Progress in Particle and Nuclear Physics 66 (2011) 549–606

Contents lists available at ScienceDirect

Progress in Particle and Nuclear Physics

journal homepage: www.elsevier.com/locate/ppnp

Review

Spin–isospin excitations probed by strong, weak and electro-magnetic interactions

Y. Fujita [a,*], B. Rubio [b], W. Gelletly [c]

[a] Department of Physics, Osaka University, Toyonaka, Osaka 560-0043, Japan
[b] IFIC, CSIC-University of Valencia, E-46071 Valencia, Spain
[c] Department of Physics, University of Surrey, Guildford GU2 7XH, Surrey, UK

ARTICLE INFO

Keywords:
Gamow–Teller transitions
β decay
Charge-exchange reactions
Isospin symmetry
High resolution
Proton-rich nuclei

ABSTRACT

Gamow–Teller (GT) transitions are the most common weak interaction processes of spin–isospin ($\sigma\tau$) type in atomic nuclei. They are of interest not only in nuclear physics but also in astrophysics; they play an important role in supernovae explosions and nucleosynthesis. The direct study of weak decay processes, however, gives relatively limited information about GT transitions and the states excited via GT transitions (GT states); β decay can only access states at excitation energies lower than the decay Q-value, and neutrino-induced reactions have very small cross-sections. However, one should note that β decay has a direct access to the absolute GT transition strengths B(GT) from a study of half-lives, Q_β-values and branching ratios. They also provide information on GT transitions in nuclei far-from-stability. Studies of $M1$ γ transitions provide similar information. In contrast, the complementary charge-exchange (CE) reactions, such as the (p, n) or $(^3\mathrm{He}, t)$ reactions at intermediate beam energies and 0°, can selectively excite GT states up to high excitation energies in the final nucleus. It has been found empirically that there is a close proportionality between the cross-sections at 0° and the transition strengths B(GT) in these CE reactions. Therefore, CE reactions are useful tools to study the relative values of B(GT) strengths up to high excitation energies. In recent $(^3\mathrm{He}, t)$ measurements, one order-of-magnitude improvement in the energy resolution has been achieved. This has made it possible to make one-to-one comparisons of GT transitions studied in CE reactions and β decays. Thus GT strengths in $(^3\mathrm{He}, t)$ reactions can be normalised by the β-decay values. In addition, comparisons with closely related $M1$ transitions studied in γ decay or electron inelastic scattering $[(e, e')]$, and furthermore with "spin" $M1$ transitions that can be studied by proton inelastic scattering $[(p, p')]$ have now been made possible. In these comparisons, the isospin quantum number T and associated symmetry structure in the same mass A nuclei (isobars) play a key role. Isospin symmetry can extend our scope even to the structures of unstable nuclei that are far from reach at present unstable beam factories.

Contents

* Corresponding author.
E-mail address: fujita@rcnp.osaka-u.ac.jp (Y. Fujita).

0146-6410/$ – see front matter © 2011 Elsevier B.V. All rights reserved.
doi:10.1016/j.ppnp.2011.01.056

1. Introduction

We shall be concerned here with spin–isospin excitations in atomic nuclei, in particular those probed with the Strong, Weak and Electro-magnetic (EM) interactions. In weak interactions in nuclear physics, such excitations are dominated by transitions with $\Delta \boldsymbol{L} = \boldsymbol{0}$ and $\Delta \boldsymbol{S} = \boldsymbol{1}$ ($\Delta S = \pm 1$ or 0), and accordingly our discussions will be largely confined to Gamow–Teller (GT) transitions and also $M1$ transitions that are analogous to them. The transitions are governed by the relatively simple isovector (IV) $\sigma\tau$ operator. It reflects the uniqueness of nuclei that they can be described as a quantum many-body system of two types of Fermion with "spin and isospin" degrees of freedom.

The main features of GT transitions can be summarised as follows:

(1) They start from a nucleus with Z and N and lead to states in a neighbouring nucleus with $Z \pm 1$ and $N \mp 1$. Thus the β^+-type GT transitions have the nature of $\Delta T_z = +1$ and the β^--type GT transitions $\Delta T_z = -1$, where T_z is defined by $(N - Z)/2$. As a result, they are of IV nature with $\Delta \boldsymbol{T} = \boldsymbol{1}$ ($\Delta T = \pm 1$ or 0). Since GT transitions involve $\Delta \boldsymbol{S} = \boldsymbol{1}$ and $\Delta \boldsymbol{L} = \boldsymbol{0}$, they also have $\Delta \boldsymbol{J}^{\boldsymbol{\pi}} = \boldsymbol{1}^+$ ($\Delta J = \pm 1$ or 0 and no parity change).
(2) They can be studied either in β decay (Weak Interaction) or in Charge-Exchange (Strong Interaction) reactions.
(3) Since the $\sigma\tau$ operator has no spatial component, transitions between states with similar spatial shapes are favoured.

(4) In a simple, independent particle picture where the individual nucleons are in an orbit with orbital angular momentum ℓ and spin s, a GT transition connects initial and final states with the same ℓ. Therefore, the transitions are among the same j orbits or the spin–orbit partners, i.e., the $j_>$ ($=\ell + 1/2$) and the $j_<$ ($=\ell - 1/2$) orbits. The $j_> \leftrightarrow j_<$ transition and the transitions between the same orbits (i.e., $j_> \leftrightarrow j_>$ and $j_< \leftrightarrow j_<$) are separated, in first order, by 3–6 MeV, the separation in energy of the spin–orbit partners.
(5) In contrast to the Fermi transitions, where only the T_z is changed by the τ operator and hence only a single state (the so-called Isobaric Analogue State) is populated in the final nucleus, GT transitions involve both the σ and the τ operators and a variety of different states can be populated. As a result one can extract more information about nuclear structure in the final nucleus.
(6) Besides the information on nuclear structure, GT transitions are also important in terms of our understanding of many processes in nuclear astrophysics.

Experimental results relevant to these features will be presented in this paper and descriptions of items (1)–(5) can be found, for example, in [1,2] and item (6) is discussed in [3].

In the study of GT transitions we are especially interested in the quantity B(GT) which is proportional to the square of the GT matrix element. The details will be discussed in Section 3. This is because, on the one hand, it can be calculated if we have a good theoretical description of both the initial and final states and, on the other hand, because it can be extracted from measurement. In β decay there exists a simple relationship between the inverse of the (partial) decay half-life $1/T_{1/2}$ and the reduced transition strength B(GT). In addition, the coefficient of proportionality has been well studied. Therefore, the absolute GT transition strengths, i.e., absolute values of B(GT), can be derived directly from β-decay studies. However the study of β decay is limited because of the Q-value. (In this article we will denote the difference in the atomic masses of the parent and daughter nuclei by Q-value or Q_β-value. Only in figures will $Q_{\rm EC}$ be used where it is necessary.) The Q-value varies from less than one MeV close to the stability line to about 12 MeV when we go far from stability (in some exceptional cases such as in very neutron-rich light nuclei, cases with 20 MeV Q-values also occur). The other limitation is that, in most cases, nuclei undergo either β^+ or β^- decay but not both.

Charge-Exchange (CE) reactions that make transitions in the β^- direction, such as the (p, n), (^{3}He, t) and (^{6}Li, ^{6}He) reactions and also in the β^+ direction, such as the (n, p), $(d, {}^2\mathrm{He})$, $(t, {}^3\mathrm{He})$ and (^{7}Li, ^{7}Be) reactions, performed at 0° (i.e., at small momentum transfer q) and intermediate incoming beam energies ($100 < E_{in} < 500$ MeV/nucleon) are good tools to study the $\sigma\tau$ response of nuclei [1,4–9] and they have features complementary to β decay. They allow access to higher excitation energies in the final nucleus. In addition it has been found that there exists a close proportionality between the 0-degree differential cross-section and the B(GT) values [10]. Therefore, CE reactions are useful tools to study the relative values of B(GT) strengths up to excitation energies of more than 20 MeV. In deriving the absolute values, reliable reference B(GT) values from β-decay studies are important. The GT transitions studied by β^--type ((p, n)-type) CE reactions can be related to those studied in β^+ decays through the isospin symmetry in the nuclear structure. Therefore, our discussion is mainly on the (p, n)-type (^{3}He, t) reaction, in which high energy resolution can be achieved. The β^+-type [(n, p)-type] CE reactions are discussed in Sections 5 and 12.

In order to combine the information from β decay and the CE reaction, we can make use of the isospin symmetry structure in nuclei and the associated equal strengths of isospin analogous transitions [11,12], i.e., the corresponding transitions between isospin analogous states. As a result, the absolute values of GT transition strength can be reliably obtained up to high excitation. As the reader will see in Section 7, the GT strengths for neutron-deficient nuclei in the *sd*- and *pf*-shell region can be deduced from such combined studies. These GT transitions are thought to play an important role in various processes of astrophysical importance [3].

The proton inelastic scattering (IE) (p, p') reactions performed at small scattering angles, especially at 0° and intermediate incoming beam energies are also a good tool to study the $\sigma\tau$ response of nuclei [13–17]. The transitions caused by the $\sigma\tau$ operator or the σ operator in the (p, p') reaction are usually called $M1$ transitions in analogy with the $M1$ transitions in γ decay due to their $\Delta \boldsymbol{J}^\pi = \boldsymbol{1}^+$ nature. However, in order to specify the spin oriented nature of these $M1$ transitions in the (p, p') reaction, we call them here the spin $M1$ transitions and they are denoted by $M1_\sigma$. The $M1_\sigma$ transitions and GT transitions in isobars can be analogous, but the isospin geometrical factors (isospin Clebsch–Gordan (CG) coefficients) associated with them are different depending on the isospin values T of the final analogue states. This allows the T value of a pair of excited analogue states to be deduced from experiment (Section 8).

The $M1$ transitions in γ decay or electron IE reactions ((e, e') reaction) [18–20], caused by the electro-magnetic (EM) interaction, also involve $\Delta \boldsymbol{J}^\pi = \boldsymbol{1}^+$. However, the $M1$ operator ($M1_{\rm EM}$ operator) causing these transitions involves not just the $\sigma\tau$ component, but other components including the $\ell\tau$ component, where ℓ is the orbital operator. Hence, by comparing the strengths of these $M1$ transitions with the strengths of analogous GT or $M1_\sigma$ transitions, the interference of the $\sigma\tau$ component with the other components in the $M1$ operator can be studied. This provides additional information on the structure of excited states (Section 9).

Comparing the properties of analogous transitions studied with different probes involving the Strong, Weak and EM interactions as the means of exciting analogue states, it is important that the data from the different probes should be of high and similar quality. In particular, it is important that they should have comparable energy resolution, since one wants to ensure that one is exciting the same states. In the (^{3}He, t), CE reaction, resolutions of 25–50 keV can now be obtained [21]. This is an improvement of one order of magnitude in resolution compared with that in the pioneering (p, n) reaction

studies [4]. This ensures a one-to-one correspondence with the transitions that can be seen in a comparison with β decay, the (p, p') reaction or γ decay. In β-decay studies, difficulties related with the systematic error due to the "Pandemonium" effect have been solved by using Total Absorption Spectroscopy (Section 4.3).

The rapid development of radioactive beam factories means that beams of nuclei far from stability will soon be available with much higher production rates. In the short to medium term this will allow much more precise studies of a wider range of β-unstable nuclei. It will also eventually allow better CE reaction studies on unstable nuclei and open up studies of GT transitions over a large part of the nuclear chart.

2. Isospin structure relevant to Gamow–Teller and $M1$ transitions

The connection between GT, spin $M1$ ($M1_\sigma$) and $M1$ ($M1_{\mathrm{EM}}$) transitions is discussed best and naturally in terms of "isospin". The τ operator involved in these transitions can connect a state having an isospin quantum number T with states of isospin $T-1$, T and $T+1$. In this section, we introduce the concepts of isospin, isobaric analogous states (analogue states) and also isobaric analogous transitions (analogous transitions). We will outline how our observations on GT, spin $M1$ and $M1$ transitions can be understood in terms of isospin and analogous transitions.

It should be noted that a similar discussion on the analogue states and analogous transitions is valid for any transitions caused by an operator that involves τ, such as the $rY_1\tau$ operator for the IV $E1$ transitions.

2.1. Isospin and analogous transitions in nuclei

In the simplest view of a nucleus, it consists of Z protons and N neutrons. Although neutrons and protons are independent fermions, they have almost the same mass and behave in the same way in purely nuclear interactions. The concept of the isospin quantum number T is based on this observation of the charge independence of the nuclear interaction. The z component of the isospin, T_z, is defined as $(N-Z)/2$. In a nucleus characterised by Z and N, this means that the minimum value of T that any state can have is $T = |T_z|$. If T is a good quantum number then mirror nuclei, in which the numbers of protons Z and neutrons N are interchanged, should have the same structure. Corresponding states in such a mirror pair are said to be isobaric analogue states or, more simply, analogue states. The abbreviation "IAS" is often used. In this article, we will use "IAS" to indicate the "analogue state of the ground state (g.s) of the initial nucleus" in the final nucleus.

We may now extend this idea to a series of isobars, nuclei with the same mass A and hence different T_z, where we expect to see states of the same structure and T (note that $T \geq |T_z|$). Transitions connecting corresponding analogue states are called analogous transitions and have corresponding strengths (for the detail, see e.g. [2,12]). Our main concern in this work is with GT and $M1$ transitions. Here we call the states excited by the $\beta^{\pm}$-decay type (charge-exchange type) $\sigma\tau_{\pm1}$ operator, which changes T_z by one unit, by the name "GT states" instead of identifying them as "the state excited by the GT transition", and the states excited by the inelastic type $\sigma\tau_0$ operator or σ operator by the name "$M1$ states". Various GT transitions in isobars can be analogous, and various GT and $M1$ transitions can also be analogous. They are expected to have corresponding strengths. In addition, GT states and $M1$ states can be analogue states. We will discuss several such cases in detail in this article.

In reality, the proton has charge while the neutron does not. Therefore, as far as the EM interaction is concerned, isospin is not a good quantum number. As a result there will be differences in structure between analogue states. In mirror nuclei with $\pm T_z$, it is expected that the differences will increase with the absolute value of T_z.

2.2. Isospin structure and GT and spin $M1$ transitions in $T = 0$ nuclei

The g.s of an even Z, even N nucleus (even–even nucleus) with $N = Z$, such as ^{12}C, ^{24}Mg or ^{28}Si, has $J^\pi = 0^+$ and $T_0 = |T_z| = 0$. By applying the $\sigma\tau$ or σ operator to the g.s, $J^\pi = 1^+$ states are excited.

The GT states with $T = 1$ in the neighbouring $T_z = \pm1$ nuclei are excited by the (n, p)- and (p, n)-type CE reactions, respectively, (see Fig. 1). The active operator is the $\sigma\tau$ interaction. On the other hand, in IE reactions, such as (p, p') or (e, e') reactions, $M1$, 1^+ states can be excited either by the isoscalar or isovector operator, because the isospin of the g.s is $T_0 = 0$. In the hadron IE reaction (p, p'), the $M1$ states with $T = 1$ are exclusively excited by the IV-type $\sigma\tau$ operator, while those with $T = 0$ are excited by the isoscalar (IS)-type σ operator. Thus, they can be called the "IV $M1$ states" and "IS $M1$ states", respectively (see Fig. 1).

It should be noted that the GT states excited by (p, n)-type reactions, the IV ($T = 1$), $M1$ states, and the GT states excited by (n, p)-type reactions have identical space and spin configurations. Thus, they are analogous states. They form an isobaric triplet [12], and are connected by dashed lines in Fig. 1. In addition, the transitions from the g.s of an even–even $N = Z$ nucleus to these states are analogous transitions, and have corresponding strengths.

One can readily illustrate the above point. Proton inelastic scattering, (p, p'), at 0° performed at intermediate incoming energies can excite $M1$ states with the nature of $\Delta L = 0$ excitation selectively. The IV and IS nature of these $M1$ states excited in $T = 0$, even–even nuclei can be distinguished by studying whether the analogue states are found or not in CE reactions at 0°. As an example, the ^{28}Si(p, p') spectrum measured at 0° and $E_p = 160$ MeV at IUCF, Indiana University [23], is compared with the ^{28}Si$(^3$He, $t)^{28}$P spectrum at $E = 140$ MeV/nucleon in Fig. 2. The high energy resolution of ≈35 keV

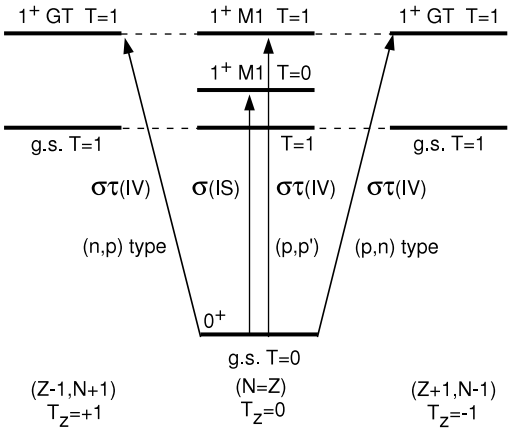

Fig. 1. Schematic isospin structure of $J^\pi = 1^+$ states excited from the g.s of an even–even $J^\pi = 0^+$ nucleus with $T = T_0 = 0$ ($N = Z$). The reactions mainly responsible for each excitation and the types of operator are shown alongside the arrows indicating the transitions. Isobaric analogue relationships among states are shown by broken lines. The Coulomb displacement energies have been removed to show the isospin symmetry of the system clearly.

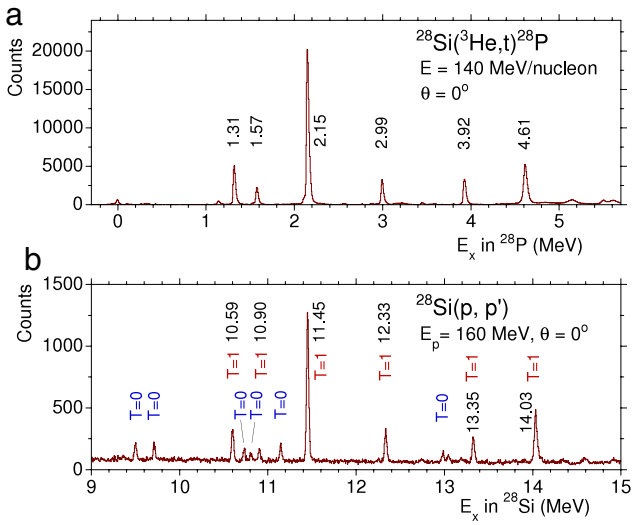

Fig. 2. A comparison of (^{3}He, t) and (p, p') spectra on the $T = 0$, ^{28}Si target nucleus. The excitation energies in spectrum (b) are shifted by 9.3 MeV, the amount of the Coulomb displacement energy. The $M1$ states observed in the (p, p') spectrum can have either $T = 1$ or $T = 0$. On the other hand, the (^{3}He, t) reaction can only excite $T = 1$, GT states that are analogous to the $T = 1$, $M1$ states. The E_x values in the (^{3}He, t) spectrum are from [22]. The E_x values and the identification of $T = 0$, $M1$ states in the (p, p') spectrum are from [15,22].

in both reactions leads to the states being well separated and clearly identified. If a pair of corresponding states is observed in both (^{3}He, t) and (p, p') spectra, the $M1$ state in ^{28}Si can be identified to be $T = 1$ [22]. In addition, we see that the corresponding GT and $M1$ states, i.e., analogue states, are excited with corresponding strengths.

2.3. Isospin structure and GT, spin M1 and Fermi transitions in T = 1/2 nuclei

In a pair of $T_z = \pm 1/2$ mirror nuclei, every state has an analogous state of similar structure in the conjugate nucleus (see Fig. 3). Such states should have the same half-integral J values and parity. Examples of $T_z = \pm 1/2$ mirror nuclei are ^{9}Be and ^{9}B, ^{23}Na and ^{23}Mg or ^{27}Al and ^{27}Si.

Because of the symmetry structure of the $T_z = \pm 1/2$ mirror nuclei, $M1$ and GT transitions from the same state (or its analogue) to another state (or its analogue) are all analogous. Analogous transitions are expected to have similar energies and strengths. Therefore, the mirror and thus isospin symmetry properties can be investigated by combining the strength and energy information for analogous transitions.

Most of the $T_z = +1/2$ nuclei in the *sd*-shell region are stable (e.g. ^{9}Be, ^{23}Na, and ^{27}Al) while the mirror $T_z = -1/2$ nuclei (e.g. ^{9}B, ^{23}Mg, and ^{27}Si) undergo β decay. Therefore, analogous GT transitions with $T_z = \pm 1/2 \rightarrow \mp 1/2$ are studied by (p, n)-type CE reactions and β^+ decay, respectively. Since the ground states are mutual IASs, the Fermi strength is concentrated in

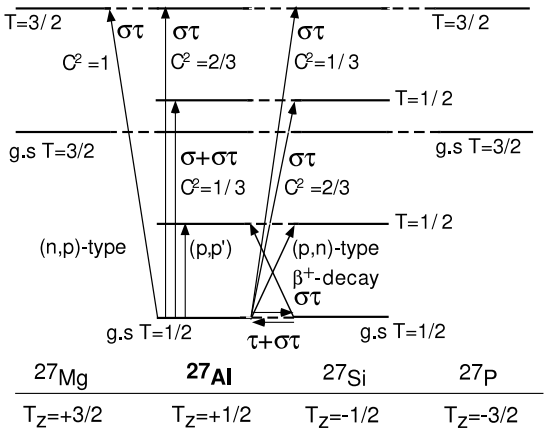

Fig. 3. Schematic isospin symmetry structures for $T_z = \pm 1/2$, odd-A mirror nuclei and the neighbouring $T_z = \pm 3/2$ nuclei for the $A = 27$ system, where ^{27}Al is stable. The Coulomb displacement energies have been removed to show the isospin symmetry of the system clearly. Analogous transitions connecting the ground states with excited states in the same nucleus and in the isobars are indicated by arrows. The squared values of associated isospin Clebsch–Gordan coefficients (C^2) are shown alongside the arrows.

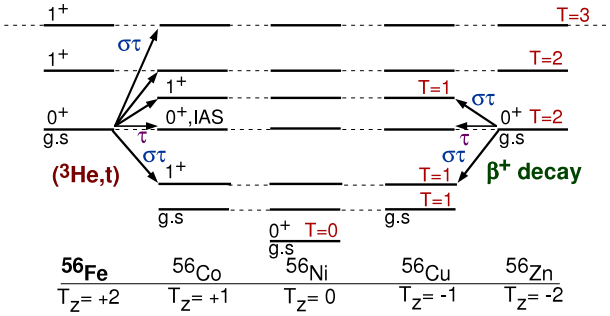

Fig. 4. Schematic view of the isospin structure of the $T = 2$ isobaric system with $A = 56$, as an example, where ^{56}Fe is stable. The Coulomb displacement energies have been removed to show the isospin symmetry of the system clearly. A similar symmetry structure in isospin is expected in $T = 1$ systems and in systems with $T = 3$ and larger.

the g.s–g.s transition. In addition, the g.s has non-zero half-integral J value. Thus the GT strength and the total Fermi strength of $B(\mathrm{F}) = |N - Z| = 1$ co-exist (see the discussion in Section 2.6.1) in this transition as an incoherent sum of strengths.

The low-lying states of the $T_z = \pm 1/2$ mirror nuclei have isospin $T = 1/2$. However, above a certain excitation energy (about $E_x = 10$ MeV), members of the $T = 3/2$ multiplet states can also exist. The IE and (p, n)-type CE reactions on a stable $T_z = +1/2$ nucleus (e.g. ^{27}Al in Fig. 3) excite both $T = 1/2$ and $3/2$ states with analogous structure in $T_z = +1/2$ and $-1/2$ nuclei, respectively. However, the CG coefficients associated with the transitions are different, as shown in Fig. 3. This difference can be exploited to allow the identification of the isospin values T of the excited states as discussed later in Section 8.2. The GT states with $T = 3/2$ in the neighbouring $T_z = +3/2$ nucleus are excited by the (n, p)-type CE reactions.

The active operator in the CE reactions is always the $\sigma\tau$ interaction. On the other hand, due to the finite value of the g.s isospin $T_0 = 1/2$, the active operators in IE reactions depend on the T values of the final states; the low-lying $T = 1/2$, $M1$ states are excited by both the $\sigma\tau$ and the σ operator, while the $T = 3/2$, $M1$ states in the higher energy region are excited only by the $\sigma\tau$ operator.

Various properties of the $T_z = \pm 1/2$ mirror nuclei are discussed later for the pairs ^{7}Li and ^{7}Be, ^{9}Be and ^{9}B, ^{11}B and ^{11}C (Section 6.1), ^{23}Na and ^{23}Mg, ^{25}Mg and ^{25}Al (Section 6.2) and ^{27}Al and ^{27}Si (Section 8.2).

2.4. *Isospin structure and analogous transitions in $T = 1, 3/2, 2$ and larger T isobaric systems*

The isospin structures of the $T = 2$ and $T = 3/2$ isobaric systems are shown in Figs. 4 and 5, respectively. The Coulomb displacement energies have been removed so that the isospin symmetry of the system is clearly evident. As a result, analogue states are aligned in the figures.

The structures of the integer T ($T = 1, 2, \ldots$) and half-integer T systems ($T = 3/2, 5/2, \ldots$) are similar to those given in Figs. 4 and 5, respectively. In addition, the isospin structures of these integer T and half-integer T systems are also similar except that the symmetry line is at the $T_z = 0$ nucleus in the former, while it is between the $T_z = +1/2$ and $-1/2$ nuclei in the latter.

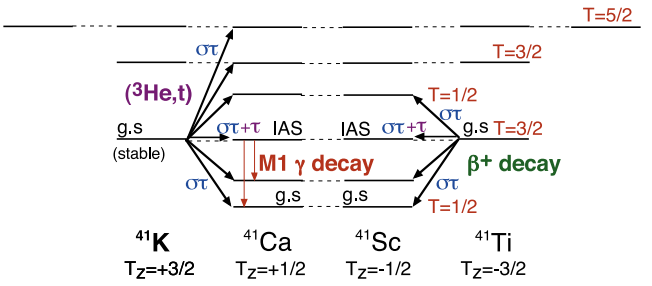

Fig. 5. Schematic view of the isospin structure of the $T = 3/2$ isobaric system with $A = 41$, as an example. The Coulomb displacement energies have been removed to show the isospin symmetry of the system clearly. A similar symmetry structure in isospin is expected in $T = 5/2$ and larger T systems.

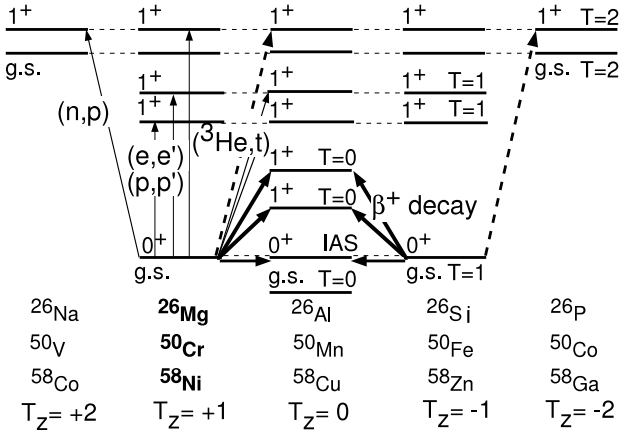

Fig. 6. Schematic view of the isospin analogue states and isospin analogous transitions for $T_z = \pm 2, \pm 1$ and 0 isobaric nuclei in $A = 26$, 50 and 58 systems, where analogue states are connected by horizontal broken lines. The Coulomb displacement energies have been removed to show the isospin symmetry of the system clearly. The stable nuclei ^{26}Mg, ^{50}Cr and ^{58}Ni can be the targets in CE reactions. The corresponding mirror proton-rich nuclei ^{26}Si, ^{50}Fe and ^{58}Zn undergo β decay. The (^{3}He, t) reaction allows us to study the $T_z = +1 \rightarrow 0$ GT transitions and excites $T = 0$, 1 and 2 states, while in the β decay, the analogous transitions with $T_z = -1 \rightarrow 0$ are studied.

Let us think of analogous GT and $M1$ transitions and their strengths. Stable target nuclei used in CE and IE reactions have $T_z \geq 0$. The isospin analogous GT and $M1$ transitions starting from nuclei, as an example, with g.s isospin $T_0 = T_z = 1$ (e.g. ^{26}Mg, ^{50}Cr and ^{58}Ni) are shown in Fig. 6. The figure also shows their analogous GT transitions that can be observed in the β decay from the $T_z = -1$ mirror nuclei (e.g. ^{26}Si, ^{50}Fe and ^{58}Zn). These analogous relationships are expected for the transitions starting from nuclei with g.s isospin $T_0 = 1, 3/2, 2$ or larger.

An (n, p)-type CE reaction (reaction in the β^+ direction) on a $T_z \geq 1$ target nucleus increases T_z by one unit. Therefore, all final states have $T_0 + 1$. On the other hand, a (p, n)-type (^{3}He, t) reaction (reaction in the β^- direction) decreases the T_z by one unit. They can reach the GT states with isospin values $T_f = T_0 - 1, T_0$ and $T_0 + 1$. Their analogous transitions can be studied by the β^+ decay of the proton-rich nuclei with $-T_z$ for the energy region up to the Q_β-value (pairs of thick solid arrows).

The transitions exciting $T_0 + 1$ states in the (n, p)-type, $T_z \rightarrow T_z + 1$ reactions are analogous with those from the $T_0 = T_z$ g.s to the $T_0 + 1$ excited states observed in the (^{3}He, t) reaction (thick broken arrow). This transition is also analogous with the exotic $-T_z \rightarrow -T_z - 1$ transition (thick broken line on the right), which cannot be observed easily today.

The IE reactions, such as (p, p') or (e, e') reactions, on the $T = T_0 = T_z$ g.s excite $T_f = T_0$ and $T_0 + 1$ states in the same nucleus. These states are analogous with the T_0 and $T_0 + 1$ states excited by the (p, n)-type and the $T_0 + 1$ states in the (n, p)-type reactions, respectively. However, the CG coefficients associated with the transitions are different in these reactions, as shown in Fig. 7. The difference can be exploited to identify the isospin values T of the excited states (see Section 8.1).

As seen from Fig. 4, analogous GT and Fermi transitions can be studied in the ^{56}Fe(^{3}He, t)^{56}Co reaction and the ^{56}Zn $\rightarrow$ ^{56}Cu β decay. The measurement of these analogous transitions is discussed in Section 11.2. The correspondence of the analogous transitions in the $A = 52, T = 2$ system is discussed in Section 11.1. The isospin symmetry structure of the $A = 41, T = 3/2$ system shown in Fig. 5 is described in Section 7.1.

2.5. Isospin Clebsch–Gordan coefficients of Gamow–Teller transitions from $T_z = 1, 3/2, 2$ and larger T_z nuclei

As will be described in Section 3.2, the GT transition matrix elements in the β^--type GT transitions starting from positive T_z ($T_z > 1/2$) nuclei are proportional to the isospin Clebsch–Gordan (CG) coefficient $C_{\rm GT} = (T_0 T_z 1 - 1 | T_f T_z - 1)$ that comes

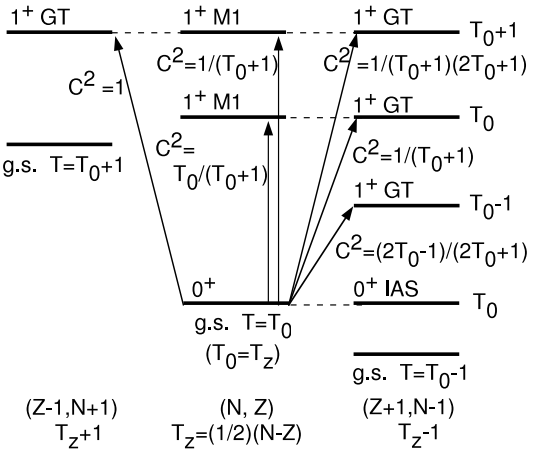

Fig. 7. Schematic view of the transitions starting from the $T = T_0 = T_z$ g.s of the nucleus having $T_z = (N - Z)/2$, where $N > Z$ (i.e. positive T_z value) is assumed. Note that, as in earlier figures, the Coulomb displacement energies have been removed. Isospin analogue states are connected by horizontal broken lines and isospin analogous transitions excited by GT and $M1$ transitions are shown by the arrows. The squared values of CG coefficients (C^2) are given alongside the arrows showing the transitions. The mirror scheme and the same CG coefficients are valid for the transitions starting from an $N < Z$ nucleus.

Table 1
The squared values of the isospin Clebsch–Gordan (CG) coefficients C^2 for the β^--type GT transitions starting from the ground states of $N \geq Z$ ($T_z \geq 0$) nuclei with various initial values of isospin T_0. The same CG coefficients are valid for the β^+-type transitions in the mirror $N \leq Z$ ($T_z \leq 0$) systems.

T_0 (=$\lvert T_z \rvert$)	Isospin of final state T_f		
	$T_0 - 1$	T_0	$T_0 + 1$
0	–	–	1
1/2	–	2/3	1/3
$T_0 \geq 1$	$(2T_0 - 1)/(2T_0 + 1)$	$1/(T_0 + 1)$	$1/(T_0 + 1)(2T_0 + 1)$
1	1/3	1/2	1/6
3/2	1/2	2/5	1/10
2	3/5	1/3	1/15
3	5/7	1/4	1/28
4	7/9	1/5	1/45
$T_0 \gg 1$	≈1	$\approx 1/T_0$	$\approx 1/T_0^2$

out when they are reduced in terms of isospin by applying the Wigner–Eckart theorem, and thus each GT transition strength is proportional to the $C_{\rm GT}^2$ (see Eqs. (2) and (3) in Section 3.2). When the transition is from the $T = T_0 = T_z$ g.s of the nucleus having $T_z = (N - Z)/2 \geq 1$ (i.e., $N \geq Z + 2$) the strength is distributed to $T_f = T_0 - 1$, T_0 and $T_0 + 1$ states in the β^--type transitions. The $C_{\rm GT}^2$ values for different isospin T_f are given in Fig. 7. On the other hand, in the β^+-type transitions, the strength is concentrated in the $T_0 + 1$ states, and thus the $C_{\rm GT}^2$ values are unity. The calculated $C_{\rm GT}^2$ values for the β^--type transitions are summarised in Table 1.

It should be noted that the same absolute value of $C_{\rm GT}$ and thus the same $C_{\rm GT}^2$ values are valid for the GT transitions starting from negative T_z ($T_z < -1/2$) nuclei. These GT transitions starting from proton-rich nuclei can be studied in β^+ decay.

For a nucleus with $T_0 = 1$, the $C_{\rm GT}^2$ values are 2/6, 3/6 and 1/6 for the $T = 0$, 1 and 2 final states, respectively. On the other hand, for a nucleus with large neutron excess (large T_0), the $C_{\rm GT}^2$ are almost unity, $1/T_0$ and $1/T_0^2$, respectively, for the $T_f = T_0 - 1$, T_0 and $T_0 + 1$ states, suggesting that most of the GT strength is concentrated in the $T_0 - 1$ states (see Table 1).

The IE and (p, n)-type CE reactions excite both $T = T_0$ and $T_0 + 1$ states with analogous structure in T_z and $T_z - 1$ nuclei, respectively. However, the CG coefficients associated with the transitions are different. The detail will be discussed in Section 8.

The large effect of the $C_{\rm GT}^2$ values on the distribution of the GT strength to different T_f states in the β^--type reaction can be illustrated from the spectra of (^{3}He, t) measurements that have been systematically performed on $T_0 = 1$, 2, 3 and 4 Ni isotopes ^{58,60,62,64}Ni [24,25]. In Fig. 8, the spectra obtained are aligned simply as a function of the excitation energy of the final nuclei. In both the spectra on ^{58}Ni and ^{64}Ni target nuclei (^{58}Cu and ^{64}Cu spectra), we see similar bump-like GT resonance (GTR) structures at $E_x \approx$ 8–9 MeV [24,25]. On the other hand, the GTR structures are less clear in the ^{60}Cu and ^{62}Cu spectra. It seems there is no good systematics of the strength distribution seen for the four spectra as a function of mass A. The "hidden" systematic change of spectra becomes apparent when the spectra are aligned by the excitation energy of the IAS peak as shown in Fig. 9. We clearly see that the GTR structure at ≈8 MeV above the IAS moves to lower energy as A increases and comes closer to the IAS, and finally in ^{64}Cu the GTR structure is situated only ≈3 MeV above the IAS. The same movement of the GT strength near to the IAS is reported in the (p, n) reaction on nickel isotopes (see Fig. 2 of [26]).

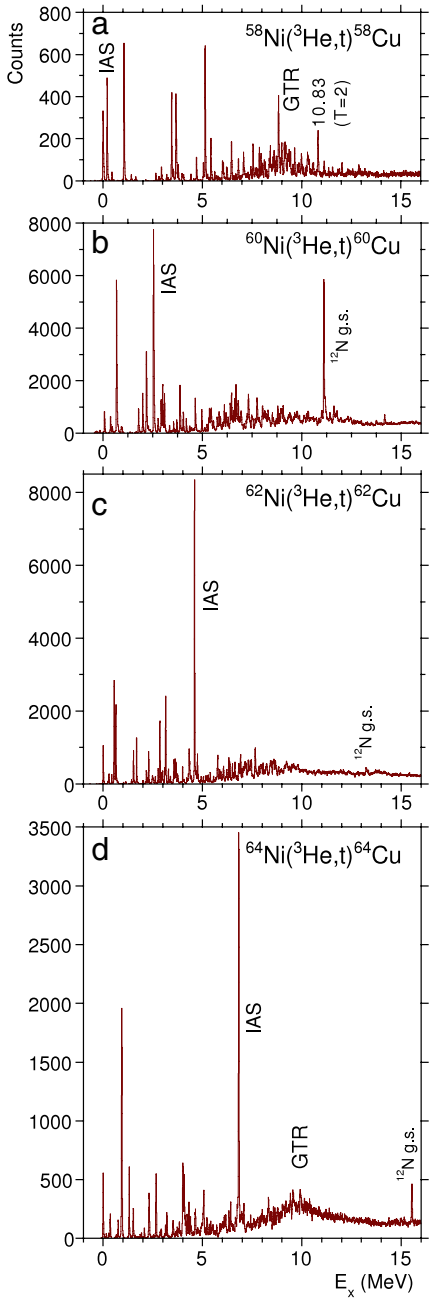

Fig. 8. The (^{3}He, t) spectra on nickel target nuclei. All spectra are aligned simply as a function of the excitation energy in the final copper nuclei. The clear bump-like structure associated with a GT resonance is observed at a similar excitation energy in the ^{58}Cu and ^{64}Cu spectra.

It should be noted that the $T = T_0 - 1$, GT excitations are inherent to the final copper nuclei (isotopes) and they are constructed on the g.s of the copper nuclei. On the other hand, the T_0 excitations are the structure constructed on the g.s of the initial nickel nuclei. They are called the spin $M1$ excitations in the initial nuclei and are observed in IE reaction experiments. Since the analogue state of the g.s of the initial nucleus is the IAS in the final nucleus, the isospin analogous structure of the T_0, $M1$ excitations, i.e., $T = T_0$, GT excitations, is constructed on the IAS.

In a simple, independent particle picture (shell-model picture), the single-particle (s.p) transitions $j_> \to j_>, j_< \to j_<$ and $j_> \to j_<$ can contribute to the GT excitations. Among them, only the $j_> \to j_<$ transition can contribute to the $M1$ excitations as neutron (ν) and/or proton (π) excitations. The $j_<$ shell is situated at higher energy than the $j_>$ by the amount of $L \cdot S$ splitting, i.e. $\Delta E_{LS} \approx$ 5–6 MeV for the $f_{5/2}$–$f_{7/2}$ pair in the nickel region. In addition, since the IV-type particle–hole (p–h) residual interaction is repulsive, it is expected that the $T = T_0$, $M1$ excitations involving $j_> \to j_<$ s.p transitions are

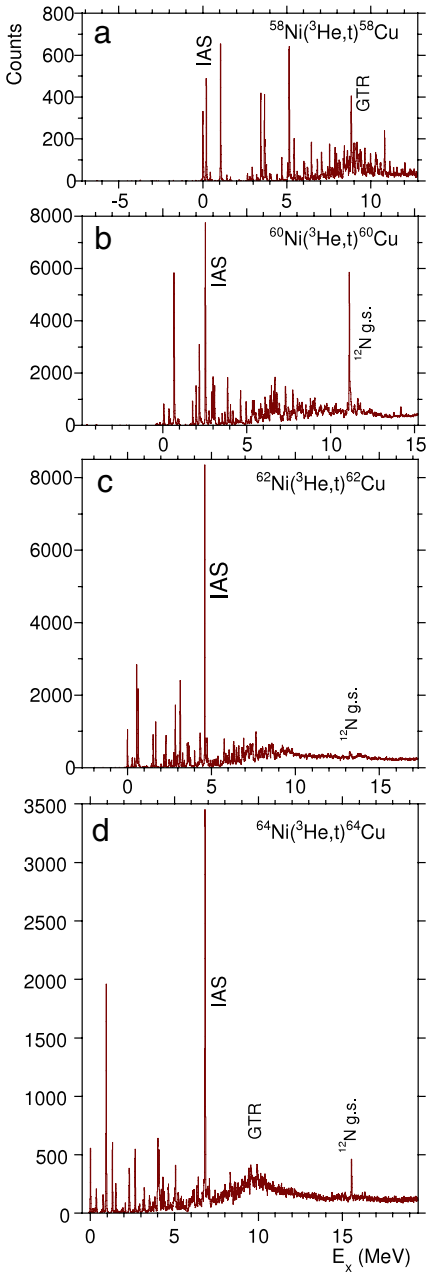

Fig. 9. The (^{3}He, t) spectra on nickel target nuclei aligned by the excitation energy of the IAS peak. The main part of the GT strength comes closer to the IAS peak as A increases.

pushed up by another few MeV to ≈7–10 MeV in nickel isotopes. Therefore, the corresponding GT excitations with T_0 nature in copper isotopes are expected at an excitation energy about 7–10 MeV higher than the IAS.

In the β^--type GT excitations starting from the neutron excess $T_0 = T_z \geq +1$ nuclei, $T_0 - 1$ GT states are also excited. In these excitations, the $j_> \rightarrow j_>$ and/or $j_< \rightarrow j_<$ transitions, in addition to the $j_> \rightarrow j_<$ transition, can contribute due to the CE nature of the excitation, i.e., transitions of the $\nu \rightarrow \pi$ nature are also allowed. In the GT excitations from nickel to copper, most of these transitions make configurations with p–h nature in the final copper isotopes. Since the residual interaction is repulsive in these p–h configurations, the main part of the strength is pushed up. It should be noted that the $T_0 - 1$, GT excitation is the structure constructed on the g.s of the $T_z = T_0 - 1$ final nucleus. Therefore, the main part of the $T_0 - 1$, GT strength is expected about 7–10 MeV above the g.s of the final nucleus.

The observed distribution of the GT strength in the daughter copper isotopes can be explained by combining the above argument with a knowledge of the CG coefficients. For the $T_0 = 1$ target nucleus ^{58}Ni, the $C^2_{\rm GT}$ value is largest for the

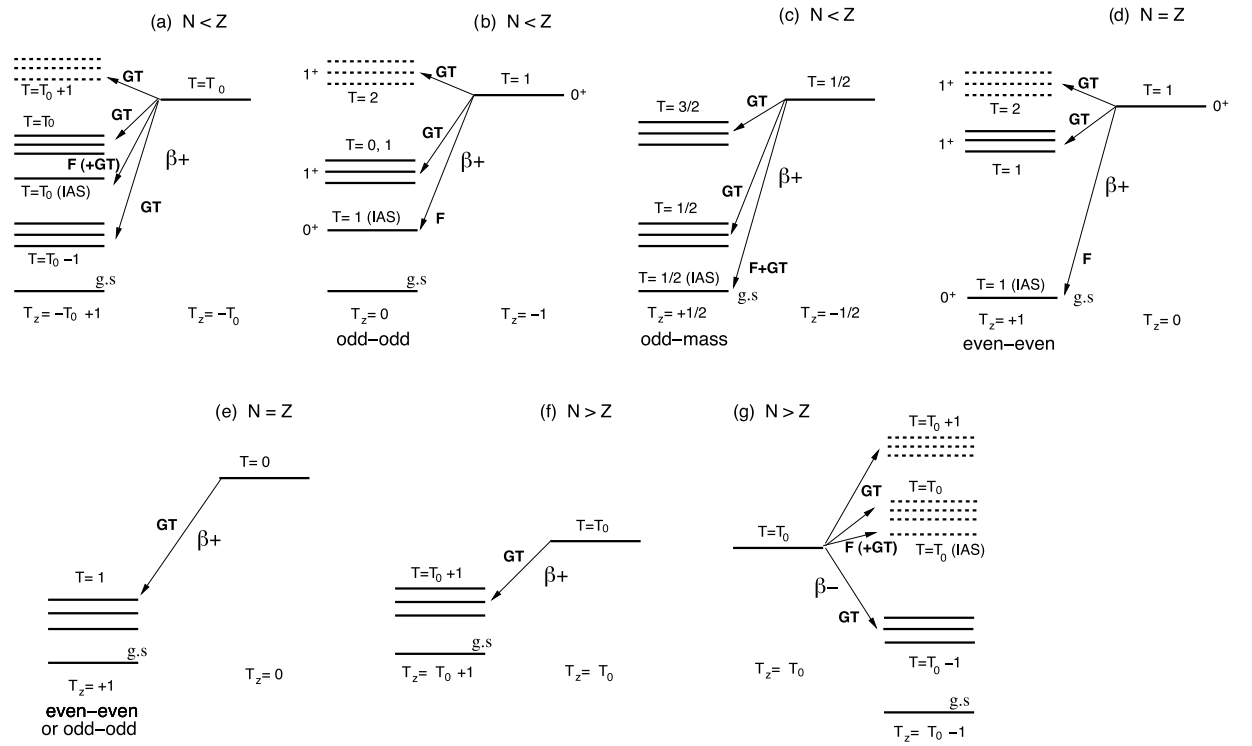

Fig. 10. The Fermi and GT transitions are shown schematically for β^+ and β^- decays from a variety of nuclei with different values of initial T and T_z. Levels shown by dashed lines indicate that the transitions to them are hindered, usually because of the configurations involved. Panels (a)–(f) represent β^+ decays. They move progressively from nuclei of negative T_z ($N < Z$) through $T_z = 0$ ($N = Z$) to nuclei with larger T_z ($N > Z$). The nuclei with $N \simeq Z$ are given in detail although the odd–odd cases are not fully covered (see text). Panel (g) shows the situation for a typical β^- decay. In panels (a), (f), and (g), the isospin of the g.s is given as T_0.

transitions to the $T = T_0 = 1$ states (see Table 1). On the other hand, for the $T_0 = 4$ target nucleus ^{64}Ni, the C_{GT}^2 values are 7/9, 1/5 and 1/45 for the $T_0 - 1$, T_0 and $T_0 + 1$ transitions, respectively. Thus the GT strength mostly goes to the $T_0 - 1$, GT states and we see the concentration of strength ≈9 MeV above the g.s of ^{64}Cu, but only 3 MeV above the IAS. The resulting conclusion is that the bump-like GTRs in ^{58}Cu and ^{64}Cu with a similar shape have different natures in terms of their isospin; the GTR in ^{58}Cu has $T = T_0$ character, while the GTR in ^{64}Cu has $T = T_0 - 1$.

2.6. Fermi and Gamow–Teller transitions in β decay

In contrast with CE reactions, which have no restrictions in energy, β decay is restricted to those cases which are offered by Nature. Accordingly, it is worthwhile summarising here which cases are allowed, especially from the point of view of isospin. Fig. 10 shows several representative decay schemes for β decays and gives an idea of where the Fermi and GT transitions occur and the isospin values of the states populated. Among them, the β^+ decays shown in panels (a) and (b) represent the β^+ decays already shown in Figs. 4 and 6, and those in panel (c) represent the β^+ decays shown in Fig. 3. The reader will recall that the corresponding mirror transitions can be studied in the β^--type CE reactions as discussed in Sections 2.3 and 2.4. As we will see below, the transitions which occur in β-decay depend on where the nuclei are situated relative to the $N = Z$ line and also on the occupancy of the proton and neutron orbits.

2.6.1. Fermi transitions in β decay

We have already discussed the GT transitions caused by the $\sigma\tau$ operator, but have said little about the Fermi transitions caused by the τ operator. In Fermi transitions neither the radial nor spin part of the wave function changes. Consequently $\Delta T \pm 1$ transitions are not allowed because of the antisymmetrical nature of the total wave function. Hence the selection rules in this case are $\Delta L = 0$, $\Delta S = 0$, $\Delta T = 0$ and $\Delta T_z = \pm 1$.

Since they connect states of the same structure in the initial and final nuclei, i.e., IASs, such transitions are strong in both CE reactions and β-decay. They carry the total Fermi sum rule strength of $B(\mathrm{F}) = N - Z$ (except for the case shown in Fig. 10(d)). It often happens that they dominate the decay process and effectively determine the decay half-life. It should be noted, however, that the transition to the IAS is not always possible in β decay.

In β^+ decay, Fermi transitions are allowed when the T_z of the initial nucleus is negative ($N < Z$) (Fig. 10(a)–(c)) and in the decay of odd–odd $T_z = 0$ nuclei when $T = 1$ (Fig. 10(d)). On the other hand, they are not allowed in the β^+ decay of

odd–odd or even–even $T_z = 0$ nuclei when $T = 0$ (Fig. 10(e)). In addition, they are not allowed in the β^+ decay from nuclei with positive T_z ($N > Z$) (Fig. 10(f)), which means that Fermi transitions are forbidden for all nuclei with positive T_z values situated "north-west" of the valley of stability in the Chart of the Nuclides.

Let us now look at the $T_z = 0$ ($N = Z$) nuclei in more detail. All such nuclei decay by β^+ emission. In general we expect that they have a g.s with $T = 0$ (Fig. 10(e)) and hence the Fermi transition is not allowed (see the discussion in Section 2.2). There, only GT decay or forbidden transitions are possible. However, there are odd–odd, $T_z = 0$ nuclei where, due to the strong proton–neutron pairing interaction, the $T = 1, J^\pi = 0^+$ state is located below the $T = 0$ states and becomes the g.s (Fig. 10(d)). Its IAS also has $J^\pi = 0^+$ and $T = 1$ and is the g.s of the even–even, $T_z = 1$, final nucleus. The transition between these two states is a super-allowed Fermi transition with a log ft value around 3.5. Among the sd- and f-shell nuclei, examples are seen in the β^+ decay of ^{34}Cl $\rightarrow$ ^{34}S, ^{42}Sc $\rightarrow$ ^{42}Ca, ^{46}V $\rightarrow$ ^{46}Ti, ^{50}Mn $\rightarrow$ ^{50}Cr and ^{54}Co $\rightarrow$ ^{54}Fe [27–30], and the same transitions in the reversed direction from the g.s of the final nuclei excite the g.s of the initial nuclei as the IAS in CE reactions (see [31] and Fig. 39). The decay to GT states with $J^\pi = 1^+$ is also possible, but these GT states lie at high excitation energy and are weakly populated. In this case, the Fermi transition takes more than 99% of the decay [27] and accordingly such transitions are used to determine the vector coupling constant g_V [30].

In β^- decay, the T_z of the initial nucleus is always positive ($N > Z$) and the Fermi transition from the $T = T_0$ parent state to the IAS with $T = T_0$ in the $T_z = T_0 - 1$ daughter nucleus is allowed in terms of isospin (Fig. 10(g)). However, the IAS is always outside the Q_β window. This is mainly because the Coulomb displacement energy is always positive since the daughter nucleus has one proton more than the parent nucleus. On the other hand, in β^--type CE reactions on positive T_z nuclei, where such energy restrictions do not apply, IASs can always be observed. Today, however, such studies are restricted to stable targets and will not provide information far from stability.

2.6.2. Gamow–Teller transitions in β decay

For $Z > N$ nuclei with large Q-values, β^+/EC-decay is the only possible process and the GT decays follow the selection rules for isospin $\Delta T = \pm 1$ or 0 (Fig. 10(a)). The orbits occupied by protons are empty on the neutron side and usually p–h configurations consisting of $j_>$ and $j_<$ orbits will contribute to GT transitions. Since Fermi decay is also allowed, the half-lives of $Z > N$ nuclei are usually short.

On the neutron-rich side of the $N = Z$ line, both β^+/EC and β^--decays are possible, depending on where the nucleus lies relative to the valley of stability. In the β^- case final GT states with all three isospins, i.e., $T_0 - 1$, T_0 and $T_0 + 1$, are possible starting from the nucleus with $T = T_0$ (Fig. 10(g)). However, the allowed orbits for the transition are often at high excitation energy in the final nucleus and consequently outside the Q-window. This effect is further exacerbated by the fact that the repulsive nature of the residual interaction in the configuration with p–h nature pushes most of the strength to high excitation energy, an effect which is discussed in Section 10 and is clearly seen in CE reactions. In the β^+ case only $T = T_0 + 1$ final GT states are possible (Fig. 10(f)). Moreover we transform a proton into a neutron in a nucleus which is already proton deficient. This means that, in general, all the allowed neutron orbits are occupied. However there are exceptions, such as when the protons occupy the $j_>$ orbit and the $j_<$ orbit is empty on the neutron side. This is exactly the case for ^{150}Ho decay as presented in Section 10.3.

In general, states with lower isospin are lower in energy. However, the $T = 1, J^\pi = 0^+$ states in $T_z = 0$ odd–odd nuclei can be located below the $T = 0$ states and become the g.s (Fig. 10(d)), as discussed in Section 2.6.1. Consequently, the decay pattern and, as a result, half-lives can be different from the usual case (Fig. 10(e)). For the same reason, in the decay of $T_z = -1$ nuclei into $T_z = 0$ nuclei (Fig. 10(b) and also Fig. 6), the IAS can lie below the $T = 0$, GT states. Such examples are presented in Sections 7.3 and 10.1.

Finally, let us think of the β decays from half-integer T_z nuclei. As discussed in Section 2.3, both the Fermi and GT transitions can contribute to the population of the IAS when the decay is from $T_z = -1/2$ nuclei (Fig. 10(c)). The same happens for the β^+ decay of $T_z = -3/2, -5/2$ and smaller values (Fig. 10(a)) and for the β^- decay of $T_z = +3/2, +5/2$ and larger values (Fig. 10(g)).

It should be noted that Fig. 10 is not comprehensive and does not cover all odd–odd cases.

3. Properties of Gamow–Teller, electro-magnetic $M1$ and spin $M1$ transitions

Let us consider the properties of GT, electro-magnetic $M1$ ($M1_{\rm EM}$), and spin $M1$ ($M1_\sigma$) transitions, which are studied typically in β decay or CE reactions, γ decay or electron IE reaction [(e, e')], and proton IE reaction [(p, p')], respectively. They are caused by the $\sigma\tau$ operator, magnetic dipole (μ) operator, and σ or $\sigma\tau$ operators, respectively.

3.1. Selection rules for J^π values of states

The selection rules for the ΔJ^π values in GT, $M1$ and Fermi transitions from a state with J_i to a state with J_f are;

GT and $M1$: $\Delta J = 0, \pm 1$ (but no $J_i = 0 \rightarrow J_f = 0$), no parity change;

Fermi: $\Delta J = 0$, no parity change (transitions are between isobaric analogue states).

In a highly deformed nucleus in which K, the projection of the total angular momentum J on the axis of deformation, becomes a good quantum number, the ΔK selection rules for GT and $M1$ transitions are important;

GT and $M1$: $\Delta K = 0, \pm 1$ (but not $K_i = 0 \rightarrow K_f = 0$).

3.2. Strengths of Gamow–Teller and $M1$ transitions

Our aim is to compare the strengths of analogous GT transitions, GT and $M1_{EM}$, or GT and $M1_\sigma$ transitions [32]. It is most appropriate to compare the strengths of these transitions in terms of the "reduced transition strength (probability)" "$B(\alpha)$", where α is the name of the operator, such as GT or $M1$. The expression for $B(\alpha)$ values reduced in spin (J) are found in text books (see e.g. [19,33,34]). In order to compare transition strengths for analogous GT and/or $M1$ transitions, however, it is important to reduce the matrix element in terms of isospin [32]. Therefore, we start here with the reduced matrix elements in spin (J) but not in isospin and follow the convention of Edmonds [35].

The reduced GT transition strength B(GT) for the transition from the initial state with spin J_i, isospin T_i, and z-component of isospin T_{zi} to the final state with J_f, T_f, and T_{zf} is given by [36]

$$B^{\pm1}(\mathrm{GT}) = \frac{1}{2J_i+1}\left|\langle J_f T_f T_{zf}\|\frac{1}{\sqrt{2}}\sum_{j=1}^{A}(\boldsymbol{\sigma}_j\tau_j^{\pm1})\|J_i T_i T_{zi}\rangle\right|^2, \tag{1}$$

where $\tau^{\pm1} = \mp(1/\sqrt{2})(\tau_x \pm i\tau_y)$ and transforms as a tensor of rank one. By applying the Wigner–Eckart theorem in isospin space, we get

$$B(\mathrm{GT}) = \frac{1}{2J_i+1}\frac{1}{2}\frac{C_{\mathrm{GT}}^2}{2T_f+1}\left|\langle J_f T_f\|\sum_{j=1}^{A}(\boldsymbol{\sigma}_j\boldsymbol{\tau}_j)\|J_i T_i\rangle\right|^2 \tag{2}$$

$$= \frac{1}{2J_i+1}\frac{1}{2}\frac{C_{\mathrm{GT}}^2}{2T_f+1}[M_{\mathrm{GT}}(\sigma\tau)]^2, \tag{3}$$

where C_{GT} is the isospin Clebsch–Gordan (CG) coefficient $(T_i T_{zi} 1 \pm 1|T_f T_{zf})$, and the $M_{\mathrm{GT}}(\sigma\tau)$ is the IV spin-type GT matrix element.

From this expression for the GT "reduced" transition strength, the important thing to note is that B(GT) consists of the squared transition matrix element and the spin and isospin geometrical factors. Therefore, even if the initial and final states are common, transitions in reverse directions have different B(GT) values. For example, a GT transition from a state having $|J\ T\ T_z\rangle$ of $|0\ T_0\ T_0\rangle$ to the $|1\ T_0-1\ T_0-1\rangle$ state has three times larger B(GT) than that in the inverse direction. This is because of the different number of sub-states; a $J=1$ state has three sub-states with $J_z=-1$, 0 and $+1$, while a $J=0$ state has only one.

In intermediate energy hadron IE reactions, such as (p,p'), $M1$ states excited by the $M1_\sigma$ transitions become prominent at forward angles including 0°. They can, in principle, be excited by the σ and $\sigma\tau$ terms of the effective nuclear interaction. In reality, however, since the $\sigma\tau$ term is much stronger, the excitations are mainly caused by the $\sigma\tau$ term [1,37], if they start from a g.s with $T_0 \geq 1/2$. Then, as in GT transitions, we can define the reduced spin $M1$ transition strength $B(M1_\sigma)$. After replacing the $\tau_j^{\pm1}$ in Eq. (1) by τ_j^0 and applying the Wigner–Eckart theorem in the isospin space, we get

$$B(M1_\sigma) = \frac{1}{2J_i+1}\frac{1}{2}\frac{C_{M1}^2}{2T_f+1}\left|\langle J_f T_f\|\sum_{j=1}^{A}(\boldsymbol{\sigma}_j\boldsymbol{\tau}_j)\|J_i T_i\rangle\right|^2 \tag{4}$$

$$= \frac{1}{2J_i+1}\frac{1}{2}\frac{C_{M1}^2}{2T_f+1}[M_{M1}(\sigma\tau)]^2, \tag{5}$$

where C_{M1} is the isospin CG coefficient $(T_i T_{zi} 10|T_f T_{zf})$, where $T_{zf} = T_{zi}$, and the $M_{M1}(\sigma\tau)$ is the IV-type spin $M1$ matrix element. The $M_{M1}(\sigma\tau)$ is slightly different from the $M_{\mathrm{GT}}(\sigma\tau)$, because the contribution of the so-called meson exchange currents (MEC) is different as will be discussed at the end of this section.

The operator $\boldsymbol{\mu}$ for $M1_{EM}$ transitions and magnetic moments consists of an orbital part $g_\ell\boldsymbol{\ell}$ and a spin part $g_s\boldsymbol{s}[=(1/2)g_s\boldsymbol{\sigma}]$. It can be rewritten as the sum of IS and IV terms (for example, see [33,34]) as,

$$\boldsymbol{\mu} = \left[\sum_{j=1}^{A} g_\ell\boldsymbol{\ell}_j + g_s\boldsymbol{s}_j\right]\mu_N = \left[\sum_{j=1}^{A}(g_\ell^{\mathrm{IS}}\boldsymbol{\ell}_j + g_s^{\mathrm{IS}}\boldsymbol{s}_j) - \sum_{j=1}^{A}(g_\ell^{\mathrm{IV}}\boldsymbol{\ell}_j + g_s^{\mathrm{IV}}\boldsymbol{s}_j)\tau_{zj}\right]\mu_N, \tag{6}$$

where μ_N is the nuclear magneton, the z-component of the isospin operator $\tau_{zj}=1$ for neutrons and -1 for protons, and τ_{zj} is τ_j^0. The coefficients g^{IS} and g^{IV} are the IS and IV combinations of gyromagnetic factors (g factors): $g_\ell^{\mathrm{IS}} = \frac{1}{2}(g_\ell^\pi + g_\ell^\nu)$, $g_s^{\mathrm{IS}} = \frac{1}{2}(g_s^\pi + g_s^\nu)$, $g_\ell^{\mathrm{IV}} = \frac{1}{2}(g_\ell^\pi - g_\ell^\nu)$, and $g_s^{\mathrm{IV}} = \frac{1}{2}(g_s^\pi - g_s^\nu)$. For bare protons and neutrons, the orbital and spin g factors are $g_l^\pi = 1$ and $g_l^\nu = 0$, and $g_s^\pi = 5.586$ and $g_s^\nu = -3.826$, respectively. Therefore, we get $g_\ell^{\mathrm{IS}} = 0.5$, $g_s^{\mathrm{IS}} = 0.880$, $g_\ell^{\mathrm{IV}} = 0.5$, and $g_s^{\mathrm{IV}} = 4.706$.

Starting from the reduced matrix elements in spin but not in isospin, and following the convention of Edmonds [35], the reduced $M1_{EM}$ strength B(M1) can be written [36] as

$$B(M1) = \frac{1}{2J_i+1}\frac{3}{4\pi}\left|\langle J_f T_f T_{zf}\|\boldsymbol{\mu}\|J_i T_i T_{zi}\rangle\right|^2 \tag{7}$$

$$= \frac{1}{2J_i+1}\frac{3}{4\pi}\mu_N^2\left|\langle J_f T_f T_{zf}\|\sum_{j=1}^{A}\left(g_\ell^{\rm IS}\boldsymbol{\ell}_j + g_s^{\rm IS}\frac{1}{2}\boldsymbol{\sigma}_j\right) - \sum_{j=1}^{A}\left(g_\ell^{\rm IV}\boldsymbol{\ell}_j + g_s^{\rm IV}\frac{1}{2}\boldsymbol{\sigma}_j\right)\tau_j^0\|J_i T_i T_{zi}\rangle\right|^2, \tag{8}$$

where $T_z = T_{zf} = T_{zi}$ for $M1$ transitions. By again applying the Wigner–Eckart theorem in isospin space, we get

$$B(M1) = \frac{1}{2J_i+1}\frac{3}{4\pi}\mu_N^2\left|\langle J_f T_f\|\sum_{j=1}^{A}\left(g_\ell^{\rm IS}\boldsymbol{\ell}_j + g_s^{\rm IS}\frac{1}{2}\boldsymbol{\sigma}_j\right) - \frac{C_{M1}}{\sqrt{2T_f+1}}\sum_{j=1}^{A}\left(g_\ell^{\rm IV}\boldsymbol{\ell}_j + g_s^{\rm IV}\frac{1}{2}\boldsymbol{\sigma}_j\right)\boldsymbol{\tau}_j\|J_i T_i\rangle\right|^2 \tag{9}$$

$$= \frac{1}{2J_i+1}\frac{3}{4\pi}\mu_N^2\left[\left(g_\ell^{\rm IS}M_{M1}(\ell) + g_s^{\rm IS}\frac{1}{2}M_{M1}(\sigma)\right) - \frac{C_{M1}}{\sqrt{2T_f+1}}\left(g_\ell^{\rm IV}M_{M1}(\ell\tau) + g_s^{\rm IV}\frac{1}{2}M_{M1}(\sigma\tau)\right)\right]^2 \tag{10}$$

$$= \frac{1}{2J_i+1}\frac{3}{4\pi}\mu_N^2\left[M_{M1}^{\rm IS} - \frac{C_{M1}}{\sqrt{2T_f+1}}M_{M1}^{\rm IV}\right]^2. \tag{11}$$

The isospin CG coefficient $C_{M1} = (T_i T_{zi} 10|T_f T_{zf})$ comes out explicitly by the use of reduced matrix elements, where $T_{zf} = T_{zi}$. The matrix elements are

$$\text{IS terms:}\quad M_{M1}(\ell) = \langle J_f T_f\|\sum_{j=1}^{A}\boldsymbol{\ell}_j\|J_i T_i\rangle, \qquad M_{M1}(\sigma) = \langle J_f T_f\|\sum_{j=1}^{A}\boldsymbol{\sigma}_j\|J_i T_i\rangle, \quad \text{and} \tag{12}$$

$$\text{IV terms:}\quad M_{M1}(\ell\tau) = \langle J_f T_f\|\sum_{j=1}^{A}\boldsymbol{\ell}_j\boldsymbol{\tau}_j\|J_i T_i\rangle, \qquad M_{M1}(\sigma\tau) = \langle J_f T_f\|\sum_{j=1}^{A}\boldsymbol{\sigma}_j\boldsymbol{\tau}_j\|J_i T_i\rangle. \tag{13}$$

Since the $g_s^{\rm IV}$ coefficient is the largest, the contribution from the IV spin term is often the largest [18,19]. The $M_{M1}^{\rm IS}$ and $M_{M1}^{\rm IV}$ are the IS and IV terms of the $M1$ matrix element, respectively. They are

$$M_{M1}^{\rm IS} = g_\ell^{\rm IS}M_{M1}(\ell) + \frac{1}{2}g_s^{\rm IS}M_{M1}(\sigma), \quad \text{and} \tag{14}$$

$$M_{M1}^{\rm IV} = g_\ell^{\rm IV}M_{M1}(\ell\tau) + \frac{1}{2}g_s^{\rm IV}M_{M1}(\sigma\tau), \tag{15}$$

where the IV term is usually larger than the IS term. The IS term, therefore, may interfere destructively or constructively with the IV term. In addition, the orbital term may interfere constructively or destructively with the spin term. These interference effects are dependent on the configurations of the initial and final states.

In $\Delta T = 0$ analogous $M1$ transitions in $T_z = \pm T$ ($T \geq 1/2$) mirror nuclei, both IS and IV contributions are expected. It should be noted that the sign of the isospin CG coefficient C_{M1} in Eq. (11) changes for these analogous transitions. For $T_z = \pm T$, Eq. (11) can be rewritten as

$$B(M1)_\pm = \frac{1}{2J_i+1}\frac{3}{4\pi}\mu_N^2\left[M_{M1}^{\rm IS} \mp \frac{|C_{M1}|}{\sqrt{2T_f+1}}M_{M1}^{\rm IV}\right]^2, \tag{16}$$

where $|C_{M1}| = \sqrt{1/3}$ for the $T = 1/2$ case. If an $M1$ transition has more than average strength, the IV contribution in the transition is usually about one order of magnitude larger than the IS contribution [18,19]. Under such a condition, we can separately extract the IS and the IV transition strengths $B_{\rm IS}(M1)$ and $B_{\rm IV}(M1)$ in the $\Delta T = 0$, $M1$ transition by solving Eq. (16) as simultaneous equations

$$B_{\rm IS}(M1) \equiv \frac{1}{2J_i+1}\frac{3}{4\pi}\mu_N^2[M_{M1}^{\rm IS}]^2 \tag{17}$$

$$= \frac{1}{4}\left[\sqrt{B(M1)_+} - \sqrt{B(M1)_-}\right]^2, \tag{18}$$

and

$$B_{\rm IV}(M1) \equiv \frac{1}{2J_i+1}\frac{3}{4\pi}\mu_N^2\frac{C_{M1}^2}{2T_f+1}[M_{M1}^{\rm IV}]^2 \tag{19}$$

$$= \frac{1}{4}\left[\sqrt{B(M1)_+} + \sqrt{B(M1)_-}\right]^2. \tag{20}$$

It is known that the $\sigma\tau$ terms of the $M1$ and GT operators are both quenched. The reduction is partly attributed to the core polarisation [12] and partly to the so-called meson exchange currents (MEC). The core polarisation modifies the initial and final wave functions, and thus the effects on the analogous $M1$ and GT transitions would be the same. On the other hand, the MEC effect can be different, because the $M1$ operator involves τ_0, while the GT operator involves $\tau_\pm$. The different contributions of the MEC to the $M1$ and GT operators have been studied theoretically [38,39] and experimentally [22,40–43]. These effects are expressed by the ratio

$$R_{\mathrm{MEC}} = [M_{M1}(\sigma\tau)]^2/[M_{\mathrm{GT}}(\sigma\tau)]^2. \tag{21}$$

The most probable value $R_{\mathrm{MEC}} = 1.25$ is deduced for nuclei in the middle of the *sd* shell [32,40–43].

3.3. Magnetic moments

The magnetic moment μ of a state with spin J and isospin T is defined by the diagonal matrix element of the z component of the magnetic dipole operator μ_z

$$\mu = \langle JJTT_z|\mu_z|JJTT_z\rangle. \tag{22}$$

By applying the Wigner–Eckart theorem in the spin space,

$$\mu = \frac{(JJ10|JJ)}{\sqrt{2J+1}}\langle JTT_z\|\boldsymbol{\mu}\|JTT_z\rangle, \tag{23}$$

where the CG coefficient $(JJ10|JJ) = \sqrt{J/(J+1)}$. By further applying the Wigner–Eckart theorem in the isospin space, and by using Eq. (6), we get

$$\mu = \frac{\sqrt{J}}{\sqrt{(J+1)(2J+1)}}\mu_N\left[M^{\mathrm{IS}}_{M1} - \frac{C_{M1}}{\sqrt{2T+1}}M^{\mathrm{IV}}_{M1}\right], \tag{24}$$

where the IS and IV matrix elements are obtained by making the initial and the final states the same in the definitions given by Eqs. (14) and (15), respectively. The CG coefficient is $C_{M1} = (TT_z10|TT_z)$.

4. β-decay studies

The common modes of radioactive decay, α-, β and γ-emission, were discovered at the beginning of the 20th century. The study of β decay is inherently more difficult than the other two because the spectra of the emitted β particles are continuous and not discrete. This is because of the three-body nature of this process, which was explained by Pauli [44] in 1932 by introducing the idea of the simultaneous emission of the neutrino and the β particle.

Fermi's theoretical explanation [45] of β decay followed Pauli's hypothesis in just a few years. In the theory he postulated that the interaction takes place at a point. In this allowed approximation, as it is called, no angular momentum can be transferred in the decay. Thus the only change in the total angular momentum J in β decay must come from the spins of the particles. In other words, if we write

$$\Delta\boldsymbol{J_i} = \Delta\boldsymbol{J_f} + \Delta\boldsymbol{L} + \Delta\boldsymbol{S} \tag{25}$$

where $\boldsymbol{J_i}$ and $\boldsymbol{J_f}$ are the total angular momentum (spins) of the initial and final nuclear states, $\Delta\boldsymbol{L}$ is the orbital angular momentum carried away by the leptons and $\Delta\boldsymbol{S}$ is the vector sum of the intrinsic spins of the electron and the neutrino, then in the allowed approximation, where $\Delta\boldsymbol{L} = \boldsymbol{0}$ by definition, we can distinguish between two cases by $\Delta\boldsymbol{S} = \boldsymbol{0}$ or $\boldsymbol{1}$. They were called Fermi and Gamow–Teller decays, respectively, in honour of the work of the physicists who first recognised their nature. They are the types of transition governed by the $\sigma\tau$ and τ operators mentioned in Section 1. As indicated earlier allowed decays follow the selection rules $\Delta\boldsymbol{J} = \boldsymbol{0}$ or $\boldsymbol{1}$, $\Delta\boldsymbol{L} = \boldsymbol{0}$, with Fermi decay characterised by $\Delta\boldsymbol{S} = \boldsymbol{0}$ and Gamow–Teller by $\Delta\boldsymbol{S} = \boldsymbol{1}$. Eq. (25) also tells us that for GT transitions 0^+ to 0^+ transitions are not possible. Such transitions can thus only proceed by Fermi decays.

Fermi's assumption of a point interaction was a good one and was fully borne out by the later discovery of the relevant $W^\pm$ exchange particles with masses of about 80 GeV/c^2. Transitions with $\Delta L \geq 1$ do occur but, not surprisingly, they are suppressed relative to allowed transitions. Historically they were designated as "forbidden" transitions because of this, a name which is not really appropriate but has stuck. The transition probability is more suppressed with increasing L. This is normally expressed in terms of the degree of forbiddenness.

As explained in Section 3.2, the strengths of GT transitions are most readily compared in terms of the reduced transition strength B(GT). The definitions of this quantity appear in Eqs. (2) and (3). In this article our interest lies in the comparison of B(GT) values derived from measurements of CE reactions and β decay, which can subsequently be compared with theoretical predictions of the same quantity. In Section 5 we will describe how one can extract B(GT) values from experiments on CE reactions. Here we will discuss how they are obtained in β-decay studies.

In β-decay experiments, the B(GT) value for a GT transition to a level j with an excitation energy E_j is expressed in terms of the f_jt_j value, where t_j is the partial half-life to level j and f_j is the phase-space factor. Similarly, the Fermi transition strength,

B(F), is related to the partial Fermi half-life t_F and f_F. Thus we have the relationships

$$B_j(\mathrm{GT})\lambda^2 = K/f_j t_j \quad \text{and} \quad B(\mathrm{F})(1-\delta_c) = K/f_F t_F, \tag{26}$$

where $K = 6143.6(17)$ [30], $\lambda = g_A/g_V = -1.270(3)$ [46] and δ_c is the Coulomb correction factor [47]. The Fermi transition strength is concentrated in the transition to the IAS and has the value $B(\mathrm{F}) = |N-Z|$. The GT transition strength is spread over a number of states B_j(GT) and each individual value depends strongly on the details of the structure of the initial and final states. If the β decay is from a state with a half-integral J value and the final state is its isobaric analogue state, the transition strength is the incoherent sum of the Fermi and GT transition strengths. A good example is the strength of the g.s–g.s transition between a pair of $T_z = \pm 1/2$ nuclei (see panel (c) of Fig. 10). In such transitions, the two parts in Eq. (26) should be combined to give

$$B(\mathrm{GT})\lambda^2 + B(\mathrm{F})(1-\delta_c) = K/ft. \tag{27}$$

The partial half-life t_j is related to the total half-life $T_{1/2}$ of the β-decay parent state by

$$t_j = T_{1/2}/I(E_j), \tag{28}$$

where $I(E_j)$ is the beta feeding to the state j. The phase-space factor, $f(Z, Q_\beta - E_x)$, can be calculated accurately but it demands a knowledge of the Q_β-value and the excitation energy of the level fed in the decay. Therefore, we have to combine the values of these quantities in order to obtain accurate B_j(GT) values.

As we have pointed out, a major limitation in β-decay studies is the Q_β-window; we cannot access the states situated above this window. In addition, there is a further limitation in that the f-factor decreases as E_x of the final state increases; the value depends on approximately $(Q_\beta - E_x)^5$. Thus the observed intensities of the beta transitions to higher-lying levels are strongly suppressed in intensity.

4.1. Q-value measurements

In order to determine the B(GT) with precision, it is necessary to have an accurate Q_β-value, which is defined as the difference in mass between the initial (parent) state and the g.s of the final (daughter) nucleus in β decay. For many years Audi and Wapstra [48–50] have carried out evaluations of all the available data on masses: an evaluation which is not a simple compilation since there are many cross-links between the initial results. These evaluations provide a continuously updated, consistent set of masses, which is the first port of call if one needs to know a mass or a Q-value.

The methods for the mass measurements can be divided into "indirect" and "direct" methods. The former are based on mass difference measurements, either reaction Q-values or Q-values in radioactive decay. If one of the masses is well known, then the other can be deduced. Direct methods are important, not because they are "absolute" mass measurements, but because they are always made relative to some "well-known mass reference" which is used to calibrate the setup. Over the last few decades two direct methods have been steadily developed which now offer the possibility of high precision measurements of masses. Mass measurements with Penning traps and mass measurements at storage rings, have so many advantages over previously used techniques that they now dominate the present activity in this field and look likely to be pre-eminent in the future as well.

In the Penning trap methods the ions are injected at low energy after being created and selected in either an Isotope Separator On-Line (ISOL) or fragmentation facility. The trap has a strong homogeneous magnetic field B and an axially symmetric static electric quadrupole field and this allows the storage of ions. In the trap they perform a complicated motion consisting of a circular motion around the magnetic field with cyclotron frequency $\omega_c = (q/m)B$ plus two types of radial motion, which are usually called reduced cyclotron motion and magnetron motion. Various methods are used but in essence all of them involve a measurement of the cyclotron frequency and hence of the mass of the singly charged ions. The reader is referred to [51,52] for the details.

Mass measurements at storage rings have been pioneered at the highly successful Experimental Storage Ring (ESR) at GSI. The great advantage of this method is that it allows the simultaneous measurement of the masses of many different nuclear species. At GSI relativistic fragments from fragmentation or fission reactions are filtered in A and Z by the FRagment Separator (FRS) and injected into the ESR. Two methods, the isochronous method and the Schottky method, are then available to determine the mass. Both of these methods essentially rely on having a long time-of-flight path over many passages round the ring [53].

4.2. Half-life measurements

The (total) half-life ($T_{1/2}$) of a β-decaying state is one of the three main ingredients needed to determine the β-decay strength B(GT) and hence the transition probability. Half-lives vary over a wide range reflecting the detail of the nuclear structure. For instance the $T_{1/2}$ of ^{44}Ti with $Z = N = 22$ is 58.9(3) years [54] while that of ^{46}V with $Z = N = 23$ is only 422.50(11) ms [55]. In the decay of ^{44}Ti, the Fermi transition is isospin forbidden (see panel (e) of Fig. 10) and possible GT transitions are outside the beta window. In contrast, the Fermi transition is allowed in the decay of ^{46}V (see panel (d) of Fig. 10). Indeed, Fermi transitions are fast since the sum rule strength is concentrated in a single state, the IAS. The GT transition strength can be distributed among many levels, and the full sum rule strength can never be observed due to the Q-window limitation in a β decay.

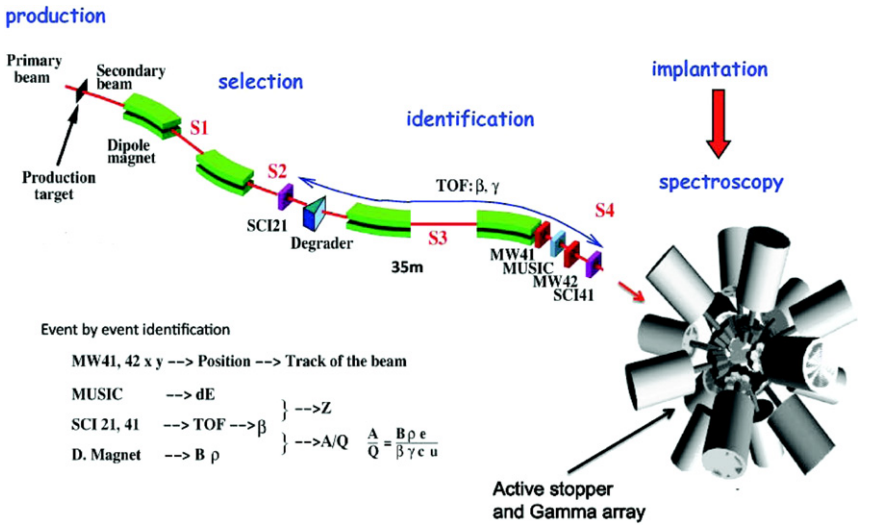

Fig. 11. A schematic view of the Fragment Recoil Separator at GSI [59]. Radioactive ions are produced in fragmentation or fission of an ≈1 GeV/nucleon heavy ion beam from the SIS-18 synchrotron. In the first half of the separator the ions are selected. After passing through a variable thickness degrader the ions are identified event-by-event in A, Z and charge q by measuring the time-of-flight between two scintillators (SC21 and SC41), the $B\rho$ of the magnets in the second half of the FRS and the energy loss (ΔE) in the multi-wire ionisation chamber (MUSIC). The ions leaving the separator are implanted into double-sided Si strip detectors (DSSDs). This active stopper serves to detect the implantation of the ion and any subsequently emitted β particles. The β-delayed γ rays are detected in the RISING γ-detector array.

It may seem simple to determine $T_{1/2}$ values. However far from the line-of-nuclear-stability when the conditions are not ideal, either from the point of view of the purity of the radioactive samples or the signal-to-noise ratio in the measurements, or from the statistical point of view, their determination can become complex and fraught with difficulty. We want to emphasise here that systematic errors due to the wrong correlation of events are often the main difficulty and source of error in reported values in the literature.

The simplest way to determine the $T_{1/2}$ of a β-decaying state, most commonly the g.s of the nucleus, is to accumulate a sample of the radioactive species of interest over a given period, then stop and measure the resulting radiation as a function of time. In the simplest case one can measure either the βs or radiation emitted promptly following the beta decay process. The most common β-delayed radiation is γ rays but in nuclei far from stability, where the Q_β-value is large and exceeds the particle separation energy, it may also be β-delayed neutrons or protons.

In a clean environment where a single decay is involved, the behaviour of the radiation as a function of time will follow the exponential law and one can readily extract the $T_{1/2}$ value with high precision. An example drawn from studies of super-allowed Fermi decays can be seen in Fig. 1 of [56]. These ideal conditions are very seldom fulfilled. Often the daughter and its progeny are also radioactive and form a decay chain. The usual way to deal with this complication is to measure either the characteristic γ radiation, which is associated with one particular decay or, in the case of nuclei far from stability, where the states in the daughter nucleus are proton or neutron unbound but those in the granddaughter are bound, one can follow the decay of the β-delayed neutrons or protons. Examples can be found in [57,58].

In the most common type of experiment to date, the delayed γs are detected with Ge detectors, which have good resolution and thus ensure that one is following the decay of the nucleus of interest since the γ-decay pattern is highly characteristic. There is, however, a price to pay because the low efficiency of Ge detectors means that the statistics of the resulting measurements is often poor. Where one is detecting protons or neutrons the detectors usually have better efficiency, typically of the order of 30%–50%. Consequently the results are statistically more significant.

This technique of accumulating, then stopping and measuring the activity is typically employed at ISOL facilities, where a mass separator and sometimes chemical or other kinds of separation are used to produce clean sources of the nuclei of interest. In order to achieve clean conditions and ensure that the daughter activity(ies) does(do) not dominate the spectra, a tape transport system is usually used, either to place the accumulated activity in front of the detectors, or to remove the accumulated activity if the range of the $T_{1/2}$ is short (less than one s). In the case of short half-lives and, if the measurement takes place at the collection point, one can follow the growth and decay of the activity and fit the corresponding equations, but this method can be applied only where the accumulation is constant or follows a well defined function, which cannot always be guaranteed.

The determination of the half-life in experiments at fragmentation facilities is more difficult. Ions are filtered through the separator [59–62] and later implanted in a highly pixellated detector. Fig. 11 shows a schematic view of a typical setup for such measurements at the Fragment Recoil Separator (FRS) at GSI with radioactive ions being implanted into an active detector in the centre of the RISING γ-ray array [63]. An experiment using this particular setup is described later in Section 7.3. However, full physical separation is seldom achieved, and sometimes deliberately not pursued since several

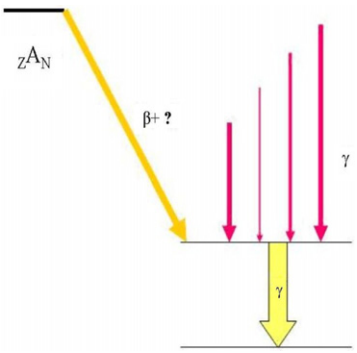

Fig. 12. Feeding of a typical level in the daughter nucleus in a hypothetical β decay (see text).

species can be measured at the same time. Instead one tries to take advantage of the fact that one ends up with a "cocktail" beam; a mixture of nuclear species lying close together in A and Z. In the subsequent off-line analysis, the ions can be identified on an individual basis from the measurements of the $B\rho$ of the ion in the separator magnets, the time-of-flight (TOF) and the ΔE. The signal induced by the implantation of the incoming ion defines $t = 0$ for the subsequent decay of the ion. The time of decay is then determined by the subsequent detection of the βs emitted in the decay and observed in the same or a neighbouring pixel. Other radiations such as γs, neutrons or protons can be recorded in coincidence with the β signal. In the analysis, the time correlation between an implant and a decay is sought over a reasonable time interval, usually at least several times longer than the half-life in question.

In ideal conditions, where the total implantation rate per pixel is low and the half-lives are short, the association between the implant and subsequent decay can be reasonably good. However in real conditions random coincidences are often the main source of error. To avoid systematic errors, it is important to have a clear definition of the randoms. One method is to associate each decay not with the previous implant as one might do intuitively (which will deform the decay curve towards shorter half-lives) but with the previous implant and several implants before. This ensures that the real correlation is included for every decay but at the expense of a high background due to the randoms. The corresponding advantage is that the background is made up of uncorrelated events and therefore can be defined by some other means. Several examples of this kind of analysis, where the resulting background is flat, can be seen in [58].

Another difficulty arises when the production method includes a time structure which affects the definition of the random background. One example of how to deal with this situation can be seen in [64]. Another example will be presented in Section 7. In studies of the nuclei farthest from stability, where the production rate is small, the number of ions observed can be small. In this case one has to extract the half-life using the maximum likelihood method. The application to rare β decays is given in [65].

4.3. Determination of β feeding and the Pandemonium effect

Even if the number of branches in a β decay to states in the final nucleus is small, it is difficult to disentangle the different components in the β-ray spectrum and thus to determine the β feedings. Instead we are compelled to deduce it from measurements on β-delayed radiation.

The simplest and most common approach is to measure the spectrum of β-delayed γ transitions using a set or array of Ge γ-ray spectrometers. They have the advantage of good energy resolution and are not disturbed by Doppler effects in this application since the sources are stationary. In practice, decay schemes are first established on the basis of γ–γ coincidences, then one can deduce the feeding to a level in the daughter nucleus from the difference between the total intensities of the feeding and de-exciting transitions. It turns out, however, that this simple prescription for experiment has a flaw in it. Although Ge detectors are well suited to determining decay schemes, they have only modest efficiency for detecting high energy γ rays; they have, in the best case, efficiencies of about 20% for γ rays of 1332 keV energy, and much lower efficiencies for higher energy γ rays.

In order to illustrate this flaw, we assume a hypothetical, simple decay scheme shown in Fig. 12. The level in the daughter nucleus is fed directly by a β transition and indirectly by γ transitions from above. If many weak high energy γ rays are not observed due to the lower efficiency of Ge detectors, their strengths may add up to a significantly large value. We may get an incorrect result for the β feeding and hence the $\log ft$ values. In other words, by the use of γ-ray detectors of limited efficiency, we are unable to extract reliable β feedings and $\log ft$ values. This problem will, in general, be exacerbated as we move away from stability. Here Q_β-values will increase with a resulting increase in the fragmentation of the β feeding because the level density increases rapidly with increasing excitation energy. This will, in general, result in a reduction in the average γ-ray intensity and fewer γ transitions will be observed. There will also be more feeding of levels at higher energies, which will be de-excited by higher energy γ rays on average and the efficiency for detecting them is lower. In addition, the effect is more serious in heavier nuclei where the level density is higher. Hardy et al. [66] recognised this difficulty and named it the "Pandemonium effect" [67].

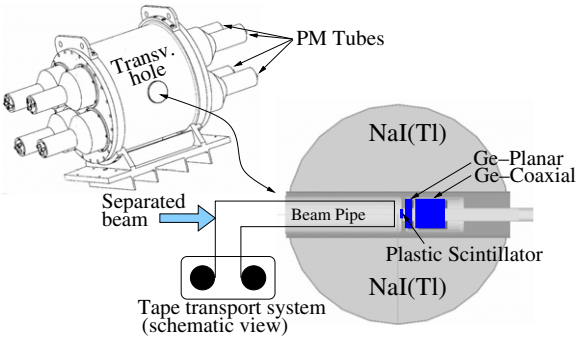

Fig. 13. A typical schematic setup of a Total Absorption Spectrometer such as Lucrecia [68] at an ISOL facility. The cylindrical NaI(Tl) scintillator, shown on the upper left, has a transverse hole in the centre. The beam pipe is inserted into one side of this hole. As we see in the lower part of the figure, the mass separated beam is directed onto a tape at the collection point. The tape is then moved at suitable intervals to carry the source into the centre of the NaI detector. If a study of a very short-lived activity is needed, it is possible to deposit the activity directly in the centre of the TAS. Additional detectors, such as a plastic scintillator to detect β particles and/or a Ge detector telescope to detect X rays and γ rays, can then be inserted into the transverse hole from the opposite side.

In order to overcome this difficulty of determining the β feeding strength from the delayed-γ measurements, one can use the Total Absorption Gamma Spectroscopy (TAS) method. The ideal γ-ray spectrometer used in this method is a 4π detector with 100% detection efficiency for all γ rays. In the resulting γ-decay energy spectrum, one would then observe the summed energy from all the γ rays in the cascade that de-excite the level fed by the β decay. Thus the population of the levels is observed directly. An ideal TAS is impossible to construct, but several of them are now available with sufficiently high efficiency to make the method work [68,69]. Fig. 13 shows schematically a typical experimental setup for measurements with such a device. An experiment using this setup is described later in Section 4.3.

The analysis of the data from these devices is not trivial. The relationship between the β feeding $I(E_j)$ of a jth state at $E_x = E_j$ in the final (daughter) nucleus and the data d_i measured in channel i in the TAS spectrum is given by

$$d_i = \sum_{j=1}^{j_{\max}} R_{ij} I(E_j), \tag{29}$$

where R_{ij}, the response function, is the probability showing how many counts are expected in the ith channel of the TAS spectrum for the unit feeding of the state at E_j. To determine R_{ij} we need to know how the TAS spectrometer responds to individual γ rays and also β particles as a function of their energy. One also requires a knowledge of the branching ratios for the γ transitions de-exciting the levels. To determine the β feeding we must solve the inverse problem represented by Eq. (29). This equation falls into the category of ill-posed problems and their solution is neither trivial nor straightforward. However Tain and Cano-Ott have found how to optimise the solutions [70,71].

In the analysis, which proceeds as an iterative process, a set of $I(E_j)$ values that can best reproduce the measured TAS spectrum is sought. In the process, a precise decay Q-value is needed to determine the energy distribution of β particles. It is also necessary to have a knowledge of the γ-decay branching ratios of the levels or make a plausible assumption about them. Thus the methods must be applied with due care and attention to the individual case under study. Examples of the use of the TAS method will be given in Sections 4.4 and 10.3.

4.4. Measurement of nuclear shapes in β decay

The shape of the nucleus is one of the simplest of its macroscopic nuclear properties to visualise, but it turns out to be difficult to measure. The shapes of the nuclei with $A \approx 70$–80 and $N \simeq Z$ are of special interest because of the symmetry associated with the neutrons and protons filling the same orbits. This, together with a low single-particle level density, means that one finds rapid changes in deformation with the addition or subtraction of only a few nucleons. One finds the co-existence [72,73] of states of quite different shapes in these nuclei e.g. in the Se and Kr nuclei [74,75]. Shape co-existence is also predicted for the lightest Sr nuclei.

There are a number of methods of measuring the g.s deformation in unstable nuclei based on the interaction of the electric quadrupole moment of the nucleus with an external electric field gradient [76–78]. These methods do not apply to nuclei with $J = 0$ or $1/2$, because they do not have a spectroscopic electric quadrupole moment. In addition, to distinguish between oblate and prolate shapes, the sign of the quadrupole moment should be determined, but this is not easy.

We introduce here a way of deducing the shape of the g.s of the initial (mother) nucleus by the accurate study of the GT strength [B(GT)] distribution as a function of E_x in the final (daughter) nucleus. The idea was first put forward by Hamamoto et al. [79] and then pursued in more detail by Sarriguren et al. [80]. In the latter case they begin by looking for local minima in the potential energy surface. Because of the shape co-existence, they found two minima which, depending on the case, may be spherical, prolate or oblate. They then calculate the B(GT) distribution assuming these deformations. In some cases

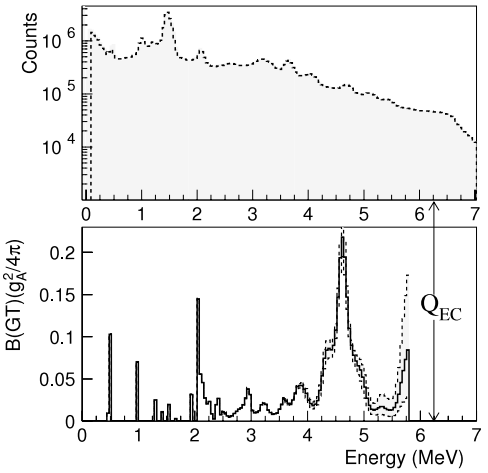

Fig. 14. Singles spectrum of ^{76}Sr decay overlaid with the spectrum recalculated (dashed line) after analysis (upper panel) [81] and the B(GT) distribution extracted from these data as a function of excitation energy in the daughter nucleus (lower panel). The dashed lines indicate the experimental uncertainty. Note that the uncertainty increases rapidly near the Q-value because of the smaller phase-space factor (f-factor).

they find that the calculated distributions differ markedly within the Q_β-window depending on the shape of the g.s of the parent nucleus.

A number of cases have been studied with the TAS spectrometer "Lucrecia" at CERN-ISOLDE [68]. The example here is of the even–even nucleus ^{76}Sr [81], where the g.s is amongst the most deformed known, based on the measurement [82] of the energy of the first excited 2^+ state and Grodzin's formula [83], an empirical relationship between the deformation and the energy of the $2^+ \rightarrow 0^+$ transition. This tells us, however, nothing about the sign of the deformation.

The CERN-ISOLDE facility provides, at present, the most intense, mass separated, low energy beams of neutron-deficient Sr nuclei. The ^{76}Sr beam with a half-life of just 8.9 s was collected on a tape and transported to the centre of the spectrometer Lucrecia where the delayed γ cascades were measured. In the final nucleus ^{76}Rb, the proton separation energy (S_p) is 3.5 MeV. As a result β-delayed proton emission has been observed in the region with $E_x = 4.8$–5.8 MeV [84]. However, this contribution was as small as 2% in B(GT), i.e., very small compared to the decay via β-delayed γ rays. The details of the measurement are given in [81].

The analysis of the TAS spectrum was carried out following the methods described in [70,71]. The shaded area in the upper part of Fig. 14 shows the experimental total absorption spectrum of the β decay of ^{76}Sr. The dashed line indicates the recalculated spectrum after the analysis. This spectrum extends beyond the ^{76}Sr Q-value because of the daughter activity and pile-up [85]. In the lower panel, we see the B(GT) distribution derived from this spectrum with the dashed lines indicating the experimental uncertainty. The marked strength at 0.5, 1.0 and 2.1 MeV is to states already known [86], but the B(GT) values reported were larger than the values obtained from the TAS measurements as a result of the "Pandemonium" effect described above.

The theoretical derivation [80] of the B(GT) distribution started with the construction of the self-consistent quasi-particle basis from a deformed Hartree–Fock (HF) calculation using density dependent Skyrme forces and pairing correlations in the BCS framework. From the minima in the total HF energy versus deformation plot Sarriguren et al. deduced the possible g.s deformations. In the case of ^{76}Sr two minima were found; one is prolate with $\beta_2 = 0.41$, the other is oblate with $\beta_2 = -0.13$. Using these results the quasi-random-phase approximation (QRPA) equations were solved with a separable residual interaction derived from the same Skyrme force used in the HF calculation. To calculate the B(GT), it was assumed that the states populated in the final nucleus have the same deformation as the initial state. Fig. 15 shows the cumulative sum of B(GT) strengths calculated with the SK3 force, where results for both prolate and oblate cases are shown. It also shows the experimental cumulative sum of B(GT) values. The shading indicates the experimental uncertainty. As we see, the experimental result agrees well with the calculation assuming the prolate shape over the energy range of 0.5–6 MeV, but not with the calculation assuming the oblate shape. Thus our results confirm the large deformation, deduced from the in-beam γ spectroscopy [82] and provide the first experimental evidence that the deformation is of prolate character.

The result also indicates that this method of determining the g.s deformation works. This method was also applied to the case of ^{74}Kr [87], where earlier measurements [88] of the decay of the isomeric, first excited 0^+ state had indicated strong mixing of the oblate and prolate shapes. Again the TAS measurements were made at CERN-ISOLDE. Fig. 16 shows the cumulative sum of B(GT) as a function of E_x for both theory and experiment for this case. The form of the cumulative sum as a function of energy reflects the fact that the B(GT) strength is in this case smoothly distributed across the Q-window, as can be seen in Fig. 4 of Ref. [87]. This time the experimental results are not fitted by the calculations for a prolate or oblate g.s. The results show that it is likely that there is a mixture of prolate and oblate shapes in the ^{74}Kr g.s. This is confirmed by the Coulomb excitation of a beam of ^{74}Kr [89]. We note that this method relies not just on an accurate measurement of the B(GT) distribution in the Q-window but also on a correct description of the wave function of the parent state. Although the

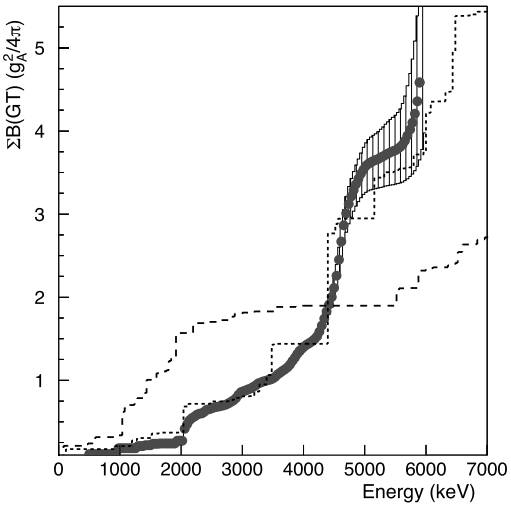

Fig. 15. The cumulative sum of the measured B(GT) as a function of the excitation energy in the final nucleus for the decay of ^{76}Sr. It is compared with the theoretical distributions for oblate and prolate shapes [81].

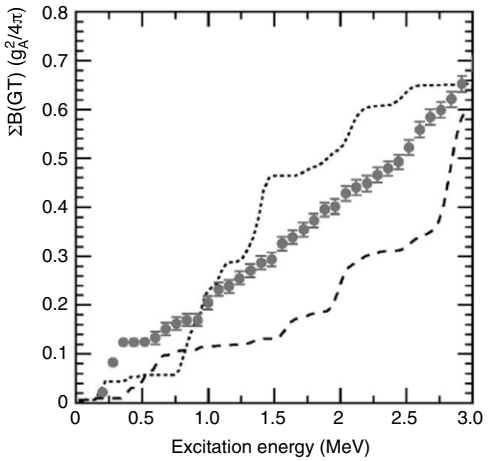

Fig. 16. As in Fig. 15, but with the corresponding data for ^{74}Kr [87]. The solid points represent experiment. The dotted and dashed lines are the theoretical distributions for oblate and prolate shapes.

two cases presented here look convincing, more cases are needed in order to fully establish the method. A number of other cases in this mass region as well as cases with $A \sim 190$ are already under study.

5. Charge-exchange reactions

In contrast to β decay, which suffers from the Q-value limitation, charge-exchange (CE) reactions, such as (p, n), (n, p), $(d, {}^2\mathrm{He})$, $({}^3\mathrm{He}, t)$ or $(t, {}^3\mathrm{He})$ reactions, can be used to study GT transitions leading to higher excited states.

In CE reactions, including $({}^3\mathrm{He}, t)$ reactions, it is known that GT excitations become prominent at intermediate energies ($\geq$100 MeV/nucleon) and at forward angles including 0°, where a small angular momentum transfer is realised. This is because of the $\Delta L = 0$ nature of GT excitations and the dominance of the $\sigma\tau$ part of the effective nucleon–nucleon interaction at small momentum transfer including $q = 0$ [1,37].

5.1. Various charge-exchange reactions

Charge-exchange reactions can be categorised into β^- type [(p, n)-like reactions] and β^+ type [(n, p)-like reactions]. Various combinations of projectiles and ejectiles are possible [90]. However, the preferred combinations are those with the following properties; (1) projectile at least has a relatively long lifetime, (2) the ejectile has a simple structure, i.e., there is no (or at most one) particle-stable excited state, and (3) the combination of the j^π values of the projectile and the ejectile

Table 2
Properties of the representative β^--type charge-exchange reactions which decrease T_z of the target nucleus by one unit. All of these reactions are endothermic. The reaction Q-values to transform projectiles into ejectiles (Q_{pe}) are given in units of MeV. The J^π values of the projectile (J_p^π) and the ejectile (J_e^π), spin transfer ΔS and the associated B(F) and B(GT) values of the projectile–ejectile sector are listed. The B(GT) values are calculated from the logft values [92] using Eq. (26) or Eq. (27) given in Section 4 and correcting the geometrical factors associated with reversed direction of transitions (see Eq. (3)).

β^- type	Q_{pe}	J_p^π	J_e^π	ΔS	B(F)	B(GT)
(p, n)	−0.782	$1/2^+$	$1/2^+$	0, 1	1.0	3.049(11)
(^{3}He, t)	−0.019	$1/2^+$	$1/2^+$	0, 1	1.0	3.02(−)
(^{6}Li, ^{6}He)	−3.508	1^+	0^+	1	0	1.577(5)
(^{12}C, ^{12}B)	−13.369	0^+	1^+	1	0	0.982(6)

Table 3
Properties of the representative β^+-type charge-exchange reactions that increase T_z of the target nucleus by one unit. The (n, p) and $(t, ^3\text{He})$ reactions are exothermic. The reaction Q values to transform projectiles into ejectiles (Q_{pe}) are given in units of MeV. The J^π values of the projectile (J_p^π) and the ejectile (J_e^π), spin transfer ΔS and associated B(F) and B(GT) values of the projectile–ejectile sector are listed. The B(GT) values are calculated from the logft values [92] using Eq. (26) or Eq. (27) given in Section 4 and correcting the geometrical factors associated with reversed direction of transitions (see Eq. (3)).

β^+ type	Q_{pe}	J_p^π	J_e^π	ΔS	B(F)	B(GT)
(n, p)	0.782	$1/2^+$	$1/2^+$	0, 1	1.0	3.049(11)
(d, ^{2}He)	≈ − 1.5	1^+	0^+	1	0	≈3[a]
(t, ^{3}He)	0.019	$1/2^+$	$1/2^+$	0, 1	1.0	3.02(−)
(^{7}Li, ^{7}Be^0)[b]	−0.862	$3/2^-$	$3/2^-$	0, 1	1.0	1.189(5)
(^{7}Li, ^{7}Be^1)[c]	−1.291	$3/2^-$	$1/2^-$	1	0	1.059(5)
(^{12}C, ^{12}N)	−17.338	0^+	1^+	1	0	0.871(6)

[a] From [90].
[b] ^{7}Be is in the ground state.
[c] ^{7}Be is in the first excited state at 0.429 MeV.

allows spin excitations. In addition, it is better if (4) the energy difference of the ejectile and the projectile (Q_{pe} value) is small. A larger Q_{pe} value will make the momentum transfer and hence the angular momentum transfer larger.

In addition to the (p, n) reaction, (^{3}He, t), (^{6}Li, ^{6}He), and (^{12}C, ^{12}B) reactions are the typical β^--type reactions. These reactions at 0° are good tools to study GT excitations in the neighbouring nuclei richer in protons. In these reactions, all the ejectiles are unstable against β decay. However, they all have rather long half-lives, and thus the effects from the reduction in the number of ejectiles reaching the detectors, or the background caused by the β^- decay of the ejectile are usually small. It should be noted that both Fermi (no spin-flip) and GT (spin-flip) transitions are caused by the (p, n) and (^{3}He, t) reactions, because both projectiles and ejectiles have J^π values of $1/2^+$ in these reactions. On the other hand, only GT transitions are induced by the (^{6}Li, ^{6}He), and (^{12}C, ^{12}B) reactions, because either the projectile or ejectile has $J^\pi = 1^+$ and the other has 0^+. The sensitivity (or the excitation strength) for the GT excitations is proportional to the "B(GT) value associated with the transformation of the projectile to ejectile" [91]. This can be seen from the B(GT) values associated with each of these reactions, which were derived from the β-decay study of the ejectiles and are listed in Table 2.

The (n, p) reaction is the representative β^+-type reaction. The other reactions used are (d, ^{2}He), (t, ^{3}He), (^{7}Li, ^{7}Be), and (^{12}C, ^{12}N), where ^{2}He is actually the two protons emitted in the narrow cone that form the "S-wave" ($\Delta L = 0$) correlation [90]. The $J^\pi = 1/2^-$ first excited state of ^{7}Be, in addition to the $3/2^-$ g.s, is particle bound, and it decays by the emission of a 0.429 MeV γ ray. In the transition from the $J^\pi = 3/2^-$ g.s of ^{7}Li, the (^{7}Li, ^{7}Be) reaction can selectively excite the spin-flip excitations if the first excited state of ^{7}Be is excited. On the other hand, the g.s→g.s transitions excite both the spin-flip and non-spin-flip excitations. Therefore, by measuring particle-γ-ray coincidences, it is possible to extract spin excitations. The properties of these reactions are summarised in Table 3.

5.2. Realisation of high energy resolution in (^{3}He, t) measurements

At the high energy resolution facility of RCNP, Osaka, consisting of the RCNP Ring cyclotron [93], a high dispersion beam line "WS course" [94] and a high resolution magnetic spectrometer "Grand Raiden" [95], precise beam matching techniques were fully applied [96–98] for the β^--type (^{3}He, t) CE reaction at an intermediate beam energy of 140 MeV/nucleon (see Fig. 17).

The introduction of magnetic spectrometers for the analysis of nuclear reaction products can open a new dimension in nuclear structure studies [95,99–104]. As the beam energy (momentum) of an accelerator increases, however, the energy (momentum) spread of the beam usually increases. It is clear that at higher energies the large momentum spread Δp of the beam can severely limit the resolution of momentum spectra measured with magnetic spectrometers. In order to use the full potential of a high resolution spectrometer, i.e. to derive a good quality spectrum from the measurements in the focal plane detectors, it is, therefore, important to match the beam characteristics at the target location to those of the spectrometer and to compensate for the deterioration from large Δp. The importance of beam matching was pointed out

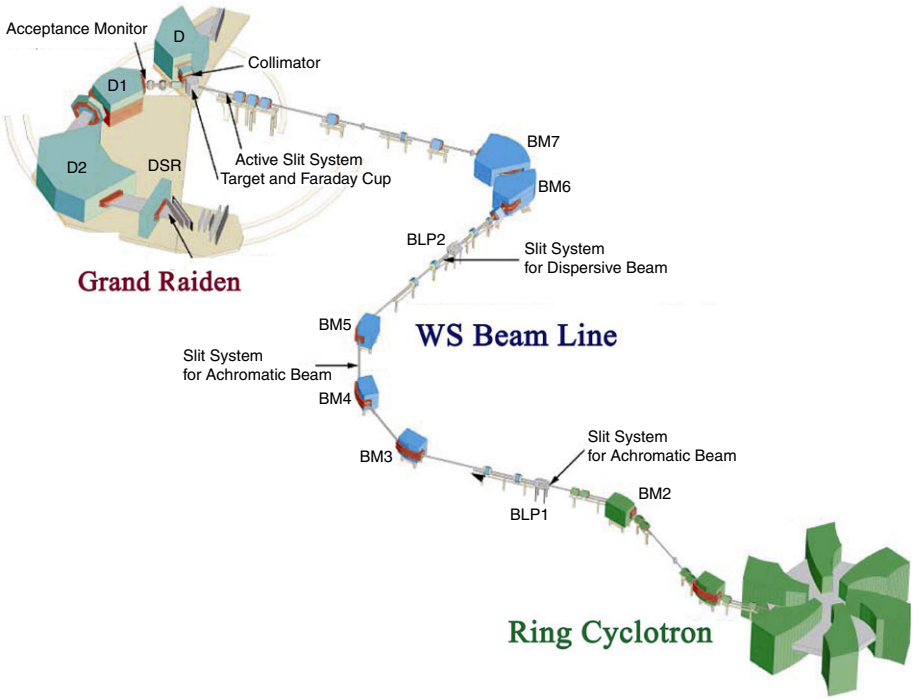

Fig. 17. A schematic view of the high energy resolution facility of RCNP, Osaka, consisting of the RCNP Ring cyclotron [93], a high dispersion beam line "WS course" [94] and a high resolution magnetic spectrometer "Grand Raiden" [95] having a mean orbit radius of 3 m and a planned momentum resolving power of 3.7×10^4. For the detailed properties, see text.

already 40 years ago [105,106]. The matching conditions *kinematic correction* (or *kinematic displacement*), *lateral dispersion matching* (or *dispersion matching* as it is usually called), *focus matching* (also called *kinematic defocusing*) and experimental procedures have been discussed in several papers [100,107,108].

Under the condition of *lateral dispersion matching*, the beam with momentum spread Δp has a finite size at the target. The beam size of the matched beam with finite energy (momentum) spread increases with the dispersion and therefore with the resolving power of the spectrometer. The spectrometer Grand Raiden has a momentum dispersion 15.45 m (15.45 cm/%) and an image magnification −0.417. Therefore, a momentum dispersion of 37.1 (=15.45/0.417) m (37.1 cm/%) is needed for the beam line [96]. This large dispersion results in a beam size of about 10 mm in the dispersive direction at the target position of the spectrometer in the (^{3}He, t) reaction at 140 MeV/nucleon, even if the energy resolution of the beam itself is as good as e.g. 140 keV ($\Delta E/E = 3 \times 10^{-4}$ or $\Delta p/p = 1.5 \times 10^{-4}$). Therefore, a high resolution spectrometer, such as Grand Raiden, suffers from a large ambiguity in determining the scattering angle due to the required large beam size needed for the realisation of the *lateral dispersion matching*. This effect can be minimised by *angular dispersion matching*. The detail of the ion optics involved is described in [96] and the essential points are discussed in Section 5.2.1. The "WS course" at RCNP shown in Fig. 17 was proposed [96] and constructed [94] as the first beam line that realises all of these conditions.

As a result, in comparison with the pioneering (p, n) work [4], nearly one order-of-magnitude better resolution ($\Delta E \leq$ 30 keV) has been achieved. Fig. 18 shows spectra from β^--type CE reactions at different resolutions. This significant improvement in the energy resolution achieved in the past twenty years is clearly seen. With higher energy resolution, fine structures have been observed even in the so-called GT resonance (GTR) region of E_x = 7–12 MeV. We recognise that the GTR in ^{58}Cu, which was observed as a bump-like structure [4], actually consists of many individual states on a smooth continuum [24].

The high energy resolution in these spectra makes it possible to study transition strengths for individual GT states. Under the concept of "isospin symmetry" described below, these strengths can be compared directly with those of analogous transitions studied by IE reaction and γ decay as well as by mirror β^+ decays.

5.2.1. Beam matching techniques

In order to realise the full potential of a high resolution spectrometer, the beam characteristics at the target location are of great importance. In order to achieve both good energy and angular resolution, it is important to realise "*matching conditions*" between the beam line and spectrometer. They were fully formulated for the first time in [96].

The ion-optical concepts of the matching conditions are illustrated in Fig. 19 for elastic scattering at 0° (small momentum transfer q) assuming a beam with small emittance. Fig. 19(a) shows the beam making an achromatic focus at the target position. Particle rays (beams) with different Δp values are "momentum analysed" by the large dispersion of a spectrometer

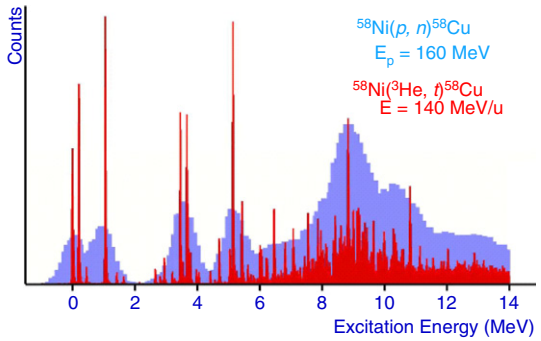

Fig. 18. Energy spectra of charge-exchange reactions at 0°. The broad spectrum is from ^{58}Ni(p, n)^{58}Cu reaction measurements in the 1980s [109]. In the recent ^{58}Ni(^{3}He, t)^{58}Cu reaction study [24], fine structure and sharp states have been observed up to an excitation energy of 13 MeV. The proton separation energy (S_p) is 2.87 MeV. An increase in the continuum background is observed above $E_x = 6$ MeV.

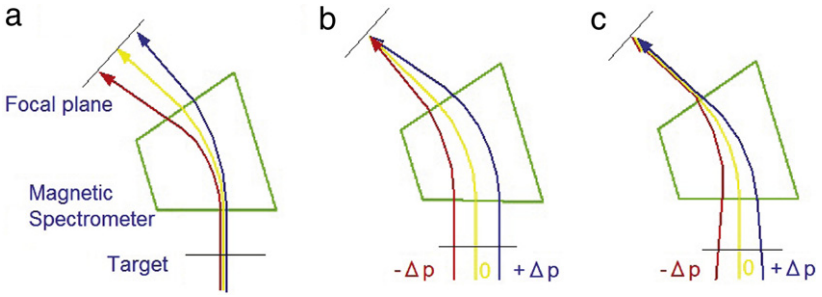

Fig. 19. Ion trajectories under different matching conditions of beam line and magnetic spectrometer: (a) when achromatic beam transportation (B.T.) is used; (b) when *dispersion matching* is realised in B.T.; (c) when both *dispersion matching* and *angular dispersion matching* are realised. The lines represent particle rays with different Δp values within a beam. For the details, see text.

and they spread spatially in the focal plane depending on the Δp value of the beam. Therefore, the resolution achieved in the spectrometer using achromatic beam transportation can never exceed the resolution determined by the spread of the beam momentum.

In order to achieve a resolution better than the momentum (energy) spread of the beam, it is necessary to realise a condition called *dispersion matching* shown in Fig. 19(b). Particle rays with different Δp values are focused at different positions on the target (dispersive monochromatic focus). The dispersion of the beam at the target is compensated by the dispersion of the spectrometer and the achromatic focus is realised in the focal plane of the spectrometer. The achievable resolution, therefore, is not affected to first order by the momentum spread of the beam.

This idea of "compensation of dispersion" can be understood in analogy with how white light with various colour components behaves in an optical system. If we think only of the focussing in the horizontal direction, a spectrometer can be represented by a magnet, which has the function of a convex lens and prism. A convex lens makes an inverted image of the source. A prism creates dispersion depending on the frequency of the light, which corresponds to the fact that the amount of bending (or the bending radius) of the beam in the magnet is dependent on the momentum of the beam. As shown in Fig. 19(b), let us think of displacing a beam with $p_0 + \Delta p$ slightly to the right of the beam with p_0, the reference beam, at the target position (source position). Due to the function of the convex lens of the magnet, the $p_0 + \Delta p$ beam is expected to arrive at the position slightly to the left of the reference beam in the focal plane (image position). However, owing to the higher momentum of this beam, it bends less. Therefore, if the amount of the displacement of the $p_0 + \Delta p$ beam at the target position is adjusted so as to make these two effects compensate each other, then we can get rid of the spacial spreading of the beam depending on the beam momentum.

Under this condition, however, rays with different Δp cross the focal plane at different angles θ_{pf}, which means that the angle measurements then have an ambiguity. Accurate angle measurements also become possible by adjusting the incident angles of rays with different Δp values, i.e., by realising *angular dispersion matching* as well (see Fig. 19(c)).

5.3. Proportionality relationship

Owing to the simple reaction mechanism of the CE reactions performed at intermediate beam energies ($E > 100$ MeV/nucleon) and angles close to 0° (to be more precise, at zero momentum transfer $q = 0$), it was found that the differential cross-sections for GT transitions are approximately proportional to their B(GT) values. The close proportionality was first noticed in (p, n) reactions at the incident energies of $E_p = 120$–200 MeV and at 0° performed at IUCF, Indiana

[10,110,111], which makes CE reactions, including the (^{3}He, t) reaction at 140 MeV/nucleon, useful probes for the study of GT transition strengths.

For specific mass A nuclei at a given incoming beam energy, the proportionality in the 0° measurement with small momentum transfer is given by

$$\frac{d\sigma_{GT}}{d\Omega}(q,\omega) \simeq K(\omega)N_{\sigma\tau}|J_{\sigma\tau}(q)|^2 B(GT) \tag{30}$$

$$= \hat{\sigma}_{GT}(q,\omega)B(GT), \tag{31}$$

where $J_{\sigma\tau}(q)$ is the volume integral of the effective interaction $V_{\sigma\tau}$ at momentum transfer q, $K(\omega)$ is the kinematic factor and $\omega = E_x - Q_{g.s-g.s}$, i.e., the total excitation energy of the final nuclear state, $N_{\sigma\tau}$ is a distortion factor, and $\hat{\sigma}_{GT}(q,\omega)$ is a unit (differential) cross-section for the GT transition [$\hat{\sigma}_{GT}(q,\omega)$ is given in units of mb/sr]. Therefore, if "a standard B(GT) value" is obtained for some GT transition in the mass A system from a β-decay study that can give an absolute B(GT) value, the unit cross-section can be determined. Then, the B(GT) values can also be derived even for transitions to higher excited states by using this close proportionality. It should be noted that Eq. (31) is exact only if (a) the reaction mechanism is simple enough that the impulse approximation can be applied, and (b) no interaction other than $V_{\sigma\tau}$ is active in the so-called 0° measurement. In reality, as will be discussed, these assumptions are not always valid.

The unit cross-section $\hat{\sigma}_{GT}(q,\omega)$ in Eq. (31) is a smooth function of the momentum transfer q and the energy loss ω. Note that the transferred momentum increases with ω even in the measurements at 0°. In the (^{3}He, t) reaction, due to the momentum mismatch between the incoming ^{3}He beam and the outgoing triton, $\hat{\sigma}_{GT}(q,\omega)$ usually decreases when E_x increases. A distorted wave Born approximation (DWBA) calculation can be used to estimate this kinematic effect (for details, see e.g. [112]). The result shows that $\hat{\sigma}_{GT}(q,\omega)$ decreases by about 5%–12% when E_x increases from 0 to 10 MeV. The amount of decrease depends on mass number A and $Q_{g.s-g.s}$, but it is rather insensitive to the specific configurations of the initial and final wave functions used in the calculation (less than a few %).

The close proportionality in a mass A system given by Eq. (31) was examined by comparing the GT transition strengths observed in the (^{3}He, t) measurements with those from mirror β^+ decays for a number of cases in which multiple pairs of analogous transitions can be compared. Such comparisons could be made for the $T = 1/2$ and 1 nuclear systems in the sd-shell region. Due to the high energy resolution achieved in the (^{3}He, t) reaction, a one-to-one comparison of the strengths of the analogous GT transitions could be made. In the $T = 1$ system, strengths were examined for analogous GT transitions starting from the g.s of the $T_z = \pm 1, A = 26$ nuclei (^{26}Mg and ^{26}Si) to the $T_z = 0$ nucleus ^{26}Al [113,112]. The isospin symmetry structure and analogous transitions for the $T = 1, A = 26$ isobaric system are shown schematically in Fig. 6. The thick arrows show pairs of analogous transitions that can be studied by the (^{3}He, t) reaction and the β^+ decay. In the $T = 1/2$ system, the proportionality was examined for the GT transitions starting from the ground states of $T_z = \pm 1/2$ mirror nuclei with $A = 27$ (^{27}Al and ^{27}Si) [43] and $A = 23$ (^{23}Na and ^{23}Mg) [114]. As a result, a proportionality within 5% has been seen in general for transitions of $\Delta L = 0$ nature and for B(GT) values larger than ≈0.04.

However, there is not always a guarantee of such good proportionality. In a naive picture, β decay and CE reactions have different sensitivities to the initial and final wave functions, i.e., CE reactions are sensitive to the surface part of the radial wave function, while β decay can occur at any point in the nucleus. The allowed GT transitions have $\Delta L = 0$, $\Delta S = 1$, $\Delta T = 1$ and thus $\Delta J = 1$. They are caused purely by the $\sigma\tau$-type interaction in β decays. In the CE reactions mediated by the "strong interaction", however, the amount of momentum transfer q is finite even in the measurement at 0° due to the finite negative Q-value of the reaction. Therefore, not only the $\sigma\tau$, but also the non-central isovector–tensor ($T\tau$) interaction (behaving like $\Delta L = 2$, $\Delta S = 1$, $\Delta T = 1$ and thus $\Delta J = 1$) can contribute. In addition, the simple "one-step" process of converting proton ↔ neutron (or u quark ↔ d quark) is guaranteed in the β decay, but more complicated "two-step" and higher order processes can also contribute in CE reactions. Thus the proportionality cannot always be guaranteed.

Exceptionally large deviations from the proportionality mentioned above were observed in some specific (and relatively weak) transitions. In the ^{34}Ar β decay to the second 1^+ state at 0.67 MeV in ^{34}Cl, a B(GT) value of 0.06 was obtained. On the other hand, in the ^{34}S(^{3}He, t)^{34}Cl reaction, the B(GT) value calculated from the good proportionality observed for strong transitions was 0.09. In order to understand such variations from proportionality, a DWBA calculation taking into account the various types of interaction is useful. DWBA analyses performed using the transition matrix elements from a shell-model calculation suggested that the contribution of the Tensor interaction is responsible for the observed differences for $A = 34$ [31]. Another example is the strength of the g.s–g.s transition between ^{58}Ni and ^{58}Cu. In the β decay of the $J^\pi = 1^+$ g.s of ^{58}Cu, a B(GT) value of 0.15 is obtained, while a DWBA calculation suggested that 20% larger strength is observed in the (^{3}He, t) reaction, again due to the Tensor contribution [115]. The common feature of these cases is that two (or more) different major $\Delta L = 0$-type s.p transitions, each of them having a large $\sigma\tau$ matrix element (e.g. $\langle d_{5/2}|\sigma\tau|d_{5/2}\rangle$ and $\langle d_{3/2}|\sigma\tau|d_{5/2}\rangle$), contribute destructively to the GT transition strength. Then, the contribution of the $\Delta L = 2$-type s.p transitions activated by the $T\tau$ (and/or the IV $\Delta L = 2$ spin) interaction becomes relatively important. Even though the contributions on their own may be small, they can play a larger role by causing constructive (or destructive) interference with the major s.p matrix elements induced by the $\sigma\tau$ interaction [31].

In addition, deviations from the proportionality (enhancement of ≈20%) were reported in (p, n) reactions performed at different incoming energies for relatively weak GT transitions involving the so-called $j_<$ ($=\ell - 1/2$) → $j_<$ s.p transitions [116,117]. Examples are the ^{35}Cl(p, n)^{35}Ar and ^{39}K(p, n)^{39}Ca g.s → g.s transition for the $d_{3/2}$ → $d_{3/2}$ s.p

transition, and the ^{13}C$(p, n)^{13}$N g.s $\rightarrow$ g.s transition for the $p_{1/2} \rightarrow p_{1/2}$ s.p transition. The same enhancement was observed in the ^{13}C(^{3}He, t)^{13}N reaction. The DWBA analysis for this reaction suggested that the $T\tau$ component is also responsible for the enhancement of these $j_< (=\ell - 1/2) \rightarrow j_<$ transitions [118].

In spite of these exceptions we can, in general, believe in the proportionality as a good way to deduce the relative values of the GT transition strength B(GT). Furthermore, if the unit GT cross-section $\hat{\sigma}_{\rm GT}$ for a specific A system can be determined, especially using the β-decay B(GT) values, reliable GT strengths can be obtained for the transitions to highly excited states.

A method using the absolute (^{3}He, t) cross-sections as a means to determine absolute B(GT) values has also been proposed [119]. It was suggested that the mass dependence of the unit GT cross-section at $q = \omega = 0$ can be expressed as $\hat{\sigma}_{\rm GT} = 109/A^{0.65}$ mb/sr.

As we have seen in Fig. 2 and will be shown in Section 8, spin-$M1$ ($M1_\sigma$) excitations that are analogous to the GT excitations can be clearly observed by using (p, p') reactions performed at intermediate beam energies ($E > 100$ MeV/nucleon) and angles close to 0°. If contributions from the minor isoscalar term (σ term) of the effective nuclear interaction and the exchange reaction process are small, a proportionality similar to Eq. (31) is expected in the measurements using proton IE scattering. The close proportionality is given by

$$\frac{{\rm d}\sigma_{M1\sigma}}{{\rm d}\Omega}(q, \omega) \simeq K(\omega) N_{\sigma\tau} |J_{\sigma\tau}(q)|^2 B(M1_\sigma) \tag{32}$$

$$= \hat{\sigma}_{M1\sigma}(q, \omega) B(M1_\sigma), \tag{33}$$

where $\hat{\sigma}_{M1\sigma}(q, \omega)$ is a unit cross-section for the $M1_\sigma$ transition. Owing to the close proportionality in both (^{3}He, t) and (p, p') reactions, it is expected that the analogue states are excited with corresponding strengths.

6. Gamow–Teller response functions for *p* and *sd*-shell Nuclei

It is expected that the strength distributions of GT transitions vary considerably reflecting the structures of initial and final nuclei. Here we show high energy resolution (^{3}He, t) spectra obtained on various p- and sd-shell nuclei at 0° and the intermediate energy of 140 MeV/nucleon, where the reaction mechanism is mainly one step. As mentioned earlier, at 0° the dominant excitations are $\Delta L = 0$ transitions. Therefore, in the region of $E_x \leq 20$ MeV, where the main part of the "structured" GT strengths are expected, all $\Delta L = 0$ transitions, except for the excitation of the IAS caused by the τ-type Fermi operator, are GT excitations caused by the $\sigma\tau$ operator. In addition, due to the proportionality, the 0° spectra provide us with a good empirical representation of the GT strength functions.

6.1. Gamow–Teller transitions in $T = 1/2$ mirror p-shell nuclei

We consider here the GT and Fermi transition strengths starting from the g.s of the $T_z = 1/2$, ^{7}Li, ^{9}Be and ^{11}B target nuclei to the g.s and the excited GT states in the $T_z = -1/2$ mirror nuclei, ^{7}Be, ^{9}B and ^{11}C, respectively. Due to the low level density, we can observe the GT states in p-shell nuclei as individual states. However, when these states are situated above the particle separation energies (either S_p or S_α), they can have a particle decay width, and if we can measure these widths we can, as we will see below, extract information about their structure. In addition, it is known that some states in these nuclei have cluster structures. We will find that the transition strengths in these nuclei are strongly related to the cluster structure.

6.1.1. Gamow–Teller transitions in $A = 7$ nuclei

The main feature of the 0°, ^{7}Li(^{3}He, t)^{7}Be spectrum shown in Fig. 20(a) is the excitation of the two low-lying states. They are the $J^\pi = 3/2^-$ g.s and the $1/2^-$, 0.429 MeV first excited state [120]. These states are stable against particle emission. Since the ground states of ^{7}Li and ^{7}Be are isobaric analogue states, the transition strength between them is the incoherent sum of the Fermi and GT strengths.

The logft values of β-decay transitions from the g.s of ^{7}Be to the g.s and the $1/2^-$, 0.478 MeV first excited state have been measured with good accuracy. As discussed in Section 2.3 and shown in Fig. 3, they are the analogous transitions to those observed in the ^{7}Li(^{3}He, t) reaction. From these logft values and assuming B(F) = 1, we obtain B(GT) = 1.20 and 1.07 for the g.s–g.s and g.s-first excited state transitions, respectively, using Eqs. (26) and (27). These large B(GT) values and the concentration of the GT strength in these transitions suggest that the $J^\pi = 3/2^-$ g.s and the $1/2^-$, 0.429 MeV state are LS-partner states.

If we magnify the vertical scale by a factor of fifty, we can identify the weakly excited $J^\pi = 3/2^-, T = 3/2$ state at 11.01(3) MeV (see Fig. 20(b)). This state is the IAS of the g.s of ^{7}He and ^{7}B [120]. The weak excitation of this state suggests that the g.s of the $T = 1/2$, ^{7}Li (and ^{7}Be) and the g.s of the $T = 3/2$, ^{7}He (and ^{7}B) have rather different spatial shapes. It has been reported that the strength of the analogous GT transition in the β^+ direction, i.e., from the g.s of ^{7}Li to the g.s of ^{7}He, observed in the (d, ^{2}He) reaction is also very weak [121].

It should be noted that the energy difference between the $J^\pi = 3/2^-$ and $1/2^-$ LS-partner states is as small as 430 keV. Since the spin–orbit force is proportional to $-(1/r){\rm d}V/{\rm d}r$, LS-partners with a large spatial extension tend to have a smaller splitting. Therefore, it is suggested that the ground states of ^{7}Li and ^{7}Be are rather diffuse.

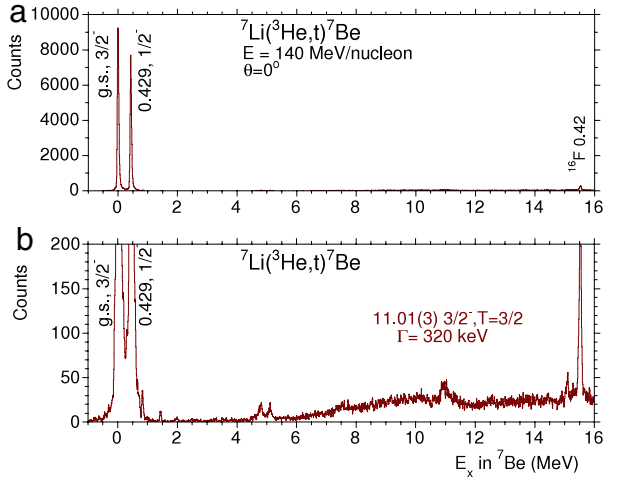

Fig. 20. Energy spectra for the ^{7}Li(^{3}He, t)^{7}Be reaction at 0° on two vertical scales. (a) The excitations of the $J^\pi = 3/2^-$ g.s and the $1/2^-$, 0.429 MeV excited state are the dominant features. (b) The same 0° spectrum, but the vertical scale is expanded by a factor of fifty. The weakly excited $J^\pi = 3/2^-$, $T = 3/2$ state is observed at 11.01(3) MeV.

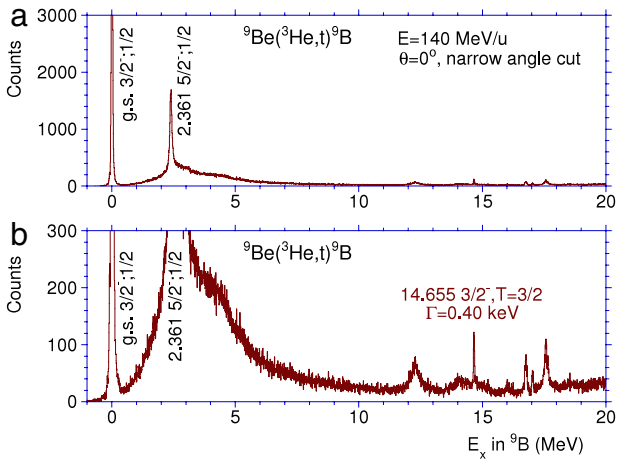

Fig. 21. The ^{9}Be(^{3}He, t)^{9}B spectrum on two vertical scales. (a) The simple structure shown in this figure was identified in earlier CE reactions. The structure of the low-lying bumps has been discussed in [123]. (b) By magnifying the vertical scale by one order of magnitude, fine structure was observed in the $E_x = 14$–18 MeV region. The 14.66 MeV state was weak but sharp.

6.1.2. Isospin selection rule and shape effects in A = 9 nuclei

Excited states above particle separation energies can have decay widths. With the realisation of high resolution in a CE reactions, it became possible to measure the decay widths even at intermediate incoming beam energies. In addition the high resolution studies provide a powerful tool for the detection of sharp but weakly excited states that co-exist with broad peaks in the high excitation region.

An interesting example is the observation of a sharp state at $E_x \approx 15$ MeV in the ^{9}Be(^{3}He, t)^{9}B spectrum. This is a $T_z = +1/2 \rightarrow -1/2$ transition. In CE spectra taken in the past, a simple structure consisting of a sharp $J^\pi = 3/2^-$ g.s and a broader 2.36 MeV state on top of a few-MeV-wide, bump-like structure was identified, just as we see in Fig. 21(a). In ^{9}B, all states are situated above the proton- and α-separation energies of $S_p = -0.186$ MeV and $S_\alpha = -1.689$ MeV, respectively [122]. Therefore, thinking in terms of the uncertainty principle, it is anticipated that states can have rather large widths at excitation energies of a few MeV (i.e., the energy of the Coulomb barrier) above these particle separation energies.

As shown in Fig. 21(b), when the vertical scale is expanded, we start to see a sharp state at $E_x = 14.66$ MeV. High sensitivity accompanied by high energy resolution of about 30 keV was essential to observe this weakly excited state on the continuum. The sharpness of the state can be explained by the isospin selection rule that prohibits proton- (and also α-) decay. It is known that this 14.6550(25) MeV state has an isospin value of $T = 3/2$ (the so-called $T_>$ state), and is the IAS of the g.s of ^{9}Li and ^{9}C [122]. The proton decay of ^{9}B results in ^{8}Be (observed as two αs in the resulting breakup). The nucleus ^{8}Be and the proton have isospin values of $T = 0$ and $1/2$, respectively. The vector sum of these two isospin values cannot

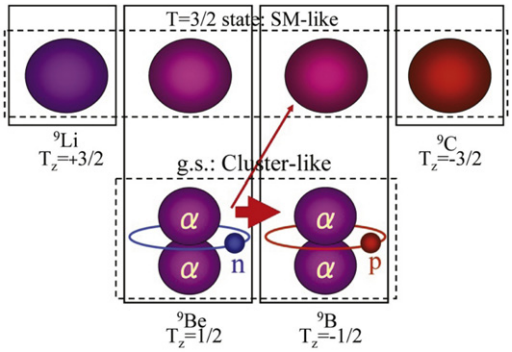

Fig. 22. ^{9}Be and ^{9}B are mirror nuclei having $T_z = +1/2$ and $-1/2$, respectively. It is thought that the main component of their ground states is $2\alpha+$ one-nucleon [124]. On the other hand, the $E_x = 14.66$ MeV, $T = 3/2$ state in ^{9}B is the IAS of the g.s of ^{9}Li and ^{9}C having a spherical shape. It should be noted that ^{9}Li and ^{9}C are the $p_{3/2}$ closed shell nuclei.

form an isospin value of 3/2; thus the proton decay is forbidden and the state is sharp. In a similar way, the isospin selection rule prohibits the α decay.

As will be discussed in Section 8.1, analysis showed that several sharp states observed above 10.8 MeV in the ^{58}Ni(^{3}He, t)^{58}Cu reaction (see Fig. 18) have $T = 2$ [24]. Although these $T = 2$ ($T_>$) states are located at nearly 10 MeV above the S_p value of 2.87 MeV, they still retain their sharpness. This is another example of the hindrance of the proton decay by the isospin selection rule.

It is known that both the g.s and this 14.66 MeV state in ^{9}B have $J^\pi = 3/2^-$. Thus, they can be connected with the $J^\pi = 3/2^-$ g.s of ^{9}Be by an allowed GT transition. However, in reality, the transition strengths differ by two orders of magnitude. It should be noted that the GT ($\sigma\tau$) operator cannot connect the states with different spatial shapes. Therefore, it is suggested that the g.s of ^{9}Be (and of ^{9}B) has a different structure from the 14.66 MeV state in ^{9}B which is the IAS of the g.s of ^{9}Li and ^{9}C (see Fig. 22). In a calculation using the method of antisymmetrised molecular dynamics (AMD), a structure consisting of $2\alpha+$ one-nucleon was predicted for the g.s of ^{9}Be and ^{9}B, while a mean field like structure is predicted for the 14.66 MeV state in ^{9}B and its IASs [124]. An *ab initio* no-core shell-model calculation [125] and a shell-model calculation with expanded $2\hbar\omega$ model space [126] shows that the GT transition from the g.s to the 14.66 MeV state is hindered. A detailed analysis of a spectrum with higher statistics is in progress [127].

6.1.3. *The "odd mass Hoyle state" in $A = 11$ nuclei*

The nuclei ^{11}B and ^{11}C are mirror nuclei. As shown in Fig. 23(a), the GT strength observed in the 0°, ^{11}B(^{3}He, t)^{11}C spectrum was fragmented. It was found that the fragmentation can be roughly understood by the coupling of a $p_{3/2}$ proton–hole (for ^{11}B) or neutron–hole (for ^{11}C) to the ^{12}C core. The coupling to the 0^+ g.s in ^{12}C produces the $J^\pi = 3/2^-$ ground states in ^{11}B and ^{11}C, and the coupling to the 2^+ first excited state at 4.44 MeV will produce a multiplet of states with $1/2^-$, $3/2^-$, $5/2^-$ and $7/2^-$. The $1/2^-$, $3/2^-$, $5/2^-$ states can be reached from the $3/2^-$ g.s by GT transitions. As reported in [128], the GT strength distribution was well reproduced by a classical shell-model calculation using the Cohen–Kurath interaction [129] with the introduction of a quenching factor, and also by an *ab initio* no-core shell-model calculation including a three-nucleon interaction [130,131]. It should be noted that the latter could reproduce the absolute B(GT) strengths without introducing the quenching factor.

Because of the excellent energy resolution in the (^{3}He, t) experiment, a peak observed at 8.4 MeV in an earlier (p, n) experiment [129] was resolved into 8.105 and 8.420 MeV states in agreement with [132]. It was found that there was almost no strength in the transition to the second excited $J^\pi = 3/2^-$ state at 8.105 MeV, although the transition from the ^{11}B g.s with $J^\pi = 3/2^-$ is allowed by the J^π selection rule. We can see this state only by magnifying the vertical scale by a factor of thirty as shown in Fig. 23(b). Interest in this state is not only due to its weak excitation, but also its absence in the shell-model calculations. These features strongly suggest that this 8.105 MeV state has a completely different spatial structure from the other strongly excited states.

The answer came from recent calculations within the antisymmetrised molecular dynamics (AMD) framework. It was shown that the second excited $3/2^-$ state in ^{11}B and ^{11}C and the first excited 0^+ state at 7.65 MeV in ^{12}C have a strong similarity from the viewpoint of cluster structure [133]. As is well known, this 7.65 MeV, 0^+ state, the "Hoyle state", is situated just above the three α threshold and is interpreted as a dilute gas state of three weakly interacting α particles [134–136]. It plays an essential role in the formation of ^{12}C by the triple alpha reaction in the Cosmos. Correspondingly, the AMD calculation shows that the second excited $3/2^-$ states in ^{11}B and ^{11}C have the well-developed cluster structures of $2\alpha + {}^3$H and $2\alpha + {}^3$He with dilute density, respectively. Therefore, these states may be called "odd mass Hoyle states". The similarity of the structures of these states was suggested experimentally by the similarity of the angular distributions of these states in the ^{11}B and ^{12}C(d, d') reactions [137].

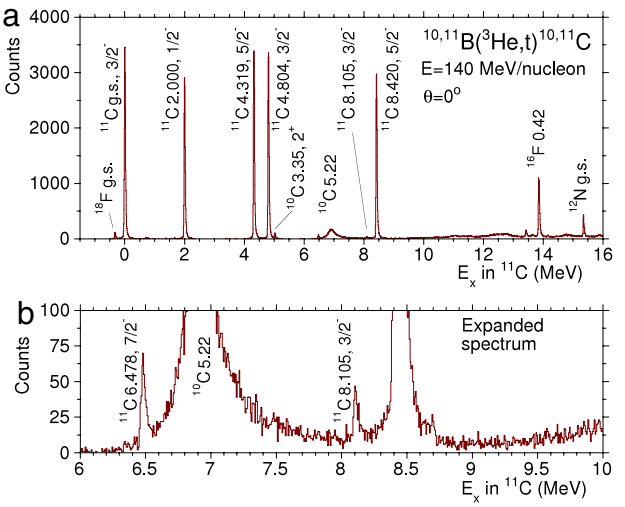

Fig. 23. Energy spectra from the ^{11}B(^{3}He, t)^{11}C reaction at 0° on two scales. (a) The spectrum up to $E_x = 16$ MeV. (b) The expanded 6–10 MeV region. The weakly excited $J^\pi = 3/2^-$, 8.105 MeV state is observed.

6.2. K selection rule in the deformed $T = 1/2$ nuclei in the middle of the sd shell

The spectra in Fig. 24 show the strengths of the $T_z = +1/2 \rightarrow -1/2$ Fermi and GT transitions starting from the g.s of ^{23}Na and ^{25}Mg target nuclei to the ground and excited GT states in the mirror nuclei ^{23}Mg and ^{25}Al. As seen, the features of these spectra are quite different in the low-lying region below $E_x = 6$ MeV. We see many prominent GT states in the $A = 23$ system [114] in contrast to the $A = 25$ system where they are very few [138]. It is known that these nuclei are deformed with a prolate shape (deformation parameter $\delta \approx 0.4$–0.5). Therefore, we can assume that low-lying states in these nuclei have the structure of a deformed (and rotating) core and a single nucleon. In strongly deformed nuclei, each single nucleon is in a Nilsson orbit labelled by the asymptotic quantum numbers [12]. When the rotation of the core is perpendicular to the z axis (the axis of symmetry), the z component K of the total spin J becomes an important quantum number. Therefore, the selection rules of $\Delta K = 0$ and ± 1, in addition to the usual selection rules of $\Delta J = 0$ and ± 1, should be taken into account [138]. Each rotational band is specified by the quantum numbers of the s.p orbit $K^\pi[Nn_z\Lambda]$, where N is the total oscillator quantum number, n_z the number of quanta along the z axis and Λ is the projection of the orbital angular momentum on the z-axis.

The proposed rotational band structure in ^{23}Na–^{23}Mg [139] is shown in Fig. 36 of Section 9.2, while that in ^{25}Al [12,140] is shown in Fig. 25.

The ground states of the $A = 23$ mirror nuclei ^{23}Na and ^{23}Mg are specified by the quantum numbers $3/2^+[2\,1\,1]$ (see Figs. 24(a) and also 36). Therefore, the transitions to the $K^\pi = 1/2^+$, $3/2^+$ and $5/2^+$ bands are allowed by the K-selection rule. Note that each Nilsson orbit specified by the asymptotic quantum numbers is filled with two nucleons. Therefore, the increase in mass number A by 2 will change the configuration of the g.s. As shown in Fig. 25, now the ground states of the $A = 25$ mirror nuclei ^{25}Mg and ^{25}Al are specified by $5/2^+[2\,0\,2]$. Therefore, the transitions from the ground states to the states of the common $1/2^+[2\,1\,1]$ band have different natures in the $A = 23$ and $A = 25$ systems with $\Delta K = 1$ and 2, respectively. Those transitions that were allowed in the $A = 23$ system are no longer allowed in the $A = 25$ system.

An interesting feature that became apparent from the comparison of these $A = 23$ and 25 systems is that at the deformation $\delta \approx 0.4$–0.5 the K selection rules are superior to the selection rules based on asymptotic quantum numbers that would start to work for large axially symmetric quadrupole deformation. One can point out that transitions from the ^{23}Na g.s of the $3/2^+[2\,1\,1]$ band to the 4.357 MeV, $1/2^+$ and 5.291 MeV, $5/2^+$ states of the $1/2^+[2\,2\,0]$ band in ^{23}Mg are, in principle, not allowed by the $\sigma\tau$ operator due to the $\Delta n_z = 1$ and $\Delta\Lambda = 1$ nature of these transitions. However, they are rather strongly excited, as seen in Fig. 24(a), because these transitions are allowed in terms of the K selection rule. Similarly, the transition to the 5.658 MeV, $5/2^+$ state of the $5/2^+[2\,0\,2]$ band is rather strong. We see that this transition is allowed by the K-selection rules, but not allowed by the n_z and Λ selection rules [138].

7. Comparison of charge-exchange and β-decay studies and the combined analysis

In order to obtain precise B(GT) values for the transitions to individual states and thus an accurate total B(GT) in the E_x region of interest, we compare and combine the knowledge of the mirror GT transitions starting from $\pm|T_z|$ mirror nuclei and ending in $\pm(|T_z| - 1)$ mirror nuclei. As we have seen, these transitions can be studied in β^--type CE reactions and β^+ decays, respectively. The (^{3}He, t) reaction can access states up to the high excitation energy region of $E_x \approx 15$–20 MeV but the GT transition strengths obtained are relative. In addition, only stable nuclei can be used as targets at present. In contrast

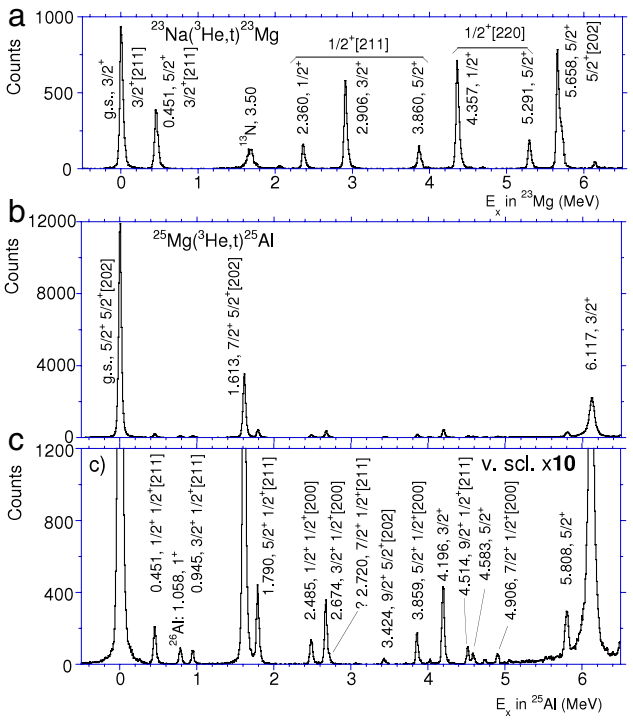

Fig. 24. Comparison of the (a) ^{23}Na(^{3}He, t)^{23}Mg and (b) ^{25}Mg(^{3}He, t)^{25}Al spectra. The ordinates of figures (a) and (b) are scaled so that states with similar B(GT) values have similar peak heights. The vertical scale of the ^{25}Mg(^{3}He, t)^{25}Al spectrum is expanded by a factor of ten in figure (c) in order to show weakly excited states more clearly.

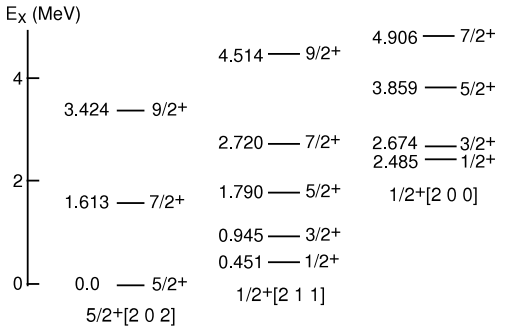

Fig. 25. Proposed band structure for the low-lying positive-parity states of ^{25}Al [12,140]. Each band is specified by the asymptotic quantum numbers $K^\pi[Nn_z\Lambda]$. Each state is identified by its E_x (in MeV) and J^π value. The identification of a new band structure at a higher energy will be discussed in Section 9.2.

absolute B(GT) values can be derived from the study of β decay, but access to states outside the Q_β window is impossible. In addition the study of feeding to the states in the upper part of the Q_β window is difficult, because the phase-space factor (f-factor) decreases rapidly with E_x. Thus, studies of the (^{3}He, t) CE reaction and β^+ decay are complementary. In order to compare the results from these two studies, however, we need to have both stable targets with, for example, $T_z = 1, 3/2, 2$ and mirror $T_z = -1, -3/2, -2$ nuclei that are particle bound and accessible in the β-decay studies.

In the p- and sd-shell nuclei, comparison of mirror GT transitions is, in principle, possible for several $T_z = \pm 1/2$ and ± 1 initial nuclei and a few $\pm 3/2$, ± 2 nuclei, but here the β-decay Q-values are low and the number of levels inside the window is small. Therefore, the comparison of strengths is possible only for the transitions to the low-lying states, but the B(GT) values obtained from the β decay can be used to normalise the CE reaction data. Above the pf shell, we run out of $T = 1, 3/2$, and 2 stable targets. At the same time the corresponding mirror β decay partners become very exotic and unbound.

For this reason nuclei at the end of the sd-shell and throughout the pf-shell are ideal for a detailed comparison of mirror transitions. Moreover GT transitions starting from stable as well as unstable pf-shell nuclei are of interest not only in nuclear physics, but also in astrophysics. They play important roles in the core-collapse stage of type II supernovae [3]. Therefore,

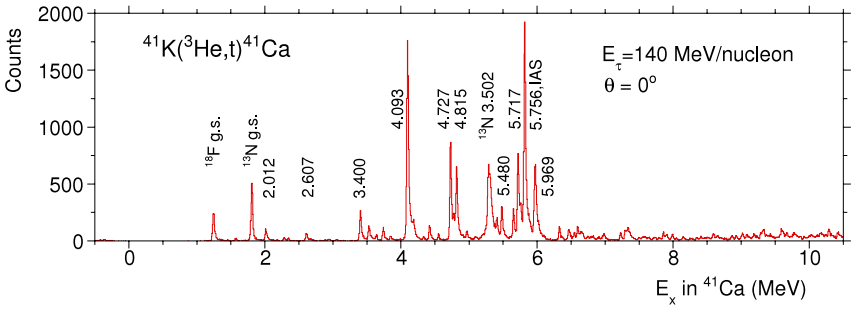

Fig. 26. The ^{41}K(^{3}He, t)^{41}Ca spectrum at 0° with an angular range up to 0.5°. A resolution of 35 keV was achieved. The main states populated in $L = 0$ GT transitions are indicated by their excitation energies.

studies of electron capture and β decay caused by charged currents and neutrino-nucleus reactions are of great astrophysical interest [141–143].

7.1. Isospin symmetry of $T_z = \pm 3/2 \rightarrow \pm 1/2$ mirror Gamow–Teller transitions in $A = 41$ nuclei

The isospin symmetry structure of the $T = 3/2$ isobaric system was discussed in Section 2.4. We examine here the strengths of $T_z = \pm 3/2 \rightarrow \pm 1/2$ analogous GT transitions and analogous $M1$ transitions within the $A = 41$ isobar quartet.

As shown in Fig. 5, the $T_z = +3/2 \rightarrow +1/2$ GT transitions from the $J^{\pi} = 3/2^{+}$ g.s of ^{41}K leading to excited $J^{\pi} = 1/2^{+}$, $3/2^{+}$, and $5/2^{+}$ states in ^{41}Ca can be measured using the ^{41}K(^{3}He, t) CE reaction. The difficulty of making a thin potassium target was solved by using a foil of $^{41}K_2CO_3$ supported by polyvinylalcohol (PVA) [144]. With a high energy resolution of 35 keV, many fragmented states were observed, and the GT strength distribution was determined up to 10 MeV excitation energy (see Fig. 26). The main part of the strength was concentrated in the $E_x = 4$–6 MeV region. The GT strength distribution obtained is shown in Fig. 27(a). The mirror symmetric $T_z = -3/2 \rightarrow -1/2$ GT transitions can be studied in the β decay of ^{41}Ti to ^{41}Sc. Two independent β-decay measurements have been reported. The work reported in [145] was performed at the ISOL facility in Jyväskylä, while that in [146] was performed at the FRS facility of GSI. As seen from Fig. 27(b) and (c), the reported B(GT) distributions were significantly different especially in the energy region above $E_x = 6$ MeV.

If isospin is a good quantum number, the transition strengths of the $T_z = \pm 3/2 \rightarrow \pm 1/2$ GT mirror transitions should not be much different. It was found that the general features of the B(GT) distribution given in [145] are similar to those observed in the ^{41}K(^{3}He, t)^{41}Ca measurement [147]. In addition, the energy resolution of 30 keV achieved in the measurement of the delayed protons after the β decay at the ISOL facility was comparable with the resolution of the (^{3}He, t) measurement of 35 keV.

By comparing the ^{41}K(^{3}He, t) and the ^{41}Tiβ decay B(GT) distributions shown in Fig. 27(a) and (b), respectively, we see similar gross features for the isospin analogous $T_z = \pm 3/2 \rightarrow \pm 1/2$ transitions. In addition, similar clustering strengths can be seen at 4.2, 4.8, and 5.7 MeV, although the strengths are distributed somewhat differently in each cluster. It should be noted that if the level density is high and if there exist forces that slightly violate isospin symmetry, such as the Coulomb force, the transition strength distribution can be somewhat different in the $T_z = \pm 3/2 \rightarrow \pm 1/2$ transitions (for the details, see [147]). By combining further the knowledge of J^{π} values of states in ^{41}Ca and ^{41}Sc evaluated in [148], correspondences of states are suggested in Table 4.

In these two experiments detecting the isospin mirror transitions, we notice that the number of observed states with appreciable B(GT) strength is identical in ^{41}Ca and ^{41}Sc, except for the weak transition to the 3.050 MeV state observed in the (^{3}He, t) reaction. The residual interaction depending on T_z, i.e., isospin asymmetric interaction, can make the GT strength distribution somewhat different. However, since J is a good quantum number, the modification of the distribution is expected only among the same J states. Rather accurate excitation energies and J^{π} values have been obtained for many of these states [148]. Therefore, the corresponding states can be assigned on the basis of excitation energies, J^{π} values, and the transition strengths from the (^{3}He, t) and β-decay measurements. Once the correspondence between analogous GT transitions became apparent, the knowledge of the J^{π} values for a pair of analogue GT states given in columns two and six of Table 4 can now be combined. The most probable J^{π} values are given in column eight. We see that the number of $J^{\pi} = 5/2^{+}$ states is the largest, while the number of $1/2^{+}$ states is smaller, suggesting a large contribution of the $d_{5/2}$ hole.

For the analogue states, the correlation of B(GT) values between analogous $T_z = \pm 3/2 \rightarrow \pm 1/2$ transitions was examined. As we see in Fig. 28, points are distributed more or less along the 45° line, but they are scattered, especially for pairs of states with smaller B(GT) values. As a result, we conclude that the gross symmetry of these isospin mirror transitions is rather well preserved, but the fine structures are somewhat different. From such differences in the fine structure of the distributions, isospin asymmetry matrix elements of ≈8 keV were deduced. A detailed discussion can be found in [147].

The Coulomb displacement energy (CDE) is dependent on the configuration of each individual state [149,150]. In order to study the CDE as a function of excitation energy, the difference of excitation energies,

$$\Delta E_x = E_x(^{41}\mathrm{Sc}) - E_x(^{41}\mathrm{Ca}), \tag{34}$$

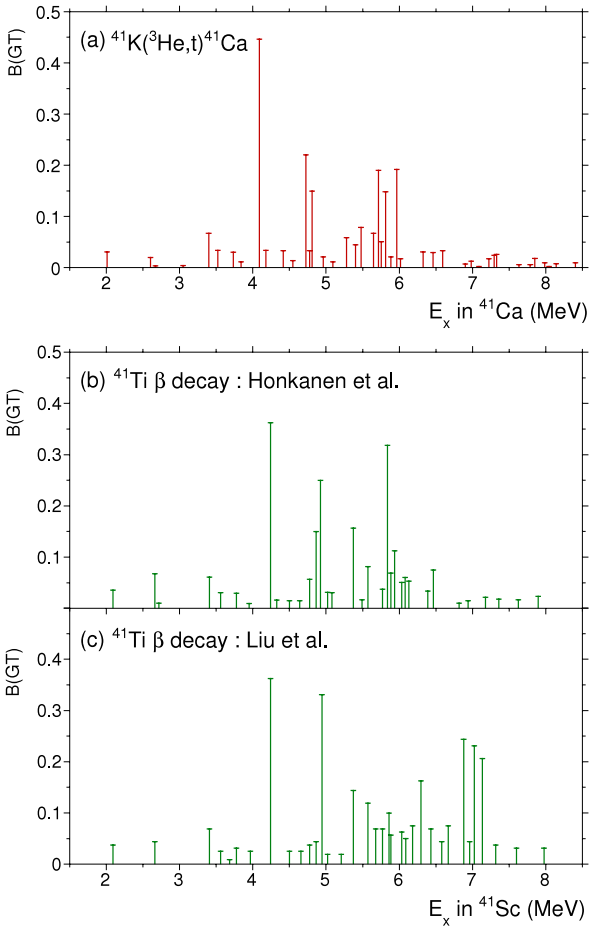

Fig. 27. Experimental B(GT) distributions from $T_z = \pm 3/2 \rightarrow \pm 1/2$ isospin mirror transitions. (a) B(GT) distribution from the ^{41}K(^{3}He, t)^{41}Ca reaction. (b) B(GT) distribution from the ^{41}Ti $\rightarrow ^{41}$ Sc β decay reported in [145]. (c) B(GT) distribution from the ^{41}Ti $\rightarrow ^{41}$ Sc β decay reported in [146]. The transition strengths of the $T_z = \pm 3/2 \rightarrow \pm 1/2$ GT mirror transitions should not be much different. It is clear that the β-decay B(GT) distribution of figure (b) is similar to that shown in figure (a). Through a detailed comparison of figures (a) and (b), a one-to-one correspondence of analogue states in ^{41}Ca and ^{41}Sc could be identified up to the excitation energy of 6 MeV, where the main transition strength was observed.

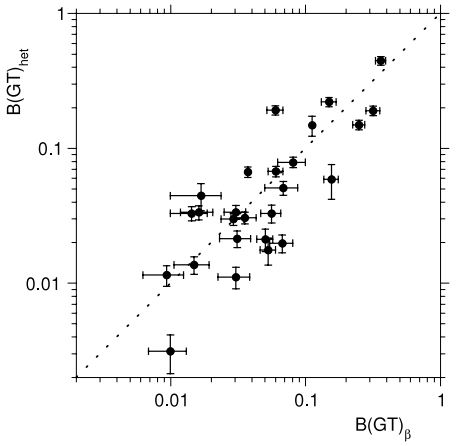

Fig. 28. A correlation between B(GT) values for analogous $T_z = \pm 3/2 \rightarrow \pm 1/2$ transitions. The $-3/2 \rightarrow -1/2$ $B(\mathrm{GT})_{\beta}$ values are from ^{41}Ti β decay [145] and the $+3/2 \rightarrow +1/2 B(\mathrm{GT})_{\mathrm{Het}}$ values are from the ^{41}K(^{3}He, t) measurement [147]. Analogue states with an ideal correlation would follow the dashed line.

was calculated for each pair of states. The ΔE_x values are given in the last column of Table 4. We see a marked increase in ΔE_x values at around $E_x = 3.8$ MeV. In the $1/2^+$ and $5/2^+$ distributions, a typical value of about 50 keV in the low-lying

Table 4
Comparison of $T_z = +3/2 \rightarrow +1/2$ and $T_z = -3/2 \rightarrow -1/2$ analogous GT transitions observed in the ^{41}K(^{3}He, t)^{41}Ca reaction and the β decay of ^{41}Ti to ^{41}Sc, respectively. The comparison is for the transitions to the states below 6.2 MeV, where the main part of the strength is concentrated.

^{41}K(^{3}He, t)^{41}Ca				^{41}Tiβ decay to ^{41}Sc[a]			Deduced values	
E_x (MeV)	$2J^\pi$; $2T$[b]	ΔL	B(GT)	E_x (MeV)	$2J^\pi$; $2T$[b]	B(GT)	$2J^\pi$[c]	ΔE_x (keV)
2.012	3^+	0	0.031(3)	2.096	3^+	0.036(7)	3^+	84
2.607	5^+	0	0.020(3)	2.667	5^+	0.067(13)	5^+	60
2.676	1^+	(0)	0.003(1)	2.719	1^+	0.010(3)	1^+	43
3.050	3^+	0	0.004(1)				3^+	
3.400	1^+	0	0.067(6)	3.411	1^+	0.061(7)	1^+	11
3.526	3^+	0	0.034(4)	3.563	$(1, 3, 5)^+$	0.031(6)	3^+	37
3.737	$(3, 5)^+$	0	0.030(3)	3.781	(5^+)	0.029(6)	5^+	44
3.845	1^+	0	0.012(2)	3.951(14)	1^+	0.009(3)	1^+	106
4.093	5^+	0	0.446(33)	4.245(4)	5^+	0.360(30)	5^+	152
4.182	(3, 5)	0	0.034(4)	4.328(3)	5^+	0.016(4)	5^+	146
4.419	3^+	0	0.033(4)	4.502(5)	3^+	0.014(4)	3^+	83
4.550		0	0.014(2)	4.644(5)	1^-	0.015(4)		94
4.727	$(3)^+$, $(5)^+$	0	0.220(17)	4.869(4)	5^+	0.150(20)	5^+	142
4.777	$(3)^+$	0	0.033(5)	4.777(5)	3^+	0.056(9)	3^+	0
4.815	5^+	0	0.149(12)	4.928(5)	$(1, 3, 5)^+$	0.250(30)	5^+	113
4.966		0	0.021(3)	5.023(5)	1^+	0.031(8)	1^+	57
5.097	3^+	0	0.011(2)	5.084(5)	3^+	0.031(8)	3^+	−13
5.283	5^+		0.059(17)	5.375(4)	5^+	0.160(20)	5^+	92
5.406	5^+	(0)	0.045(10)	5.493(5)	1^+	0.017(7)		87
5.480	$(3)^+$	0	0.079(7)	5.576(4)	3^+, 5^+	0.081(19)	3^+	96
5.652	$(5)^-$	0	0.067(6)	5.774(4)	$(1, 3, 5)^+$	0.069(20)	5^+	122
5.717	$(5)^-$	0	0.190(15)	5.840(5)	3^+, 5^+	0.320(40)	5^+	123
5.756	$(5)^+$	0	0.051(6)	5.886(12)	$(1, 3, 5)^+$	0.069(19)	5^+	130
5.814	3^+; 3[d]	0	0.148(25)	5.939(4)	3^+; 3[d]	0.110[e]	3^+	125
5.890	1^-	(0)	0.021(4)	6.038(25)	$(1, 3, 5)^+$	0.051(7)		148
5.969	$(3, 5)^+$	0	0.192(15)	6.083(20)	$(1, 3, 5)^+$	0.060(8)	1^+	114
6.019		(0)	0.018(4)	6.133(20)	3^+, 5^+	0.053(7)		114

[a] From Ref. [145].
[b] From Ref. [148].
[c] Suggested J^π values from the comparison.
[d] The IAS with $T = 3/2$. Other states are $T = 1/2$ [147].
[e] From the shell-model calculation, see Ref. [145].

region suddenly changes to more than 100 keV above 4 MeV excitation energy, where the main part of the strength appears. For the transitions in the low-lying region, mainly $d_{3/2} \rightarrow d_{3/2}$ and $f_{7/2} \rightarrow f_{7/2}$ transitions are expected in a naive single-particle model. On the other hand, at higher excitation energies the main transitions are expected to be $d_{5/2} \rightarrow d_{3/2}$ and $f_{7/2} \rightarrow f_{5/2}$. The sudden increase in ΔE_x values, corresponding to the sudden change in the CDE, suggests a change of the main configurations of the wave functions at around $E_x = 3.8$ MeV.

The $M1$ transitions strengths in ^{41}Ca from the IAS, i.e., the isobaric analogue state of the g.s of ^{41}K, to five low-lying excited states were compared with the analogous GT transition strengths derived from the ^{41}K(^{3}He, t) ^{41}Ca study (see Fig. 5) [147]. It was found that ratios of the $M1$ and GT transition strengths, except for one transition, were similar. Thus the contribution from the $\ell\tau$ term, which is inherent to an $M1$ transition and has no corresponding term in a GT transition, is small in these $M1$ transitions. As we will see in Section 9, the contribution of the $\ell\tau$ term can be large if a nucleus is deformed.

7.2. Merged analysis combining charge-exchange and β-decay information

We have been studying $T_z = \pm 1 \rightarrow 0$ mirror GT transitions for the pf-shell nuclei (see Fig. 29). Starting from the 0^+ g.s of the $T_z = \pm 1$ nuclei, the identical final 1^+ excited states are reached in these transitions. Therefore, their comparison should be simple. Thorough studies for the $T_z = +1 \rightarrow 0$ transitions have already been made using (^{3}He, t) reactions on the stable $T_z = +1$, f-shell target nuclei ^{42}Ca [151], ^{46}Ti [152], ^{50}Cr [153], ^{54}Fe [151] and ^{58}Ni [24] (see Fig. 39 for the spectra obtained).

The $T_z = -1 \rightarrow 0$ transitions have been investigated by studying the β decays of $T_z = -1$ proton-rich nuclei (for details, see [154–157]). The B(GT) values from these β decays can, in principle, be used to determine the $\hat{\sigma}_{\rm GT}(0^\circ)$ values. Once the $\hat{\sigma}_{\rm GT}(0^\circ)$ value is known, the B(GT) values can be determined for the transitions to highly excited states using Eq. (31) and the results of CE reaction studies. However, the β-decay B(GT) values for the $T_z = -1$, pf-shell nuclei have rather large uncertainties.

As we have seen, accurate values of the total half-life $T_{1/2}$, with uncertainties of $\lesssim$5%, can be obtained in β decay studies, but the study of accurate feeding ratios is more difficult. In order to overcome this difficulty, we introduce the "merged

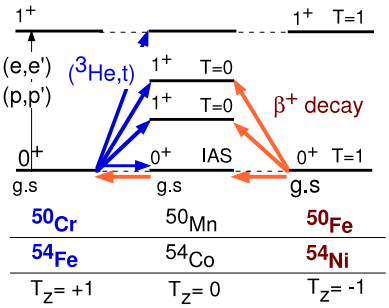

Fig. 29. Schematic illustration of the isospin symmetry GT transitions in the "$T = 1$ system" for $A = 50$ and 54. The Coulomb displacement energies have been removed to show the isospin symmetry structure. The $T_z = \pm 1 \rightarrow 0$ transitions can be studied by the (^{3}He, t) reaction and β decay, respectively, for the pf-shell nuclei. The ground states of $T_z = 0$ nuclei ^{50}Mn and ^{54}Co are the IASs of the neighbouring $T_z = \pm 1$ nuclei and have $T = 1$.

analysis", in which the relative GT strength distributions from the (^{3}He, t) reaction are combined with the total half-life $T_{1/2}$ and the decay Q-value from the β-decay study [153]. In this analysis, good symmetry for the strengths of $T_z = \pm 1 \rightarrow 0$ analogous GT transitions is assumed.

The "merged analysis" starts with the formula connecting the total β decay half-life $T_{1/2}$ and the partial half-life t_F of the Fermi transition and t_js of GT transitions

$$(1/T_{1/2}) = (1/t_F) + \sum_{j=GT}(1/t_j). \tag{35}$$

The inverse of the half-life represents the transition strength. Therefore, in this formula we assume that the total β-decay strength given on the left side is the sum of the strengths of the Fermi and GT transitions, and the contribution from forbidden transitions is small. Applying Eq. (26), one can eliminate both t_F and t_j, and we get

$$\frac{1}{T_{1/2}} = \frac{1}{K}\left[B(F)(1-\delta_c)f_F + \sum_{j=GT}\lambda^2 B_j(GT) f_j\right], \tag{36}$$

where f_F and f_j can be calculated if the decay energy is known, $B(F) = |N - Z|$, and the relative strengths proportional to $B_j(GT)$ can be studied in the (^{3}He, t) reaction (see Eq. (31)). Therefore, if the total half-life $T_{1/2}$ of the β decay is known accurately, the relative strengths of the $B_j(GT)$ studied in the (^{3}He, t) reaction can be converted into absolute values.

The first analysis was made for the $A = 50, T = 1$ isobaric system (see Fig. 6), because the decay Q-value and the total half-life $T_{1/2}$ for the ^{50}Fe $\rightarrow$ ^{50}Mn β decay ($T_{1/2} = 0.155(11)$ s and $Q_\beta = 8.15(6)$ MeV) [155] were the best known among the $T = 1$ triplets in the pf-shell region. The partial half-lives and thus the feedings were, however, unclear; only the feeding to the first 1^+ state at $E_x = 0.651$ MeV had been detected. A B(GT) value of 0.60(16) was deduced under the extreme assumption that no feeding took place to higher excited states [155]. On the other hand, in the merged analysis the ratio of unknown feedings up to a higher excitation region of the $T_z = -1 \rightarrow 0$ ^{50}Fe β decay can be deduced by multiplying the ^{50}Cr(^{3}He, t) ^{50}Mn spectrum (Fig. 30(a)) with the calculated f-factor (Fig. 30(b)). The deduced "β-decay energy spectrum" is shown in Fig. 30(c).

The properties of the states up to $E_x = 5$ MeV observed in the ^{50}Cr(^{3}He, t) ^{50}Mn measurement are summarised in Table 5. The g.s of ^{50}Mn is the $J^\pi = 0^+$ IAS of the target nucleus ^{50}Cr [158]. Since the only GT state known was at 0.651 MeV [158–160], E_x values of higher excited states were determined with the help of kinematic calculations using well-known E_x values of ^{26}Al, ^{24}Al, and ^{16}F states in the spectrum from a polyvinylalcohol (PVA)-supported $^{nat}MgCO_3$ thin foil target [144] as references. All E_x values of ^{50}Mn states were determined by interpolation. Estimated errors are about 10 keV.[1]

In order to select GT states with "$\Delta L = 0$" nature, intensities of observed states were compared in the spectra for two angle cuts $\Theta = 0°$–$0.5°$ and $1.5°$–$2.0°$. All prominent states showed 0° peaked angular distributions, suggesting a $\Delta L = 0$ nature. Since the Fermi strength is concentrated in the transition to the IAS, it is very probable that the transitions with $\Delta L = 0$ are GT transitions. Intensities of several weakly excited states increased at larger scattering angles, suggesting a "$\Delta L \geq 1$" nature (see Table 5).

As discussed, the unit GT cross-section in Eq. (31) gradually decreases as a function of excitation energy. A DWBA calculation showed that such a kinematical correction was small and amounted to only 4% at 5 MeV. The f-factors were calculated following Ref. [162]. Values normalised to unity at $E_x = 0$ are shown in Fig. 30(b). Putting the value of $T_{1/2}$ and the calculated ratio of feedings in Eq. (36), absolute GT transition strengths B(GT) were derived for all of the GT states up to

[1] There is a recent measurement of the γ-decay of these 1^+ states to the 0^+ g.s [161]. It suggests that the error is about 15 keV in the 4 MeV region.

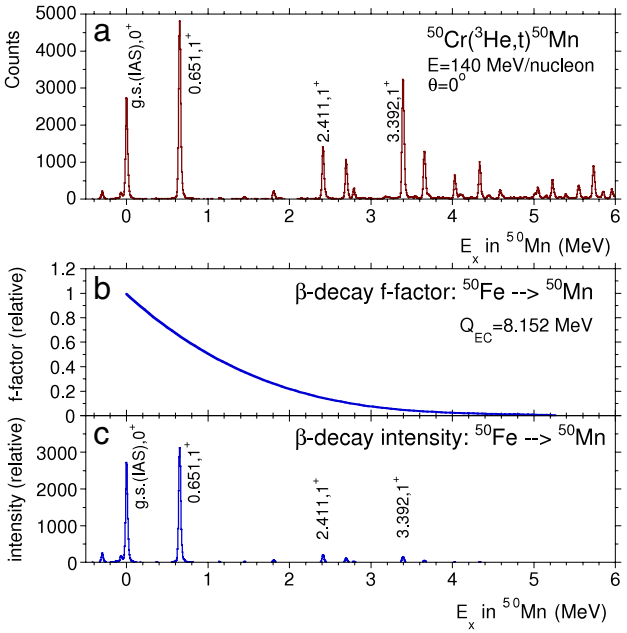

Fig. 30. (a) The ^{50}Cr(^{3}He, t) ^{50}Mn spectrum for events with scattering angles $\Theta \leq 0.5°$. An energy resolution $\Delta E = 29$ keV (FWHM) has been realised. Some of the strongly populated states with $\Delta L = 0$ are indicated by their excitation energies in MeV. (b) The f-factor for the ^{50}Fe β decay, normalised to unity at $E_x = 0$ MeV. (c) The estimated ^{50}Fe β-decay energy spectrum obtained by multiplying the ^{50}Cr(^{3}He, t) spectrum by the f-factor. Note that the IAS is stronger in the real β-decay experiment due to the different ratio of coupling constants for the τ and $\sigma\tau$-type interactions for the (^{3}He, t) reaction [153].

Table 5
States observed in the ^{50}Cr(^{3}He, t) ^{50}Mn reaction below $E_x = 4.6$ MeV. For the states populated with $\Delta L = 0$, B(GT) values assuming $T_{1/2} = 0.155(11)$ s are given.

Evaluated values[a]		(^{3}He, t)[b]		
E_x (MeV)	J^π	E_x (MeV)	ΔL	B(GT)
0.0	0$^+$[c]	0.0	0	
0.651	1$^+$	0.652	0	0.50(13)
0.800	2$^+$	0.800	$\geq$1	
1.143	3$^+$	1.147	$\geq$1	
1.802	3	1.805	$\geq$1	
		2.411	0	0.15(4)
		2.694	0	0.11(3)
		2.790	0	0.03(1)
		3.177	$\geq$1	
		3.392	0	0.35(9)
		3.654	0	0.14(4)
		4.028	0	0.07(2)
		4.333	0	0.11(3)
		4.584	0	0.03(1)

[a] From Refs. [158,159].
[b] Present work.
[c] The IAS with $T = 1$.

$E_x = 5$ MeV shown in Fig. 30(a), and they are listed in the last column of Table 5. Owing to the newly deduced feedings to higher excited GT states, the merged analysis showed that the B(GT) value of the first GT state should decrease by about 20% down to 0.50(13) compared to the value of 0.60(16) deduced from the β-decay study assuming that only one GT transition existed, i.e., the one to the 0.651 MeV state in ^{50}Mn.

It should be noted that in this merged analysis [153], the half-life is introduced from the β-decay measurement and the precise branching ratios are deduced from the high resolution spectrum obtained in the (^{3}He, t) reaction, in combination with the calculated f-factor, under the assumption of isospin symmetry. However, in the present analysis, we notice that the uncertainty originates not only from the half-life but also from the Q_β-value used for the calculation of the f-factor. The Q-value measurement will require another dedicated effort involving, e.g., the trap technique (see Section 4.1).

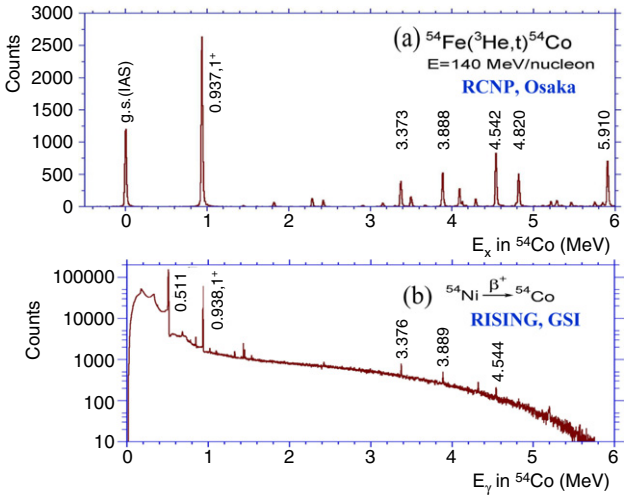

Fig. 31. (a) The ^{54}Fe(^{3}He, t) ^{54}Co spectrum for events with scattering angles $\Theta \leq 0.5°$. Major states with $\Delta L = 0$ are indicated by their excitation energies in MeV. They are excited in the $T_z = +1 \rightarrow 0$ GT transitions. (b) On-line γ-ray spectrum from the RISING array at GSI measured in coincidence with the β particles from the ^{54}Ni decay. The existence of γ-ray peaks and CE reaction peaks at corresponding energies suggests a good mirror symmetry for the $T_z = -1 \rightarrow 0$ and $T_z = +1 \rightarrow 0$ GT transitions.

7.3. β-decay experiments for the study of Gamow–Teller strengths in proton-rich f-shell nuclei

As we have seen, the β-decay B(GT) values for the $T_z = -1$, pf-shell nuclei have rather large uncertainties, and consequently a dedicated effort was required to improve them. A programme of comparing β-decay measurements with the results from the (^{3}He, t) reactions has now been undertaken for the nuclei ^{42}Ti, ^{46}Cr, ^{50}Fe, and ^{54}Ni at the GSI, Darmstadt.

The purpose of the experiments was (1) to obtain precise $T_{1/2}$ values, which are important input parameters to perform the "merged analysis", and (2) to observe the feeding to the states at high excitation energies. The nuclei of interest are clearly at the frontier where the present fragmentation facilities start to be competitive with the ISOL facilities. The reason is a combination of unfavourable chemical properties of the chemical elements of interest produced in the isotope separator ion source and the short half-lives, much shorter than the release time of the ions in the source.

The fragmentation experiment [163,164] was performed as part of the RISING stopped beam campaign [165] at the FRagment Separator (FRS), GSI. Beams of ^{42}Ti, ^{46}Cr, ^{50}Fe, and ^{54}Ni were produced in the fragmentation of a primary 680 MeV/nucleon ^{58}Ni beam of 0.1 nA on a 400 mg/cm^2 Be target. The primary beam length was 10 s with a repetition cycle of 13 s. The reaction products were separated in the fragment separator and the ions of interest, mainly fully stripped, focused at the end of the FRS and implanted into an active beam stopper system. Full separation was not achieved during the experiment, but the collected activity contained mainly the nuclei of interest (≈80%). Complete separation was achieved in the off-line analysis using TOF, $B\rho$ values and ΔE signals. The implantation detector consisted of three layers of double-sided silicon strip detectors (DSSDs) with an area of 50 × 50 mm and 16 × 16 strips. The same detector registered the ΔE signals produced by the βs in the decay. The high pixellation was essential for the determination of the correct implantation-β correlations. The detector system was surrounded by the RISING γ-ray array composed of 15 EUROBALL cluster Ge detectors. The overall γ-ray detection efficiency was about 15% at 1.33 MeV. This sensitive array was a key piece of equipment for the detection of γ rays of high energy.

The production rate of the four $T_z = -1$ nuclei, ^{42}Ti, ^{46}Cr, ^{50}Fe, and ^{54}Ni was relatively high, up to 500 counts/s distributed mainly in two DSSD detectors. As an example, we show the results for the $A = 54$ system. The spectrum from the ^{54}Fe(^{3}He, t) ^{54}Co measurement [151] and the delayed-γ spectrum from the ^{54}Ni → ^{54}Co β decay are compared in Fig. 31. Due to the high production rate for ^{54}Ni and the good detection efficiency of the RISING setup, high energy delayed γ rays could be seen (Fig. 31(b)) at the energies corresponding to the GT states observed in the ^{54}Fe(^{3}He, t) ^{54}Co measurement [151]. Prior to our work, only the first excited state, at 937 keV was reported in the literature [156].

The branching ratios to all the excited states are based on the intensity analysis of the β-delayed γ rays. Based on the fact that we are dealing with a relatively light system and simple de-excitation patterns (mainly 1^+ to 0^+ g.s), we considered that the Pandemonium effect in this case must be small. An important and delicate issue in order to obtain correct branching ratios, and thus the intensities to the states at high energy is a good calibration of the efficiency of the γ detectors at energies around 4 MeV. This is far from trivial and demands a combination of calibration source measurements and Monte Carlo simulations. The analysis is still in progress, but an interesting observation is that the states populated in ^{54}Co by GT transitions from ^{54}Ni decay mainly by direct γ transitions to the 0^+ g.s, and little or no γ branching is observed to the first 1^+ state.

The analysis of the $T_{1/2}$ [161], as mentioned in Section 4.2, can be based either on the βs or on the β-delayed γs. The first has better statistics, but the second is more specific to the decay under study. However, in a fragmentation experiment

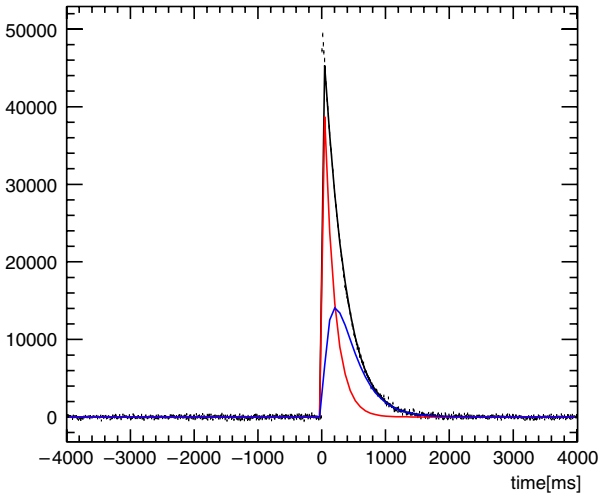

Fig. 32. Heavy ion implantation–β correlations for identified ^{54}Ni ions produced at GSI (see text). The random background has been subtracted. The flat baseline of zero counts for negative as well as for positive long correlation times gives an indication of the correctness of the background subtraction. The fit includes the ^{54}Ni decay curve as well as the growth and decay curve for the ^{54}Co daughter activity; see text.

of this kind the big advantage is that one can, in principle, associate the βs detected in a pixel with the implantation of the heavy ion. This is a clean method to identify a specific decay, but the randoms have to be evaluated properly. In Fig. 32, we show the fit for the decay curve of ^{54}Ni and the growth and decay curve for the ^{54}Co daughter activity after the randoms have been subtracted. As can be seen, a perfect fit is obtained for the combination of the two activities. The precise ^{54}Co half-life value of 193.271(63) ms [30] was used as an input in the fit. From the present fit, a preliminary value for the ^{54}Ni $T_{1/2}$ of 114.4(10) ms was obtained, where the fitting error is 0.2 ms and the quoted error originates from possible systematic errors. Any variation in the fitted half-life due to changes in the dead time was explored by repeating the analysis for events which occur at different times during the synchrotron beam spill. A small variation was found near the end of the spill. Provided this was avoided the half-life obtained was stable to within 1 ms. Similarly, any systematic effects due to mis-identified ions being included in the $A = 54$ window were explored using the information from the γ-ray spectrum. Such effects were also found to cause a variation of less than one ms. This value is in agreement with the previous value of $T_{1/2} = 106(12)$ [156] and with a recent value of 115(12) ms measured at the Leuven ISOL facility in Louvain-la-Neuve [166].

In [156], a B(GT) value of 0.68(16) was obtained for the transition to the 0.937 MeV state assuming that all β-decay GT strength is concentrated in this decay. However, the longer half-life and the finding of the feeding to higher excited states in the ^{54}Fe(^{3}He, t) ^{54}Co reaction [151] suggest that the GT transition strength to the $E_x = 937$ keV state should be smaller. In the "merged analysis" presented in Section 7.2, we obtain B(GT) $= 0.46(8)$; a value smaller by about 30% compared to the previous one. The transition strength to this state has also been measured in an ^{54}Fe(p, n) reaction at $E_p = 135$ MeV [167]. Compared to their B(GT) value of 0.74(5), which was derived from their own systematics, our new value is more than 35% smaller.

8. Identification of isospin T by the comparison of charge-exchange reactions and inelastic scattering

As discussed in Section 5.2, given the high energy resolution achieved in the ^{58}Ni(^{3}He, t) ^{58}Cu reaction, many individual GT states have been observed (see Fig. 18) even in the so-called GT resonance (GTR) region of $E_x = 7$–12 MeV [24]. The (^{3}He, t) reaction on the $T_z = +1$ target nucleus ^{58}Ni with a g.s isospin $T_0 = 1$ excites $T = 0$, 1 and 2, GT states in the final nucleus ^{58}Cu. In general, the $T = 0$, GT states appear in the lower-lying region, the $T = 1$ states in the middle, and the $T = 2$ states in the higher excitation region due to the isospin symmetry term of the nuclear interaction (see [2] and the discussion in Section 2.4), but in the real spectrum they are not separated, but mixed with each other.

From the $T = T_0$ g.s of a target nucleus with T_z ($=T_0$), final states with $T_0 - 1$ (if $T_0 - 1 \geq 0$), T_0 and $T_0 + 1$ are excited in the $T_z - 1$ nucleus (see Section 2.4). We call them $T_<$, T_0 and $T_>$ states, respectively. (If the transition is from $T_0 = T_z = +1/2$ nucleus, only $T = 1/2$ and 3/2, i.e., T_0 and $T_>$ states are excited in the $T_z = -1/2$ final nucleus, see Section 2.3.) Our interest here is to separate the GT strength distribution into these different isospin components. For that purpose, we can use the 0° (p, p') spectrum measured for the same target nucleus as a reference. This reaction excites the T_0 and $T_>$ spin $M1$ states ($M1_\sigma$ states), analogous to the corresponding states seen in the (^{3}He, t) reaction. Therefore, those states that are not observed in the (p, p') reaction should be the $T_<$ states [168]. In order to distinguish the $T_>$ states from the T_0 states, we can further use the fact that the CG coefficients in the excitation of these different T states are different for the (^{3}He, t) and (p, p') reactions (see the CG coefficients shown in Figs. 3 and 7).

We summarise the squared values of CG coefficients C^2 and their ratios in the (^{3}He, t) reaction and also the (p, p') reaction for the transitions to the $T_>$ (T_0+1) and T_0 states in Table 6. As seen, the ratios of CG coefficients between the $T_>$ and T_0 states

Table 6
The squared values of the isospin Clebsch–Gordan (CG) coefficients C^2 for the T_0 and $T_0 + 1$ excitations in the (^{3}He, t) and (p, p') reactions for various values of T_0, the initial isospin. The ratio of $C^2(T_0 + 1)$ divided by $C^2(T_0)$ shows that the $T_0 + 1$ excitation is enhanced in the (p, p') reaction compared to the (^{3}He, t) reaction. The enhancement factor is shown in the last column.

Initial T_0	(^{3}He, t)			(p, p')			Enhancement in (p, p')
	$C^2(T_0)$	$C^2(T_0 + 1)$	Ratio[a]	$C^2(T_0)$	$C^2(T_0 + 1)$	Ratio[a]	
1/2	2/3	1/3	1/2	1/3	2/3	2	4
1	1/2	1/6	1/3	1/2	1/2	1	3
3/2	2/5	1/10	1/4	3/5	2/5	2/3	8/3
2	1/3	1/15	1/5	2/3	1/3	1/2	5/2

[a] Ratio of $C^2(T_0 + 1)$ divided by $C^2(T_0)$.

are always larger in the (p, p') reaction than in the (^{3}He, t) reaction, suggesting that the excitation of $T_>$ states, compared to the excitation of T_0 states, will be enhanced in the (p, p') reaction, compared to the (^{3}He, t) reaction, by the factors shown in the last column. Therefore, if we compare the (p, p') and (^{3}He, t) spectra normalised by the strengths of the analogous transitions to T_0 states, we should see the enhancement of the transitions to the $T_>$ states in the (p, p') spectra.

It should be noted that GT transitions observed in (n, p)-type reactions are analogous to the transitions to $T_>$ states observed in the (^{3}He, t) reaction. The associated CG coefficient in (n, p)-type reactions is always unity. For these GT transitions in the β^+ direction, it is usually hard to find a β decay that enables us to study the unit GT cross-section. Therefore, the B(GT) values determined in the $T_0 \rightarrow T_>$ transitions in the high resolution (^{3}He, t) reaction (after correcting for the isospin CG coefficients) can provide good standard for B(GT) values in the (n, p)-type reactions. In a similar way, $B(M1_\sigma)$ values studied in the (p, p') reaction (see Eq. (5)) can be calibrated using the B(GT) values of the analogous transitions studied in the (^{3}He, t) reaction.

8.1. *Identification of isospin T in the $T_z = 0$ final nucleus ^{58}Cu and the isospin selection rule*

The electron-capture rates from *pf*-shell nuclei are important at various stages of stellar evolution [3]. The rates are determined by the GT strengths of transitions in the β^+ direction. Since analogous transitions can be studied as the $T_0 \rightarrow T_0 + 1$ transitions in the (^{3}He, t) reaction, it is intriguing to identify the $T_0 + 1$, GT states in the (^{3}He, t) spectra [24].

As seen from Fig. 7, the (^{3}He, t) reaction on the target nucleus ^{58}Ni with g.s isospin $T = T_0 = 1$ and $J^\pi = 0^+$ excites $J^\pi = 1^+$ GT states with $T = 0$ ($T_<$), 1 (T_0) and 2 ($T_>$) in ^{58}Cu. On the other hand, only the $T = 1$ and 2 analogue states are observed in the ^{58}Ni(p, p') reaction as excited 1^+ states in ^{58}Ni. Therefore, if states are observed only in the (^{3}He, t) reaction, they are the $T = 0$ ($T_<$) states. The 0.203 MeV state in ^{58}Cu is the isobaric analogue state of the $J^\pi = 0^+$, $T = 1$, g.s of ^{58}Ni [169]. Therefore, it is expected that the $T = 1$ and also $T = 2$, GT states in ^{58}Cu have E_x values about 200 keV higher than the parent $M1$ states in ^{58}Ni. In order to distinguish between $T = 1$ and 2 states, we can use the difference of CG coefficients in the (^{3}He, t) and (p, p') reactions.

The ^{58}Ni(^{3}He, t) experiment was performed at RCNP, while the ^{58}Ni(p, p') experiment was performed at IUCF [23,24]. The high resolution (p, p') experiment at 0° is difficult to carry out [23]. Such measurements have been successful only at IUCF, RCNP and iThemba-LABS (Cape Town, South Africa), where good magnetic spectrometer systems are available. The detailed procedure in the experiment is described in [17].

The (^{3}He, t) and (p, p') spectra obtained at 0° are shown in Fig. 33(a) and (b) for the $E_x = 8.5$–12.5 MeV region. The (^{3}He, t) spectrum is shifted by 0.203 MeV, i.e., the E_x value of the IAS in ^{58}Cu, in order to identify the corresponding GT and $M1$ states with $T = 1$ and 2. Most of the states showed forward-peaked angular distributions, suggesting that they are the states with $\Delta L = 0$. However, a detailed analysis of the ^{58}Ni(p, p') spectrum showed the existence of several extra peaks that had no corresponding partner in the (^{3}He, t) spectrum [24]. By consulting the nuclear resonance fluorescence (NRF) measurement on ^{58}Ni [170], those states were identified as Coulomb-excited $E1$ states. The Coulomb excitation is stronger as the Z of the target nucleus increases.

The vertical scales of the two panels in Fig. 33 have been adjusted so that the corresponding 8.837 MeV state in the (^{3}He, t) spectrum and the 8.667 MeV state in the (p, p') spectrum have the same heights. This pair of states is known to have $T = 1$ [169]. In addition to this pair, we see many corresponding states by comparing the two spectra in Fig. 33, and the properties of the pairs of GT and $M1$ states are summarised in Table 7. From Table 6, we anticipate that the transitions to the $T = 2$, $M1$ states are enhanced by a factor of three in the (p, p') spectrum for the $T_0 = 1$ initial nucleus ^{58}Ni. It is clear that the 10.664 MeV state in the (p, p') spectrum is enhanced by a factor of about three over the corresponding 10.825 MeV GT state in the (^{3}He, t) spectrum. It is seen that several other peaks are enhanced in the (p, p') spectrum and they are the candidates for $T = 2$ ($T_>$) states. We name the enhancement factor for the peak in the (p, p') spectrum as "R_{GT}" and give a value of three for the strongest pair of analogue $T_f = 2$ states at 10.664 and 10.825 MeV [24]. The R_{GT} values for the other pairs were calculated, including the kinematic correction factor (of the order of a few %). The R_{GT} values are listed in column six of Table 7.

Almost all pairs of analogue states below 10 MeV show the R_{GT} values of ≈1 or typically less than 1.5. A typical example is the 8.837–8.677 MeV pair (see Fig. 33). The R_{GT} value of 1.16(13) is in good agreement with the value of unity expected for a $T_f = 1$ state. On the other hand, those at higher energies show larger values between 2.1 and 3.4. (The deviation from

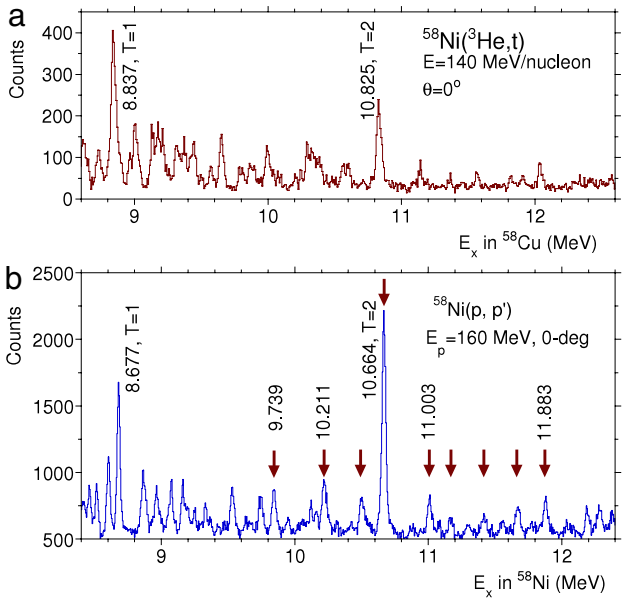

Fig. 33. The comparison of the ^{58}Ni(^{3}He, t) ^{58}Cu and ^{58}Ni (p, p') spectra taken at 0° in the excitation energy region where both $T = 1$ and 2 states coexist. (a) The 0° ^{58}Ni(^{3}He, t) ^{58}Cu spectrum measured at RCNP. (b) The 0° ^{58}Ni (p, p') spectrum measured at IUCF. Several states around $E_x = 10$ MeV are apparently enhanced in the (p, p') reaction, suggesting that they are $T_>$ ($T = 2$) states. The candidates for $T = 2$ states are indicated by arrows. For details, see the text.

Table 7
Corresponding analogue states observed in the (^{3}He, t) and (p, p') spectra and the R_{GT} values (see text). The B(GT) values (in arbitrary units), cross-sections, differences of excitation energies ΔE_x and determined T_f values are shown.

(^{3}He, t)		(p, p')		ΔE_x (MeV)	R_{GT}	T_f
E_x in ^{58}Cu (MeV)	B(GT) (a.u.)	E_x in ^{58}Ni (MeV)	Cross-section (mb/sr)			
8.837	0.190(11)	8.677	1.02(4)	0.160	1.16(13)	1
8.959	0.040(5)					0
9.000	0.077(7)	8.856	0.41(5)	0.144	1.17(20)	1
9.129	0.075(6)	8.959	0.32(4)	0.170	0.93(17)	1
9.172	0.064(7)					0
9.209	0.048(6)	9.071	0.35(4)	0.138	1.6(3)	1
9.307	0.054(7)	9.156	0.36(4)	0.151	1.4(3)	1
9.371	0.047(6)	9.242	0.17(4)	0.129	0.8(2)	1
9.444	0.044(7)	9.326	0.20(4)	0.118	1.0(3)	1
9.567	0.032(5)					0
9.645	0.073(6)	9.526[a]	0.37(4)	0.119	1.11(19)	1
9.783	0.026(6)					0
9.861	0.031(6)	9.739[b]	0.37(11)	0.122	2.6(9)	2
9.989	0.055(6)	9.835[c]	0.33(4)	0.154	1.3(3)	1
10.291	0.054(6)	10.115	0.22(4)	0.176	0.9(2)	1
10.329	0.040(7)	10.156[c]	0.17(4)	0.173	1.0(3)	1
10.388	0.027(8)	10.211[b,c]	0.41(4)	0.177	3.4(1.1)	2
10.554	0.033(6)					0
10.597	0.028(6)	10.492[b,c]	0.27(4)	0.105	2.2(6)	2
10.825	0.120(8)	10.664[b,c]	1.59(5)	0.161	3.0[d]	2
11.137	0.027(5)	11.003[b,c]	0.27(4)	0.134	2.3(6)	2
11.358	(0.014(5))	11.165	0.16(4)	0.193	2.7(1.2)	2
11.562	(0.021(5))	11.423[b]	0.15(4)	0.139	1.6(6)	(2)
11.815	(0.017(5))	11.672[b]	0.31(9)	0.143	4.2(1.9)	2
11.903	(0.017(5))					0
12.034	0.033(6)	11.883[b]	0.29(4)	0.151	2.1(5)	2

[a] Assigned as $E1$ state in Ref. [170].
[b] A corresponding state was found in the (d,^{2}He) spectrum [171,172].
[c] A corresponding state was observed in the (e, e') spectrum and identified to be $T = 2$ [173].
[d] R_{GT} value of 3.0 is given from the ratio of CG coefficients.

the value of three may come from the uncertainty in the background subtraction and/or the contribution of the isoscalar component in the (p, p') reaction.) It is rather clear that pairs of states are divided into two groups by the value of R_{GT}, and

it is suggested that those pairs with large R_{GT} have $T = 2$. The $T = 2$ states identified in the comparison are indicated by arrows in Fig. 33(b) [24].

For the identification of T, it is essential to find a one-to-one correspondence in the analogous GT and $M1_\sigma$ excitations. In this respect, high resolution measurements in IE and CE reactions were essential in the assignment of the isospin values of states.

The difference of the excitation energies of the analogue states in ^{58}Cu and ^{58}Ni, i.e., $\Delta E_x = E_x(^{58}\text{Cu}) - E_x(^{58}\text{Ni})$, are listed in column five of Table 7. The average value of 148 keV was smaller than the excitation energy of 203 keV of the IAS in ^{58}Cu.

As we see from Fig. 7, these $T = 2$ states are selectively excited in (n, p)-type reactions. The overall distribution of the GT strengths derived in the present T-decomposition analysis is in agreement with the result from the ^{58}Ni$(t, {}^3\text{He})$ ^{58}Co reaction performed at NSCL, MSU using a beam of $E(t) = 115$ MeV/nucleon with an energy resolution $\Delta E = 250$ keV (FWHM) [115], and also the result from the ^{58}Ni$(d, {}^2\text{He})$ ^{58}Co reaction performed at KVI using a beam of $E(d) = 85$ MeV/nucleon with $\Delta E \approx 130$ keV [171,172]. However, it was suggested that the GT strength distribution from the ^{58}Ni$(n, p)^{58}$Co reaction [174] was not consistent with that from the $(t, {}^3\text{He})$ reaction [115]. From a theoretical viewpoint, only shell-model calculations can predict the detail of these GT strength distributions in pf-shell nuclei. Large scale shell-model calculations have been performed using modern interactions, such as KB3G [175,176] or GXPF1 [177], and a comparison of the various theoretical results can be found in [178]. The comparison between the experimental and theoretical results is discussed in [24,115].

In both the ^{58}Ni$({}^3\text{He}, t)$ ^{58}Cu and ^{58}Ni(p, p') reactions, sharp states were observed with our resolution of ≈30 keV. As we have discussed in Section 6.1.2, states above the particle separation energies can have measurable widths. The proton separation energy S_p and the neutron separation energy S_n are 8.17 MeV and 12.2 MeV, respectively, in ^{58}Ni. Thinking of the Coulomb barrier (effectively ≈ several MeV high) which hinders the proton decay and also the centrifugal potential which hinders both proton and neutron decays, it is understandable to see no extra width even for the states with $E_x \sim 12$ MeV. Similarly, S_n in ^{58}Cu is as large as 12.43 MeV, but S_p is only 2.87 MeV.

In order to understand the existence of sharp peaks even in the $E_x \approx 10$–12 MeV region of ^{58}Cu, i.e., the region about 8 MeV above S_p, we have to consider the isospin selection rule associated with the proton decay. As we have seen, these sharp states are mainly of $T = 2$ ($T_>$) nature. After the decay, ^{58}Cu becomes a proton with $T_z = -1/2$ and $T = 1/2$ and ^{57}Ni with $T_z = -1/2$ and g.s isospin $T = 1/2$. Since the vector sum of two $T = 1/2$ states gives only $T = 0$ or 1, the proton decay from the $T = 2$ states in ^{58}Cu to the $T = 1/2$ g.s or other $T = 1/2$ states in ^{57}Ni is not allowed. The decays are possible only to the $T = 3/2$ excited states above $E_x = 5.2$ MeV in ^{57}Ni [179]. This means that the effective S_p for a $T = 2$ state in ^{58}Cu becomes 8.1 (=2.9 + 5.2) MeV or more. Therefore, the $T = 2$ GT states identified in the present analysis can, in principle, decay by proton emission, but due to the hindrance of the decay by the Coulomb barrier and the centrifugal potential, we find that they still retain their narrow widths even though they have high excitation energies of more than 10 MeV.

8.2. *Identification of isospin T in the $T_z = -1/2$ final nucleus* ^{27}Si

The schematic isospin structure and the transitions in $T_z = \pm 1/2$ and the neighbouring $T_z = \pm 3/2$ nuclei are shown in Fig. 3. Our interest here is to distinguish between the $T = 1/2$ and 3/2 states that can co-exist in the higher excitation region.

The $A = 27$ mirror nuclei ^{27}Al and ^{27}Si have $T_z = +1/2$ and $-1/2$, respectively and the low-lying states have $T = 1/2$. The lowest $T = 3/2$ (i.e., $T_>$) state appears at 6.814 and 6.626 MeV in ^{27}Al and ^{27}Si, respectively [180], and thus above these excitation energies, both $T = 1/2$ and 3/2 states can co-exist. For the identification of the $T_<$ and $T_>$ states of the analogous GT and $M1$ states and also for the study of the symmetry structure at higher energies in these $T_z = \pm 1/2$ nuclei, we can compare the spectra from the $({}^3\text{He}, t)$ and (p, p') reactions on the same initial nucleus ^{27}Al.

As explained in Section 5.3, the $\sigma\tau$-type interaction becomes important in the (p, p') reaction at 0° and the transition strengths are approximately proportional to those of the analogous GT transitions studied in the $({}^3\text{He}, t)$ reaction (see Eqs. (31) and (33)). However, the CG coefficients related to exciting the $T = 1/2$ and 3/2 states are different in these two reactions. The squared values of the CG coefficients (C^2) are 2/3 and 1/3 in the $({}^3\text{He}, t)$ reaction and 1/3 and 2/3 in the (p, p') reaction, suggesting that the transition strengths of the $T = 3/2$ states are enhanced by a factor of four in the (p, p') reaction compared to the $({}^3\text{He}, t)$ reaction, if the strength is normalised by the lower-lying $T = 1/2$ states, as summarised in Table 6.

The 0°, ^{27}Al$({}^3\text{He}, t)$ experiment was performed at RCNP using a ^{3}He beam with an energy of 140 MeV/nucleon, while the ^{27}Al(p, p') experiment at 0° was performed at IUCF, Indiana University using the $E_p = 160$ MeV proton beam [23]. The experimental details can be found in [24]. The $({}^3\text{He}, t)$ and (p, p') spectra obtained at 0° are shown in Fig. 34(a) and (b) for the $E_x = 8$–14 MeV region. The analysis of the angular distributions showed that most of the states observed in the $({}^3\text{He}, t)$ reaction, except weak ones, have $\Delta L = 0$ nature, suggesting that they are GT states. Since the g.s of ^{27}Al has a J^π value of $5/2^+$, the possible J^π values of the final states are $3/2^+$, $5/2^+$ and $7/2^+$. The vertical scales in the two panels of Fig. 34 are adjusted to get agreement for the heights of discrete states in the 8 MeV region, where it is known that states are mainly of $T = 1/2$ character. We can readily observe corresponding structures with similar intensities up to $E_x = 11$ MeV in both spectra although the final nuclei are different. In the higher E_x region, however, the level density becomes large and, in addition, we see many strongly excited states only in the (p, p') spectrum. It looks as if the spectra are different in this

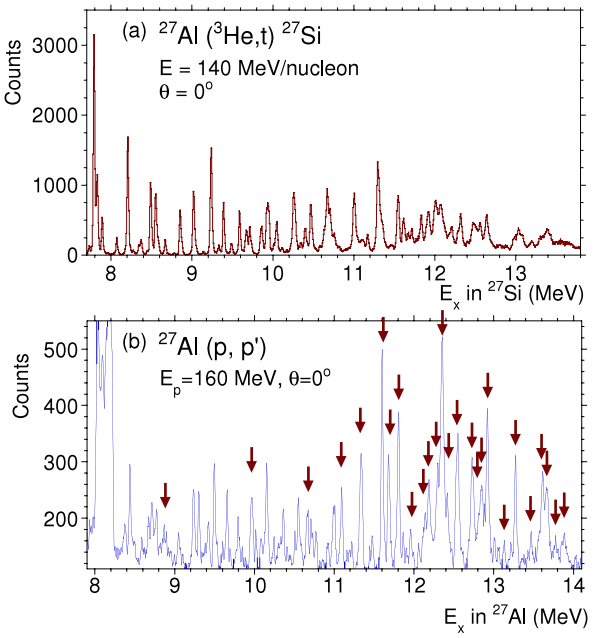

Fig. 34. The comparison of the ^{27}Al(^{3}He, t) ^{27}Si and ^{27}Al (p, p') spectra measured at 0° in the region of excitation energy where both $T = 1/2$ and 3/2 states co-exist. (a) The 0° ^{27}Al(^{3}He, t) ^{27}Si spectrum measured at RCNP with a resolution of 30 keV. (b) The 0° ^{27}Al (p, p') spectrum measured at IUCF with a resolution of 35 keV. Many states around $E_x = 12$ MeV are apparently enhanced in the (p, p') reaction, suggesting that they are $T_>$ $(T = 3/2)$ states. The candidates for $T = 3/2$ states are indicated by arrows. For details, see the text.

region. A closer look, however, shows the existence of corresponding structures, and in addition, corresponding states can be identified because of the energy resolutions of about 30 keV in both spectra.

Owing to the symmetry energy of the nuclear interaction, the centroid of the $T_>$ strength is situated at higher E_x than that of the $T_<$ strength, and thus it is expected that $T = 3/2$ states in ^{27}Si become dominant at higher excitation. Since excitation of these $T = 3/2$ states should be enhanced by a factor of four as a result of the difference in the CG coefficients, we selected states that are strongly enhanced in the (p, p') spectra as good candidates for $T = 3/2$ states. In the comparison, attention should be paid to the fact that the excitation energy of corresponding states as well as the transition strength may not be as perfect as is expected from the assumption of isospin symmetry. It is known that the Coulomb displacement energy of the corresponding states becomes larger as a function of E_x [43]. In addition isospin mixing can modify the strength distribution. The difference in the active operators is also important. In the (^{3}He, t) reaction, only the $\sigma\tau$-type nuclear interaction can make a contribution to the excitation of both $T_<$ and $T_>$ states, whereas for the $T_<$ excitation in the (p, p') reaction, the σ-type as well as $\sigma\tau$-type nuclear interaction and exchange term can contribute. Although it is usually said that the transition matrix element of the σ term is one order of magnitude smaller than that of the $\sigma\tau$ term at small q transfer [37], the cross term between the σ and $\sigma\tau$ terms can be large. Accordingly, the strengths of the $T = 1/2$ excitations in the (p, p') reaction may not represent the pure $\sigma\tau$ response of nuclei.

Those peaks which are enhanced in the (p, p') spectrum up to $E_x = 14$ MeV in ^{27}Al are indicated by arrows in Fig. 34(b). It should be noted that these $T = 3/2$ states in ^{27}Al in Fig. 3 are the analogues of the states in the $T_z = \pm 3/2$ nuclei ^{27}Mg and ^{27}P, which can be studied in the (n, p)-type reaction on ^{27}Al and the exotic (p, n)-type reaction on the unstable nucleus ^{27}Si, respectively. An ^{27}Al(d, ^{2}He) ^{27}Mg measurement at RIKEN [181] using an $E_d = 135$ MeV/nucleon beam showed the existence of a bump at $E_x = 5.6$ MeV in the GT strength with their resolution of about 600 keV. Since the g.s analogue of ^{27}Mg is at 6.8 MeV in ^{27}Al, we find that this bump structure corresponds well to the concentration of the discrete $T = 3/2$, $M1$ states seen around 12.5 MeV in Fig. 34(b). It should be noted that the structure of ^{27}Mg is not well known [182]. However, we could deduce its structure up to $E_x \approx 7.2$ MeV through the identification of $T = 3/2$ states up to $E_x = 14$ MeV. It is also suggested that the possible J^π values of these final states are $3/2^+$, $5/2^+$ or $7/2^+$.

It is rather difficult to study in detail the structures of $T_z = \pm 3/2$ nuclei in *sd* shell. However, if isospin symmetry is assumed, it was found that the structures of such $T_z = \pm 3/2$ nuclei can be deduced by identifying the $T = 3/2$ states in the highly excited region of $T_z = \pm 1/2$ nuclei.

9. Comparison of Gamow–Teller and $M1_{EM}$ transitions

Our aim in this section is to compare the transition strengths for the analogous $M1$ (or more precisely $M1_{EM}$) and GT transitions. As discussed in Section 3.2, there is a similarity in the form of the GT and $M1$ operators. The $\sigma\tau$ (IV spin) term is

common to both operators and is usually dominant. However, in the $M1$ operator, there are additional terms. They are the $\ell\tau$ (IV orbital) term and the isoscalar term. They can interfere constructively or destructively with the IV spin term.

9.1. Isoscalar and orbital contributions in $M1_{\rm EM}$ transitions

In the comparison of GT transitions with the analogous $M1$ transitions, a simple relationship is obtained for the transition strengths if the $\sigma\tau$ term is dominant in the $M1$ transition. From the comparison of Eqs. (10) and (3) in Section 3.2, and using $R_{\rm MEC}$ defined by Eq. (21), the "quasi" proportionality between B(GT) and $B(M1)$ is expressed as

$$B(M1) \approx \frac{3}{8\pi}(g_s^{\rm IV})^2\mu_N^2\frac{C_{M1}^2}{C_{\rm GT}^2}R_{\rm MEC}B({\rm GT}) = 2.644\mu_N^2\frac{C_{M1}^2}{C_{\rm GT}^2}R_{\rm MEC}B({\rm GT}). \tag{37}$$

Therefore, the value "renormalised $B(M1)$" defined by

$$B^R(M1) = \frac{1}{2.644\mu_N^2}\frac{C_{\rm GT}^2}{C_{M1}^2}B(M1) \tag{38}$$

can be compared directly with the values of B(GT).

In order to examine the interference of IS and IV orbital terms with the IV spin term in an $M1$ transition, we define the following ratio taking the effects of the MEC (Eq. (21)) into consideration [43],

$$R_{\rm ISO} = \frac{1}{R_{\rm MEC}}\frac{B^R(M1)}{B({\rm GT})}. \tag{39}$$

By comparing Eqs. (10) and (3), it is seen that $R_{\rm ISO} > 1$ usually indicates that the IS term and/or the IV orbital term make a constructive contribution to the IV spin term, while $R_{\rm ISO} < 1$ shows a destructive contribution. As discussed in [32,114], the contribution of the IS term is minor. Therefore, it is expected that the deviation of $R_{\rm ISO}$ from unity mainly shows a contribution of the IV orbital term in each $M1$ transition.

9.2. Large orbital contributions in the $M1_{\rm EM}$ transitions in deformed nuclei

We examine the $M1$ γ decays in the $T_z = 1/2$, ^{23}Na nucleus and compare the $M1$ transition strengths with the GT strengths obtained from the ^{23}Na(^{3}He, t) ^{23}Mg reaction. As we have seen in Section 6.2, the mirror nuclei ^{23}Na and ^{23}Mg are well deformed. The jth state with $J_j^\pi = 1/2^+, 3/2^+$, and $5/2^+$ can decay directly to the $J_0^\pi = 3/2^+$ g.s by $M1$ transitions. The $M1$ γ-transition strength $B(M1)\downarrow$ (in units of μ_N^2) from an excited state to the g.s of ^{23}Na is calculated using the measured lifetime (mean life) τ_m (in units of seconds), gamma-ray branching ratio b_γ (in %) to the g.s, $E2$ and $M1$ mixing ratio δ and the γ-ray energy E_γ (in MeV). The relationship among these quantities is given (see e.g. [33]) by

$$B(M1)\downarrow = \frac{1}{\tau_m}\frac{1}{E_\gamma^3}\frac{b_\gamma}{100}\frac{1}{1+\delta^2}\frac{1}{1.76\times10^{13}}. \tag{40}$$

The $B(M1)\downarrow$ values were calculated up to $\approx S_p$ of 8.79 MeV for all states that may possibly have these three J^π values using data compiled in [180]. The γ-decay data were far from complete, because either lifetime and/or branching ratio were often missing for many states above $E_x = 6$ MeV. For some of the transitions, the $E2$ and $M1$ mixing ratios δ were not available. For them $\delta = 0$ was assumed, and thus only upper-bound values of $B(M1)\downarrow$ were obtained. In order to determine the $B(M1)\uparrow$ values, the $2J+1$ factors for the initial and final states were corrected by

$$B(M1)\uparrow = \frac{2J_j+1}{2J_0+1}B(M1)\downarrow. \tag{41}$$

In Eq. (38), the ratio of squared CG coefficients for a transition from a $T_i = 1/2$ state to a $T_f = 1/2$ state in mirror nuclei is 2. Therefore, we find that the $B^R(M1) = (2/2.644\mu_N^2)B(M1)\uparrow$ value can be compared directly with the corresponding values of B(GT). The $B^R(M1)$ values for the excited states of ^{23}Na are shown in Fig. 35(b). From the comparison with the B(GT) distributions shown in Fig. 35(a), we see that some $M1$ transitions, even strong transitions, are strongly enhanced compared to the analogous GT transitions, suggesting large orbital contributions, while in some others, almost no orbital contribution was found. The low-lying spectra of odd-A deformed nuclei can be analysed in terms of the rotational bands formed on intrinsic configurations, which are specified by the quantum numbers of the Nilsson orbit of the odd particle. We analyse such a large difference of the orbital contributions on the basis of the different selection rules for ℓ and σ operators in transitions connecting different deformed bands [114].

Let us consider an odd A, deformed nucleus with an even–even core. Under the assumption that the nucleus is symmetrical about the z axis, the single-particle orbits (Nilsson orbits) are labelled by using the asymptotic quantum numbers $K^\pi[Nn_z\Lambda]$ (see Section 6.2 for the asymptotic quantum numbers). We note Λ and Σ ($=s_z$) are the projection of the orbital angular momentum and the spin along the z axis, respectively, and $K = \Lambda + \Sigma$ holds. On top of each single-particle orbit, a rotational band with $J = K, K+1, \ldots$ is formed.

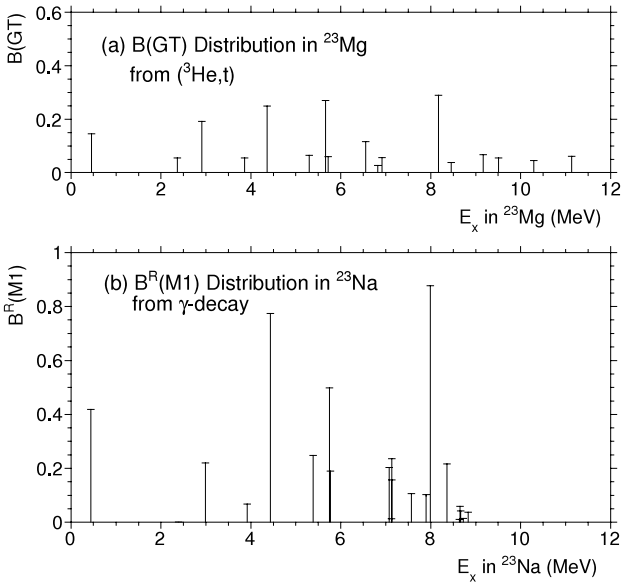

Fig. 35. Comparison of $B(\mathrm{GT})$ and $B^R(M1)$ strength distributions. (a) $B(\mathrm{GT})$ strength distribution from the ^{23}Na(^{3}He, t) ^{23}Mg reaction. (b) $B^R(M1)$ strength distribution in ^{23}Na deduced from γ-decay data.

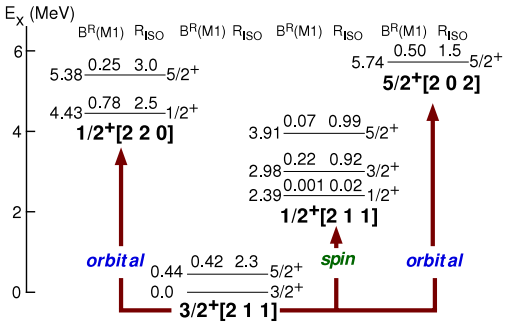

Fig. 36. Proposed band structure for the low-lying positive-parity states of ^{23}Na. Each band is specified by the asymptotic quantum numbers $K^\pi[Nn_z\Lambda]$. The $B^R(M1)$ value, which is proportional to $B(M1)\uparrow$, and the ratio R_{ISO} are also indicated. Each state is identified by its E_x (in MeV) and J^π value.

The proposed band structure for the low-lying positive-parity states of ^{23}Na, based on the Nilsson-orbit classification [139], is shown in Fig. 36. We study the possible contributions of σ and ℓ operators for the intra-band and inter-band transitions between the rotational bands specified by the asymptotic quantum numbers $K^\pi[Nn_z\Lambda]$.

(a) Intra-band transitions

In intra-band transitions, asymptotic quantum numbers of intrinsic motion do not change. The matrix elements for the operators ℓ_z and σ_z are given by

$$\langle K^\pi[Nn_z\Lambda]|\ell_z|K^\pi[Nn_z\Lambda]\rangle = \Lambda, \quad \text{and} \quad \langle K^\pi[Nn_z\Lambda]|\sigma_z|K^\pi[Nn_z\Lambda]\rangle = 2\Sigma, \tag{42}$$

respectively. Therefore both orbital and spin contributions are expected in the intra-band $M1$ transitions.

The transition from the $J^\pi = 3/2^+$ g.s to the 0.44 MeV, $5/2^+$ state is an intra-band transition (see Fig. 36). The R_{ISO} of 2.3 is much larger than unity. Since the major component of the $3/2^+[2\,1\,1]$ orbit is $d_{5/2}$, constructive interference is expected between the ℓ and σ contributions for this transition [114]. This rather large experimental R_{ISO} value suggests a relatively large orbital contribution because of this constructive interference.

Both $\ell_\pm$ and $\sigma_\pm$ operators cause inter-band transitions. However, it should be noted that they connect bands of different character.

(b) Transitions caused by the $\ell_\pm$ operator

Operators $\ell_\pm$ can cause transitions between states in different rotational bands. By applying ℓ_+, we get

$$\ell_+|K^\pi[Nn_z\Lambda]\rangle \propto |(K+1)^\pi[Nn_z \pm 1\Lambda+1]\rangle, \tag{43}$$

and by applying ℓ_-, we get

$$\ell_-|K^\pi[Nn_z\Lambda]\rangle \propto |(K-1)^\pi[Nn_z \pm 1\Lambda-1]\rangle, \tag{44}$$

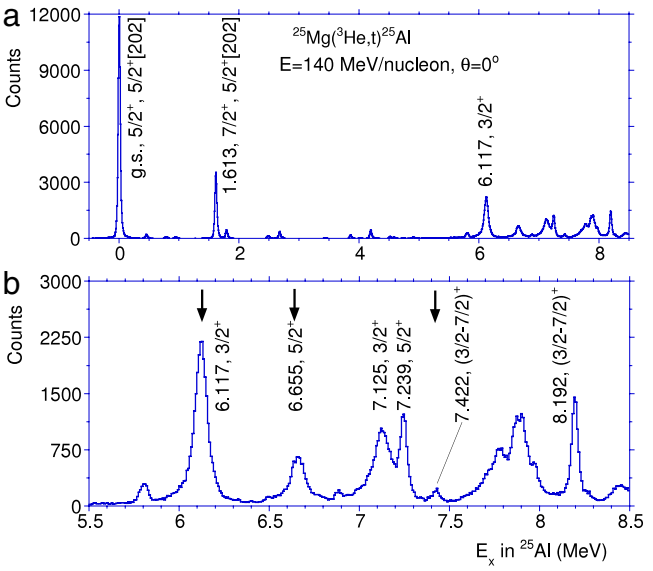

Fig. 37. The ^{25}Mg(^{3}He, t) ^{25}Al reaction spectra of (a) the range up to the excitation energy of 8.5 MeV and (b) expanded 5.5–8.5 MeV region. The members of the $3/2^+[2\,0\,2]$ rotational band are indicated by arrows. The "desert region" spreading between 2–6 MeV region is discussed in Section 6.2.

where the relationship $0 \leq n_z \pm 1 \leq N$ and $0 \leq \Lambda \pm 1 \leq N$ should hold. Therefore $\ell_\pm$ connect the bands in which the asymptotic quantum numbers n_z and Λ change by one unit.

The 4.43 MeV, $J^\pi = 1/2^+$ and the 5.38 MeV, $5/2^+$ states are assigned to be members of the $1/2^+[2\,2\,0]$ band [139]. In the transitions from the g.s to these states, the asymptotic quantum number Λ decreases by one unit. Therefore, the transitions should be caused by the ℓ_- operator, and the contribution of σ is only through the admixture of wave functions from orbits other than $1/2^+[2\,2\,0]$. The $R_{\rm ISO}$ values are large for these transitions.

The $J = 5/2$, 5.74 MeV state in ^{23}Na is assigned to be the band-head state of the band $5/2^+[2\,0\,2]$ [139], and its analogue state is at $E_x = 5.66$ MeV in ^{23}Mg [180]. The $M1$ transition from the g.s is the second strongest in the low-lying region. Because of its $\Delta\Lambda = 1$ nature, the $M1$ transition should be caused by the ℓ_+ operator. However, the $R_{\rm ISO}$ value of 1.5 obtained was not so large. It is suggested that some contribution from the σ operator exists in this case. The B(GT) value to the analogue 5.66 MeV state in ^{23}Mg is large in the analysis of the ^{23}Na(^{3}He, t) reaction (see Fig. 35(a)).

(c) Transitions caused by the $\sigma_\pm$ operator

By applying $\sigma_\pm$, we get

$$\sigma_\pm |K^\pi[Nn_z\Lambda]\rangle \propto \delta(\Omega, \Lambda \mp 1/2)|(K \pm 1)^\pi[Nn_z\Lambda]\rangle. \tag{45}$$

As expected, the $\sigma_\pm$ operator causes transitions in which the asymptotic quantum number Σ, and thus K changes by one unit.

Starting from the $J = 3/2$ g.s of the $3/2^+[2\,1\,1]$ band, transitions to the $J = 1/2$, $3/2$, and $5/2$ states of the $1/2^+[2\,1\,1]$ band at 2.39, 2.98, and 3.91 MeV are allowed by the σ_- operator. The $R_{\rm ISO}$ values obtained for the latter two transitions, assuming $R_{\rm MEC} = 1.25$ [32], are nearly unity, in agreement with the expectation that the transitions are caused mainly by the σ_- operator.

As we have seen, by comparing the strengths of analogous $M1$ ($M1_{\rm EM}$) and GT transitions, we see the contribution of the $\ell\tau$ term that is inherent to the $M1$ transition. The contribution can be large in deformed nuclei and thus the $R_{\rm ISO}$ value gives us a good hint for specifying the Nilsson orbits involved in the transition, especially in combination with the K selection rule for GT and $M1$ transitions (see Section 3.1). Since the $M1$ transitions can be studied not only in the γ-decay measurements, but also in (e, e') reactions, the $R_{\rm ISO}$ values can be obtained even for the transitions to the high E_x region.

We see a good example in the identification of the $3/2^+[2\,0\,2]$ orbit in the deformed nuclei ^{25}Mg and ^{25}Al [183]. It is the highest-lying orbit among the six Nilsson orbits in the prolate deformed *sd*-shell nuclei and was never properly identified for more than 50 years after its prediction by Nilsson [184,185]. This orbit would lie in the low-lying region for nuclei with neutron or proton numbers N or $Z \approx 19$. Therefore, the expectation was that this orbit would not be observed, because nuclei with these values of N or Z located near the stability line are not deformed due to the shell closure at Z and/or $N = 20$. Therefore, the $3/2^+[2\,0\,2]$ orbit was sought in the well deformed lighter mass nuclei ^{25}Mg and ^{25}Al but at higher E_x. As a result of an examination of the ^{25}Mg(^{3}He, t) ^{25}Al spectrum at 0°, it was found that the $E_x = 6.117$ MeV, $J^\pi = 3/2^+$ state in ^{25}Al was the band-head state of the $3/2^+[2\,0\,2]$ orbit connected by the K-allowed GT transition from the $J^\pi = K^\pi = 5/2^+$ g.s of ^{25}Mg. The excited $5/2^+$ and $7/2^+$ members were also clearly assigned at 6.655 and 7.422 MeV, respectively, as shown in Fig. 37.

In making the assignment, the difficulty was how to distinguish two possible $K^\pi = 3/2^+$ bands, i.e., (a) the $3/2^+[2\,1\,1]$ neutron–hole band made in the $\nu 3/2^+[2\,1\,1] \rightarrow \pi 5/2^+[2\,0\,2]$ transition, and (b) the $\pi 3/2^+[2\,0\,2]$ particle band made in the $\nu 5/2^+[2\,0\,2] \rightarrow \pi 3/2^+[2\,0\,2]$ transition, where both of them were expected to appear in the same E_x region. Therefore, the derived B(GT) value for the transition from the g.s of ^{25}Mg to the 6.117 MeV in ^{25}Al was compared with the $B(M1)$ values of the corresponding analogous $M1$ transition studied in γ-decay and (e, e') measurements for ^{25}Mg. It was found that the analogous $M1$ transition was weaker than the strength obtained by assuming only the $\sigma\tau$ contribution ($R_{\rm ISO} < 1$) showing that the IV spin term and the IV orbital term interfere destructively. Since constructive interference was predicted in the theoretical calculation [12] for the case (a), and destructive interference for the case (b), the experimental finding was consistent with the prediction assuming that the 6.117 MeV state is the band-head state of the $3/2^+[2\,0\,2]$ orbit.

As expected, the $3/2^+[2\,0\,2]$ band is situated higher (in the region of $E_x = 6$–7.5 MeV) than other well established bands (see Fig. 25) [12,140]. In order to compare the results with the γ-decay and (e, e') results and also to identify the band members in the region of high level density, the high resolution in the CE reaction spectrum was important.

10. Observation of Gamow–Teller resonance structures in charge-exchange reactions and β-decay

The residual interaction for a neutron and proton in a particle–hole (p–h) configuration is known to be strongly repulsive, particularly for cases where the particles are spin–orbit partners and couple to $J = 1$, e.g. in the $\pi f_{7/2}^{-1} \nu f_{5/2}$ configuration. In contrast, the residual interaction for p–p and h–h configurations is attractive [186]. A repulsive (attractive) residual interaction pushes the strength up (down) to higher (lower) excitation energy than the energy expected without such residual interactions.

It should be noted that in heavy stable nuclei, the neutron excess becomes large. Thus, the configurations of states populated by GT transitions in β^--type CE reactions from even–even nuclei have in most cases p–h nature. As a result, the main part of the GT strength in heavy nuclei is pushed up to a region higher than the energy difference of the LS partner orbits ($\Delta E_{LS} = |\epsilon(j_<) - \epsilon(j_>)|$). The resonance structures excited in GT transitions (GTR) were first reported by the Michigan group [187] and have been studied intensively at IUCF, Indiana using (p, n) reactions at intermediate energies [4,110, 188–191] and also at RCNP, Osaka [8]. However, in a few limited cases, i.e., when the initial nuclei are ^{6}He (^{6}Be), ^{18}O (^{18}Ne) or ^{42}Ca (^{42}Ti) in which two neutrons (protons) sit on top of doubly LS-closed inert core nuclei, namely ^{4}He, ^{16}O and ^{40}Ca, respectively, states of particle–particle (p–p) character can be formed by the β^--type (β^+-type) GT transitions in the final nuclei ^{6}Li, ^{18}F and ^{42}Sc. In these cases, the main part of the GT strength is pulled down to the low-lying region. As a result the GT strengths observed in such reactions exhibit a wide variety of distributions.

10.1. Development of Gamow–Teller resonance structure in pf-shell Nuclei

In nuclei lighter than the sd shell, we do not observe a prominent resonance structure in the GT strengths in β^--type CE reactions. However, in nuclei heavier than the iron isotopes, we see well-developed GTRs [4]. Therefore, it is expected that we should observe the development of the GTR structure in the f-shell region.

As mentioned above, the main configurations of the GTRs of the $N > Z$ nuclei are of p–h nature. The observation of a GTR at much higher E_x than the energy gap between the $j_<$ and $j_>$ orbits can be explained by the repulsive p–h interaction but, in a few rare cases, p–p configurations can be formed if the transitions start from nuclei having two nucleons outside a doubly closed shell.

There then arises a simple question of how the attractive p–p (or h–h) interaction competes with the repulsive p–h interaction in the IV, GT excitation. We find that such a competition can be studied by examining the mass dependence of the strength distribution of GT transitions starting from the $N = Z + 2$ ($T_z = 1$) even–even, $f_{7/2}$-shell nuclei and leading to the $N = Z$ ($T_z = 0$) odd–odd nuclei. We can study these transitions for the nuclei with $A = 42$, 46, 50 and 54, where the initial nuclei are ^{42}Ca, ^{46}Ti, ^{50}Cr and ^{54}Fe, respectively. As mass A increases, the $f_{7/2}$ orbit with $j_>$ nature will be filled gradually on top of the ^{40}Ca inert core, and the $\nu f_{7/2}$ orbit is filled completely in ^{54}Fe. On the other hand, the $f_{5/2}$ orbit with $j_<$ nature always remains empty (see Fig. 38). Therefore, the transitions between single-particle orbits contributing to the GT transitions in these $A = 42$, 46, 50 and 54 systems are always the same, i.e., $\nu f_{7/2} \rightarrow \pi f_{7/2}$ and $\nu f_{7/2} \rightarrow \pi f_{5/2}$, but their character changes from p–p, p–p starting from ^{42}Ca to h–h, p–h in the ^{54}Fe case.

Since the T_z values of the initial nuclei are all identical ($T_z = 1$), one would anticipate that the total GT strengths would be similar [90]. In addition, the strength distribution is not affected by the isospin CG coefficients that re-distribute the GT strength among the final $T = T_0 - 1$, T_0 and $T_0 + 1$ states [24,32] because the initial state always has $T_0 = 1$.

In the $A = 42$ system, as a result of GT transitions one neutron and one proton remain outside of the ^{40}Ca inert core. Therefore, we see that the two final configurations, i.e., both $(\pi f_{7/2}, \nu f_{7/2})$ and $(\pi f_{5/2}, \nu f_{7/2})$ have p–p nature formed on top of the ^{40}Ca inert core, as we see in Fig. 38. These p–p configurations should have attractive nature. As A increases, both $\nu f_{7/2}$ and $\pi f_{7/2}$ orbits are filled gradually. Accordingly the $(\pi f_{5/2}, \nu f_{7/2})$ configuration loses its p–p nature and finally in the $A = 54$ system, the $\nu f_{7/2}$ orbit in this final configuration has the nature of a pure hole. Therefore, this configuration now has repulsive p–h nature. The $(\pi f_{7/2}, \nu f_{7/2})$ configuration also loses its p–p nature as A increases, but in $A = 54$ it again has attractive h–h nature.

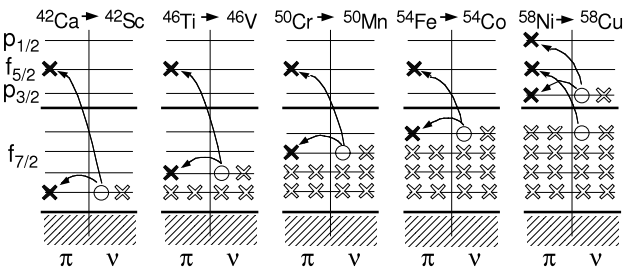

Fig. 38. Allowed configurations for GT$_-$ transitions starting from $T_Z = +1$, f-shell nuclei ^{42}Ca, ^{46}Ti, ^{50}Cr and ^{54}Fe to $T_Z = 0$ nuclei ^{42}Sc, ^{46}V, ^{50}Mn and ^{54}Co, where the simplest shell structure is assumed. The filled orbits of protons (π) and neutrons (ν) are shown by open crosses. The newly created holes and particles following the transitions are shown by the open circles and filled crosses, respectively. More configurations are involved in the transitions from the pf-shell nucleus ^{58}Ni.

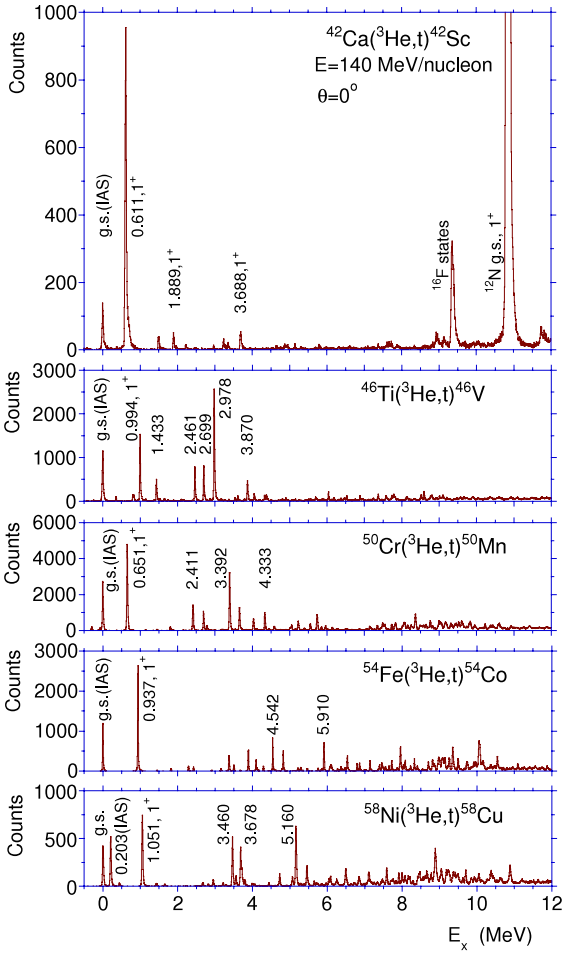

Fig. 39. High energy resolution (^{3}He, t) spectra for the f-shell, $T_z = +1$ target nuclei ^{42}Ca, ^{46}Ti, ^{50}Cr and ^{54}Fe and also for the pf-shell nucleus ^{58}Ni. An energy resolution of ≈30 keV was obtained. The angular distributions suggest that strongly populated states are GT states with $\Delta L = 0$. The vertical scale is normalised with the heights of the IAS peaks all having B(F) = 2. Since the ratio of strengths of the τ and $\sigma\tau$-type nucleon–nucleon interaction changes only slowly as a function of mass number A, we expect the heights of the peaks to reflect the B(GT) values assuming the proportionality between the 0° cross-section and the B(GT) and ignoring kinematical effects. As A increases from 42 to 54, the GT states are more fragmented and more GT strength is found in a higher energy region of 7–12 MeV. In ^{58}Cu, strengths below 4 MeV revive because of the contribution of the p-shell configurations.

With the splendid resolutions of 25–40 keV, the GT strength distributions of the transitions starting from the $T_z = +1$ target nuclei with $A = 42$–56 were studied in detail in the (^{3}He, t) reaction as shown in Fig. 39. The analysis of the angular distribution for each transition shows that most of the strong transitions have $\Delta L = 0$ nature and are GT excitations. We see that the Gamow–Teller (GT) strength that is concentrated in one low-lying state in the lightest odd–odd $N = Z$ f-shell

nucleus ^{42}Sc moves to higher energy with the increase in mass A, and finally forms a resonance structure in the heaviest f-shell nucleus ^{54}Co.

In ^{42}Sc, it is clear that the GT strengths are pulled down and accumulate in the 0.61 MeV, 1^+ state. This feature can be explained by the fact that both the $(\pi f_{7/2}, \nu f_{7/2})$ and $(\pi f_{5/2}, \nu f_{7/2})$ configurations have the attractive p–p nature in ^{42}Sc (see Fig. 38). On the other hand in ^{54}Co, where the $(\pi f_{5/2}, \nu f_{7/2})$ configuration is of the repulsive p–h character, the main part of the GT strength is pushed up. The $(\pi f_{7/2}, \nu f_{7/2})$ configuration has attractive h–h nature, but only 10%–15% of the observed GT strength remains in the first 1^+ state. The overall repulsive nature of the residual interaction in ^{54}Co can be understood in terms of the numbers of available transitions that make up the $(\pi f_{5/2}, \nu f_{7/2})$, p–h configuration and the $(\pi f_{7/2}, \nu f_{7/2})$, h–h configuration. If we assume a simple shell structure, they are 48 and 16, respectively.

It should be noted that the pure p–p configuration in ^{42}Sc (i.e., $(\pi f_{7/2}, \nu f_{7/2})$) having a small intrinsic energy can be realised due to the "charge-exchange" nature of the GT transition, in which the conversion of an $f_{7/2}$ neutron into a proton in the identical $f_{7/2}$ shell is allowed. (In IE excitations, on the other hand, a proton (or a neutron) remains as it is. Therefore, transitions inside a shell do not make any sense.) The existence of the p–p configuration is also due to the simplicity of the $\sigma\tau$ operator that cannot change the spacial part of the initial and final wave functions, and thus the simple configurations consisting of only $j_>$ and $j_<$ orbits can be excited.

10.2. Structure of Gamow–Teller resonances in a Sn isotope

In the (p, n) reactions performed at intermediate incident energies in the 1980s [4], a broad bump-like structure due to the GTR was always observed for nuclei with mass A larger than ≈60. As shown in Fig. 18, the broad bump of the GTR observed in the ^{58}Ni(p, n) ^{58}Cu reaction was resolved into fine structure and sharp states in the high resolution ^{58}Ni$(^3$He, $t)$ ^{58}Cu measurement [24]. It is thus of interest to study whether such fine structures can be found in even heavier nuclei if they are studied with high resolution. The level density of states excited in GT transitions is thus another topic of interest. We select ^{118}Sn as the target nucleus. It is a representative, spherical medium–heavy nucleus.

The ^{118}Sn$(^3$He, $t)$ ^{118}Sb spectrum taken at 0° with a resolution of 30 keV is shown in Fig. 40. The g.s of ^{118}Sb has $J^\pi = 1^+$, and the g.s–g.s transition starting from the 0^+ g.s of ^{118}Sn is a GT transition. Since the B(GT) value for this transition is well determined in the β-decay study of ^{118}Sb, we can get the unit GT cross-section $\hat{\sigma}^{\mathrm{GT}}(0°)$. Then, using Eq. (31), the B(GT) values can be deduced for the transitions to excited states. In this spectrum, the 51 keV, 3^+ state in ^{118}Sb was clearly recognised as a skirt on the g.s peak, and we expect to get a reliable cross-section for the g.s–g.s transition.

The proton separation energy S_p is 4.887(3) MeV in ^{118}Sb. Therefore, below this energy the decay width should be small and we should see discrete states. We see that the low-lying states below $E_x = 2$ MeV are well separated. In the energy region between 2–4 MeV, however, we see fine structures, but the spectra are not decomposed into states even with our resolution of 30 keV. Above this energy region, only the IAS has been clearly observed as a discrete state. The IAS is apparently wider than the g.s, with the decay width being due to isospin mixing [192,193].

In ^{118}Sb, it is interesting to see that the GT strength is divided into four parts, i.e., the g.s, the clustering states in $E_x = 1$–2 MeV, 2–4 MeV, a bump-like structure at 4–8 MeV and the GTR structure with $E_x = 8$–15 MeV. The bump-like structure at 4–8 MeV is called a pygmy GT resonance [194]. It should be stressed that the existence of such a complicated structure even in a nucleus with a relatively high mass of $A = 118$ is a challenge to the understanding of nuclear structure.

Whether fine structures exist in the bump-like structure of the GTR is another interesting subject. By analysing the high resolution ^{90}Zr$(^3$He, $t)$ ^{90}Nb data using a "wavelet analysis" technique, characteristic energy scales were extracted [195].

10.3. The Gamow–Teller resonance observed in the β^+ decay of ^{150}Ho

As explained in Section 2.6.2, when we depart from the $N \simeq Z$ region and move towards heavy, neutron-deficient nuclei, β^+ decay is, in general, inhibited (see panel (f) in Fig. 10). An exceptional case is found when the $j_>$ state is occupied by protons and the $j_<$ orbit is still empty on the neutron side. Now, only the $\pi j_> \to \nu j_<$ transition takes place. In general, such a transition proceeds to low-lying states in the daughter nucleus and no GT resonance structure is formed. However, in the decay of an odd–odd nucleus, provided that a GT transition demands the breaking of a pair of particles in the $j_>$ orbit, the final states can lie at relatively high energy but still inside the Q_β-window.

Here we present such a case, the β^+ decay of a neutron-deficient, odd–odd heavy nucleus ^{150}Ho $(Z = 67, N = 83)$ with a relatively high Q_β-value of 7.3 MeV. The nucleus ^{150}Ho with a β-decaying isomer of $J^\pi = 2^-$ is of particular interest because its β^+ decay to states in ^{150}Dy is configuration forbidden at low excitation energy, and allowed at ∼5 MeV. This is the first case where the GT resonance structure has been clearly observed in β decay. Our aim was to study both the fine structure of the GTR and obtain reliable B(GT) values. Therefore, this β^+ decay was measured using both high resolution Ge detectors and a TAS spectrometer [196,197].

Fig. 41 gives a schematic view of the relevant single-particle orbits available above the ^{146}Gd doubly closed shell [198]. It also shows the expected configuration of the ^{150}Ho, 2^- isomer with the odd neutron in the $f_{7/2}$ orbit and a proton in the $d_{3/2}$ orbit. A pair of protons, which couple to 0^+, can partially occupy all three of the $s_{1/2}$, $h_{11/2}$ and $d_{3/2}$ orbits. As we see from Fig. 41, since the only allowed GT transition is from the $\pi h_{11/2}$ to the $\nu h_{9/2}$ orbit, the decay requires the breaking of an

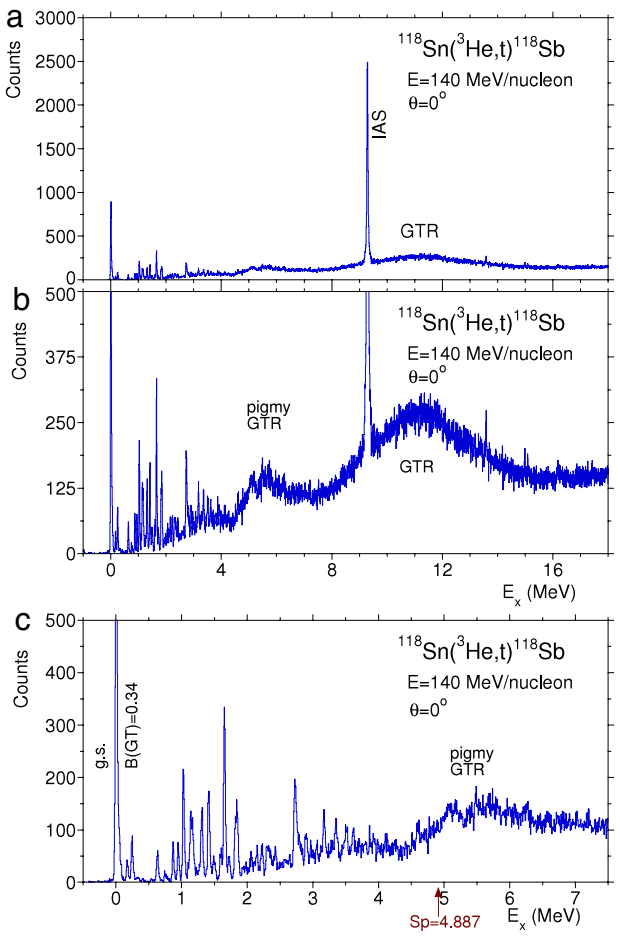

Fig. 40. (a) ^{118}Sn(^{3}He, t) ^{118}Sb spectrum. The discrete g.s, low-lying states, and the IAS are prominent. (b) ^{118}Sn(^{3}He, t) ^{118}Sb spectrum with an expanded vertical scale. (c) ^{118}Sn(^{3}He, t) ^{118}Sb spectrum with expanded vertical and energy scales.

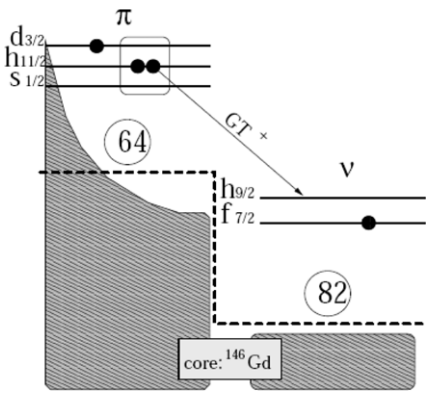

Fig. 41. Schematic view of the s.p. orbits available above the ^{146}Gd doubly closed shell and the allowed GT transition in the β^+ decay of the $J^\pi = 2^-$ isomeric state of ^{150}Ho.

$h_{11/2}$ proton pair in the parent 2^- state. This breaking of the $h_{11/2}$ pair requires extra energy and it is expected that the GT strength will lie at relatively high E_x.

The four-particle states with spins and parities $1^-, 2^-$ and 3^- populated in the ^{150}Dy daughter nucleus have the configurations $[(\pi d_{3/2} - \nu f_{7/2})\,(\pi h_{11/2} - \nu h_{9/2})]$. A simple approximation to the excitation energy of these states is just twice the pairing gap for protons plus twice the pairing gap for neutrons plus the neutron $h_{9/2}$ s.p. energy, i.e. at ≈4.5 MeV excitation energy. This is well within the Q_β-window for this decay. It should be noted that this decay is closely connected

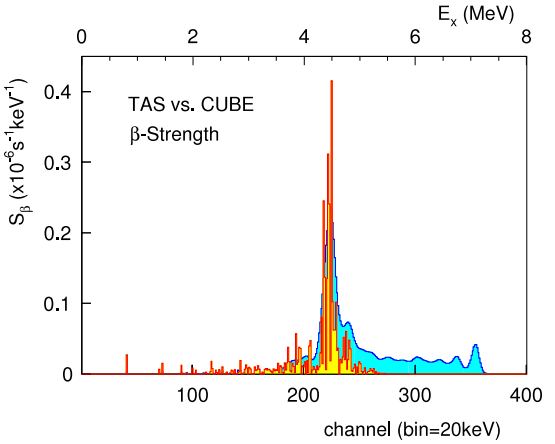

Fig. 42. The β-decay strength as a function of E_x in the daughter nucleus ^{150}Dy following the β decay of the ^{150}Ho 2^- state measured with the CLUSTER CUBE (sharp lines) and the GSI–TAS (continuous function) [197].

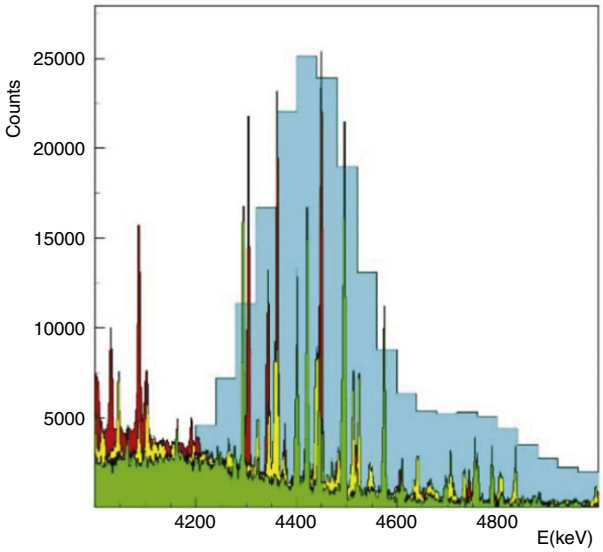

Fig. 43. Comparison of part of the GSI–TAS and CLUSTER CUBE spectra (with various coincidence gates) for the decay of the ^{150}Ho, 2^- isomer state measured with the CLUSTER CUBE (sharp peaks) and the GSI–TAS (continuous spectrum) [197]. The horizontal axis represents the excitation energy in the final nucleus for the TAS spectrum. For the γ rays (sharp peaks) the energy of the gating transition has been added to match the excitation energy.

to the decay of ^{148}Dy, a simpler case, since it has just a single proton pair outside the ^{146}Gd core. The two cases must clearly be much the same and should have a comparable logft, namely 3.95(3) [199]. It will, of course, be slightly different because of the presence of the $d_{3/2}$ proton, which will modify the probability of the proton pair occupying the $\pi h_{11/2}$ orbit. With this minor caveat we can say that we expect the ^{150}Ho, 2^- state to decay strongly to levels at $\approx$4.5 MeV with a logft of about 3.9.

The work was carried out using both the GSI–TAS [69] for the total absorption (γ-ray) spectroscopy (TAS) and a Ge array called the "CLUSTER CUBE" for the high resolution and high efficiency measurement of individual γ rays. This array consisted of six EUROBALL cluster detectors [200] in a highly compact geometry, with four of the detectors 10.2 cm from the source and the other two at a distance of 11.3 cm. The photopeak efficiency of the array was 10.2(0.5)% at 1332 keV. The number of γ-ray lines observed by the CLUSTER CUBE and located in the decay scheme was 1064, which were arranged into a decay scheme with 295 levels. These numbers show the high quality of the measurement.

In Fig. 42, β-decay strength distributions are shown as a function of excitation energy for the measurements using the GSI–TAS and the CLUSTER CUBE. In this study an analysis, based on the shell model, provided a prediction of the distribution of B(GT) strength between the 1^-, 2^- and 3^- states of 3.6:4.0:7.4 normalised to 15 arbitrary units [197]. In the experiment the possible J^π values 1^-, 2^- and 3^- of the final states could be assigned by analysing the decay pattern to the states of known J^π. Using these assignments it was possible to estimate the B(GT) strength distribution to the states with $J^\pi = 1^-, 2^-$ and 3^-. The resulting ratios of 3.4:4.2:7.4 were consistent with the theoretical estimate.

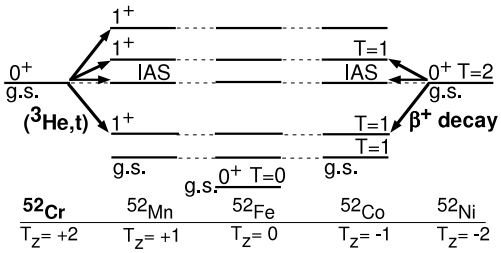

Fig. 44. Schematic view of the analogue states and the isospin symmetry transitions in the mass $A = 52$, $T = 2$ quintet, where the Coulomb energy is removed. The (^{3}He, t) reaction provides information on the $T_z = +2 \rightarrow +1$ GT transitions and the Fermi transition to the IAS, while the β decay allows us to study the analogous transitions with $T_z = -2 \rightarrow -1$.

In Fig. 42, one can see clearly the distinctive feature of the spectra from both types of spectrometer, namely the strong β feeding to a narrow interval of about 240 keV at 4.4 MeV excitation. This is the $\pi h_{11/2}$ to $\nu h_{9/2}$ transition that we expected to see. The resonance structure is similar to those observed in CE reactions on heavy nuclei. The excitation energy of this GTR structure is more or less in agreement with the predicted value [197]. The two spectra have the same shape, which gives confidence in the analysis techniques used for the TAS spectrum. There is, however, a clear loss in sensitivity in the CLUSTER CUBE spectrum at higher energies. If we take the total B(GT) up to the Q_β-window then we miss, in total, 50% of the B(GT) in this high quality Ge measurement.

On the other hand the individual levels and γ transitions can only be disentangled in the spectra from the CLUSTER CUBE. Therefore, we see a wealth of fine structure in the GTR in Fig. 43. The GTR structure measured with the GSI–TAS is compared with the spectra from some coincidence gates showing γ rays de-exciting levels in the same region. This is the clearest example of the observation of the GTR structure studied in β decay up to now.

Using the same GSI–TAS, similar resonance structures have also been observed in the study of allowed GT transitions to nuclei close to the doubly magic nucleus ^{100}Sn [201–203].

These examples demonstrate the need for the use of both TAS and high resolution Ge measurements. The TAS measurements are essential because it is the only way to obtain a proper measure of the GT decay strength in heavy nuclei. The high resolution measurements are also essential if one wants to study the details of the level scheme and the fine structure of the resonance.

11. Studies of Gamow–Teller transitions in exotic nuclei

The *rp*-process of nucleosynthesis proceeds through nuclei near the proton drip-line, in which GT transitions starting from unstable *pf*-shell nuclei play important roles. Therefore, the study of these GT transitions is one of the key issues in nuclear astrophysics [3,141]. Our knowledge of these transitions, especially the GT transitions starting from unstable *pf*-shell nuclei with $T_z[=(1/2)(N-Z)] = -2$ and larger is poor. Here we discuss the study of GT transitions in nuclei far from the line of stability by combining results from studies of the β decay for these nuclei with the detailed information on mirror transitions obtained from (^{3}He, t) reactions on stable target nuclei.

11.1. Deduction of Gamow–Teller transitions in the decay of the proton drip-line nucleus ^{52}Ni

In β-decay studies of Gamow–Teller (GT) transitions starting from *pf*-shell nuclei near the proton drip-line, half-lives can be measured rather accurately. On the other hand, the high resolution (^{3}He, t) CE reactions on mirror nuclei provide complementary information on individual GT transitions up to high excitation energies in the final nucleus. For the accurate study of GT transition strengths in the $A = 52$, $T = 2$ system, we compare and combine results from the β-decay study of the proton-rich nucleus ^{52}Ni and the measurement of the ^{52}Cr(^{3}He, t) reaction assuming that good isospin symmetry applies to the $T_z = \pm 2 \rightarrow \pm 1$ transitions, which do not share common final states as shown in Fig. 44.

In the β-decay study of ^{52}Ni, an accurate half-life of $T_{1/2} = 40.8(2)$ ms has been measured [58]. In addition the delayed-proton spectrum has been measured, but the derivation of GT transition strengths, B(GT)s, was difficult. This is because of the low production rate for these nuclei far from stability and the suppression of feeding to states at high excitation energy due to the small phase-space factors (f-factors). The isospin symmetry of analogue states and the analogous GT and Fermi transitions in the "$T = 2$ quintet" are shown in Fig. 44 for the $A = 52$ isobars. In the quintet, GT and Fermi transitions from the $J^\pi = 0^+$ ground states of the $T_z = \pm 2$ even–even nuclei to the 1^+, GT states and the 0^+, IAS in the $T_z = \pm 1$ odd–odd nucleus, respectively, are analogous. This allows us to make the $T_z = -2 \rightarrow -1$ β-decay results more informative by adding a detailed knowledge of the $T_z = +2 \rightarrow +1$ isospin analogous GT transitions studied in the ^{52}Cr(^{3}He, t) measurement.

The $T_z = +2 \rightarrow +1$, ^{52}Cr(^{3}He, t) ^{52}Mn experiment was performed at the high energy resolution facility of RCNP, Osaka. A resolution of $\Delta E < 30$ keV, achieved by using matching techniques, was crucial in separating the IAS and the nearby 1^+, GT states (see Fig. 45(a)), which was not possible in the earlier ^{52}Cr(p, n) measurement [204]. Using the proportionality (Eq. (31)) and the "merged analysis" (see Section 7.2 and [153]) which uses the $T_{1/2}$ value (40.8(2) ms) in the β decay of ^{52}Ni as an input, accurate B(GT) values can be derived.

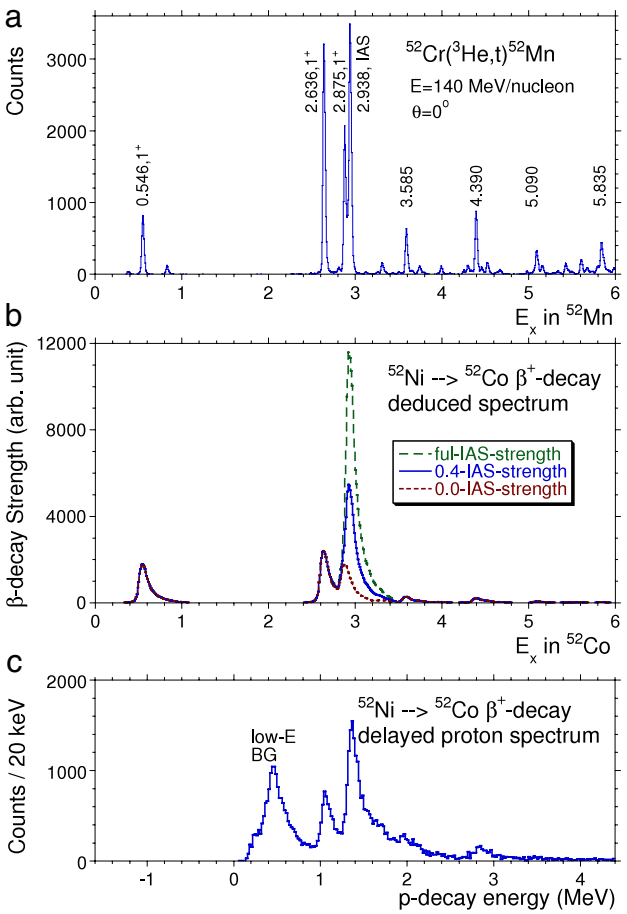

Fig. 45. (a) The ^{52}Cr(^{3}He, t) ^{52}Mn spectrum taken at the incoming energy of 140 MeV/nucleon for events within scattering angles $\Theta \leq 0.5°$. Prominent states with $\Delta L = 0$, most probably the GT states, are indicated by their excitation energies in MeV. The identification of the IAS and the low-lying 1^+ states is from [205]. (b) The estimated ^{52}Ni β-decay spectrum obtained by multiplying the calculated f-factor with the ^{52}Cr(^{3}He, t) spectrum from figure (a). The proton decay from the $T = 2$, IAS in the $T_z = -1$ nucleus ^{52}Co is not allowed by the isospin selection rule; the decay is possible only through $T = 1$ isospin impurities. Therefore, the peak corresponding to the proton decay of the IAS should be suppressed. (c) The delayed-proton spectrum obtained in the ^{52}Ni, β-decay measurement (from [58]). Note that the energy scale is shifted by the proton separation energy of $S_p = 1.58$ MeV in ^{52}Co [58].

Assuming good isospin symmetry for the $T_z = \pm 2 \rightarrow \pm 1$ GT transitions, the "β-decay spectrum" of the $T_z = -2$ nucleus ^{52}Ni can be deduced by multiplying the calculated f-factor and the (^{3}He, t) spectrum for the $T_z = +2$ target nucleus ^{52}Cr shown in Fig. 45(a). By adding the width of 150 keV corresponding to the resolution of the delayed-proton measurement, the spectrum shown in Fig. 45(b) was obtained. It should be noted that the proton decay from the IAS is suppressed by the isospin selection rule, in which the $T_z = -1$ nucleus ^{52}Co becomes the $T_z = -1/2$ nucleus ^{51}Fe with the g.s isospin $T = 1/2$ and a proton with $T_z = -1/2$ and isospin $T = 1/2$. The vector sum allows either $T = 0$ or 1. Since the IAS in the $T_z = -1$ nucleus ^{52}Co has $T = 2$, it is expected that the proton decay only occurs through the isospin impurity components in the wave functions.

The ratios of the Fermi and GT coupling constants (interaction strengths) are different in the corresponding β-decay and (^{3}He, t) reaction. It was found that the unit Fermi transition strength compared to the unit GT strength is larger by a factor of $\approx$5 in the β decay than in the (^{3}He, t) reaction for mass $A = 52$ at 140 MeV/nucleon [37,151,153]. By including this factor, the broken line in Fig. 45(b) was estimated. However, in reality, the delayed-proton spectrum (Fig. 45(c)) suggests that the proton decay of the IAS is suppressed by the isospin selection rule. By assuming the suppression factor of about 60% (the full line in the Fig. 45(b)), we could reproduce well the delayed-proton spectrum of the ^{52}Ni β decay.

Since the β-delayed proton spectrum from the nucleus ^{52}Ni was well reproduced by the spectrum reconstructed using the (^{3}He, t) spectrum on the mirror ^{52}Cr nucleus, it is suggested that the isospin symmetry holds well even for $T_z = \pm 2 \rightarrow \pm 1$ mirror transitions. The β-decay measurement suggests the E_x value of the IAS in ^{52}Cr is 2.93 MeV, which is also in good agreement with the value of 2.94 MeV in ^{52}Mn. All of this suggests that the strengths of $T_z = -2 \rightarrow -1$ GT transitions can be deduced from accurate measurements of the analogous transitions in the high resolution (^{3}He, t) reaction. It should be stressed that the strengths of these exotic GT transitions have never been well studied in direct measurements.

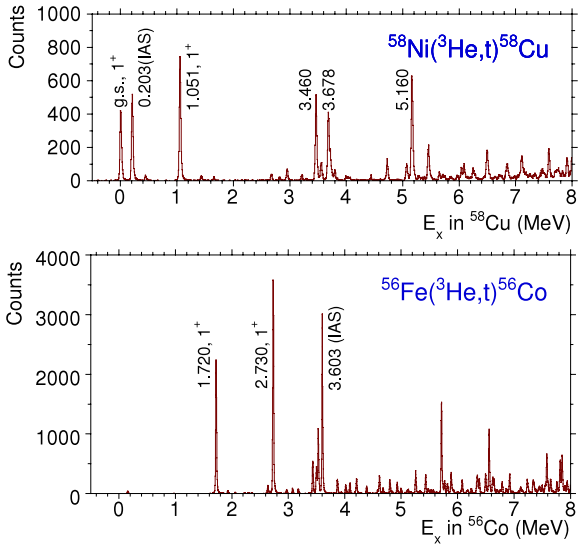

Fig. 46. The ^{58}Ni(^{3}He, t) ^{58}Cu and ^{56}Fe(^{3}He, t) ^{56}Co spectra at 0° and an intermediate incident energy of 140 MeV/nucleon. The GT transitions in these ^{58}Cu and ^{56}Co spectra are the $T_z = +1 \rightarrow 0$ (see Fig. 29) and $T_z = +2 \rightarrow +1$ (see Fig. 4) transitions, respectively. The vertical scales are normalised by the heights of the IAS peaks representing the Fermi transition strengths of $B(\mathrm{F}) = N - Z = 2$ and 4, respectively. Since the ratio of strengths of the τ and $\sigma\tau$-type nucleon–nucleon interaction changes only slowly as a function of mass number A, we expect the heights of the peaks to reflect the B(GT) values assuming the proportionality between the 0° cross-section and the B(GT) and ignoring kinematical effects.

11.2. Nuclei above the f shell

Since the proton separation energy S_p of the daughter nucleus becomes lower as the mass number A and isospin T increase, delayed-proton measurements in β decay will become important for the study of proton-rich *pf*-shell nuclei far from stability. In addition, due to the larger Q_β-values, the β^+ decay can access the GT transitions up to higher excited states in the daughter nucleus. There are, however, more experimental difficulties as A increases. One is the low production rate of such exotic nuclei, which makes it difficult to determine the absolute yields of the emitted protons and γ rays. The second is the fact that the proton transition may populate a state other than the g.s in the final nucleus, which makes it difficult to determine the excitation energy of the level fed in the decay. Finally, if the setup used is similar to the one described in 7.3 the summing of the proton signal in the implantation detector with the beta signal limits either the resolution of the proton spectrum (if the implantation detector is thick, i.e. 1 mm Si) or the β detection efficiency (if the implantation detector is thin, i.e. 0.3 mm Si).

Nevertheless a project to study the β decay of these exotic nuclei is in progress at GANIL, France. We have started with the decay of ^{58}Zn and ^{56}Zn cases with $T_z = -1$ and $T_z = -2$, respectively. They are the isospin mirror nuclei of the stable ^{58}Ni and ^{56}Fe nuclei, respectively (see Figs. 4 and 6). Moreover ^{58}Ni is the heaviest $T_z = +1$ target nucleus that exists and allows us to inspect the $T = \pm 1$ system beyond the $f_{7/2}$ shell with both CE and β-decay.

The half-lives and branching ratios obtained in the β-decay studies can be combined with the (relative) GT strength distributions from the high resolution (^{3}He, t) measurements at RCNP for the better understanding of the nuclear structure of these *pf*-shell nuclei far from stability.

The (^{3}He, t) spectra obtained for ^{58}Ni ($T_z = +1$) [24,168] and ^{56}Fe ($T_z = +2$) [206] are shown in Fig. 46. The angular distribution analysis suggests that most of the prominent excitations are the transitions to GT states (except the IAS). With an excellent energy resolution of $\Delta E = 19$ keV ($\Delta E/E = 4.5 \times 10^{-5}$) in the ^{56}Fe(^{3}He, t) measurement, it was found that the 3.5(2) MeV peak assigned as the "IAS peak" in the ^{56}Fe(p, n) reaction [109] consists of four states at 3.44, 3.50, 3.53 and 3.60 MeV. Since the proton decay from the IAS will be suppressed, as was discussed in Section 11.1, the identification of the IAS is important.

As mentioned above, we have recently carried out an experimental programme at GANIL using the LISE3 separator [207]. In the first experiment, a ^{64}Zn^{29+}, 79 MeV/nucleon beam with an average intensity of 500 enA was accelerated by the two GANIL accelerators CSS1 and CSS2 and impinged on a $^{\mathrm{nat}}$Ni production target. The ^{58}Zn nuclei produced by the 6-neutron removal fragmentation process were selected by the LISE spectrometer and the following Wien filter. In the second experiment a beam of ^{58}Ni^{26+} with 75 MeV/nucleon was used. The ^{56}Zn nuclei were produced through a double charge-exchange reaction. It was found that the production of both ^{56}Zn and ^{58}Zn was better with the ^{58}Ni beam.

The implantation detector setup at the focal plane consisted of a standard 300 μm-thick silicon detector providing the energy loss signal, a 1004 μm (first experiment) optimised for good β detection efficiency, or a 300 μm (second experiment) optimised for good proton energy resolution, double-sided silicon strip detector (DSSD) with 16 × 16 strips with a pitch of 3 mm used as the implantation device, and a 4 mm thick lithium-drifted silicon detector used as a veto detector for the

implantation events and also to detect β particles. The implantation array was surrounded by four germanium CLOVER detectors.

We obtained a preliminary value of $T_{1/2} = 90(8)$ ms for the decay of ^{58}Zn from the β-delayed γ-ray measurement in the first experiment. An experiment at ISOLDE reported a value of 86(18) ms [157]. An earlier study at GANIL gave a value of 83(10) ms [208]. In the second experiment the β-delayed protons emitted in the decay of ^{56}Zn were clearly seen with higher statistics and better resolution than in a previous experiment [58]. A full analysis of these experiments is in progress.

12. Summary and outlook

In this article we have tried to compare and contrast our present knowledge of CE reactions and β decay. We have also looked at how $M1$ transitions can provide closely related spectroscopic information. In both cases, β decay and CE reactions, there have been rapid advances in experimental methods over the last two decades or so.

Our studies of β decay have been transformed (see Section 4) not just by the increasing availability of beams of radioactive nuclei far from the line of stability with higher intensities but also by improvements in detection techniques (Sections 4.1–4.3). These improvements allowed us to observe the GT resonance for the first time in β-decay studies (Section 10.3), or to perform spectroscopic studies using fragmentation reactions (Sections 7.3 and 11).

The dramatic improvement in energy resolution achieved in the β^--type CE reaction (^{3}He, t) has allowed us to see the details of the GT transitions; details lost in the fog of poor resolution in earlier studies. Even the fine structure of GTRs can now be studied. The higher sensitivity associated with the much improved energy resolution even allows us to identify a sharp $T = 3/2$ state at $E_x = 14.66$ MeV in ^{9}B in spite of its weak excitation strength (Section 6.1.2).

All these improvements now allow us to combine studies of both processes and obtain a richer and more complete picture of GT states and the strengths of the spin–isospin excitations in nuclei. One of the best examples of how these studies can be combined is the "merged analysis" (Section 7.2) which relies on two main ideas. One is the proportionality between the (^{3}He, t) cross-section and the B(GT), and the other is the assumption that isospin is a good quantum number and hence states in mirror nuclei have identical configurations (only protons and neutrons are exchanged) and mirror transitions have identical strengths. If these conditions are fulfilled then we can combine the results from β decay and CE reactions in mirror nuclei.

As we have seen in Section 5.3, mirror transitions have been compared in the *sd*-shell nuclei, where a good proportionality was observed for the stronger transitions. However, a better comparison can be made for the *pf*-shell nuclei, because the Q-values are larger there and several states are populated in the beta decay inside the Q_β-window. We performed (^{3}He, t) measurements on $T_z = +1$, *pf*-shell nuclei to study $T_z = +1 \rightarrow 0$ GT transitions. With an energy resolution of about 30 keV, discrete GT states were identified, which allowed us to perform the merged analysis in combination with the accurate $T_{1/2}$ value from the mirror β-decay study (Section 7.2). The unknown energy spectra of the $T_z = -1 \rightarrow 0$ β-decay of exotic nuclei were estimated by multiplying the (^{3}He, t) spectra by the f-factor calculated from the Q-value of the decay. By further combining the half-life values obtained in the β-decay measurements, absolute values for GT transition strengths B(GT) were derived. Note that no feeding information, which is sometimes difficult to measure in a β decay, was used.

The B(GT) values obtained in the merged analysis, however, require an experimental validation, to this end, we have launched a series of experiments at the fragmentation facilities at GSI (Section 7.3) and GANIL (Section 11.2). All the levels which were observed in the (^{3}He, t) reactions and lie within the sensitivity limit of our setup were observed through the detection of the β-delayed γs. Although the detailed analysis for the determination of precise γ-ray intensities is in progress, a good isospin symmetry is suggested.

The merged analysis for the determination of absolute GT strengths can be extended not only to other $T = 1$ systems, but also to $T = 2$ and even higher T systems, thus allowing the GT strength distributions in proton-rich exotic nuclei to be deduced. The uncertainty in the GT strength obtained is due mainly to the ambiguities in the $T_{1/2}$ and the decay Q-value. A better knowledge of the $T_{1/2}$ and Q-values will make the merged analysis more fruitful as the means to determine the absolute GT strengths in proton-rich exotic *pf*-shell nuclei. A knowledge of these strengths is also important because they are needed to deduce astrophysical transition rates under extreme conditions.

We have also analysed the nature of the $\sigma\tau$ operator and how it transforms the initial state into states in the final nucleus. The $\sigma\tau$ operator does not modify the spatial distribution of the initial state (Sections 6.1.2 and 6.1.3), it changes a proton into a neutron, or vice versa and it can flip the spin. Consequently, parent and daughter states are closely related. This has been used to determine the shape of ^{76}Sr (Section 4.4).

In the present article, we have focused on (p, n)-type reactions. It is worth noting that the new results on GT transitions obtained in the high resolution (^{3}He, t) reaction are constructed on the bases of the accumulated knowledge and the understanding achieved by using the (p, n) reactions performed at intermediate incoming energies of $E_p = 120$–200 MeV [4,10,110,189,191,209]. In the (p, n)-type reactions, the proton separation energy S_p in the final nucleus is usually lower than the neutron separation energy S_n. Therefore, studies of proton decay from GT states (GT resonances) can provide direct information on the configurations involved or their microscopic structure. At intermediate incoming energies, proton decays were studied in coincidence with (^{3}He, t) reaction at 150 MeV/nucleon [210–212]. Since the (^{6}Li, ^{6}He) reaction has a selectivity for spin excitations, it can be used for the study of GT and other spin-flip excitations [213].

Although we could not pay much attention to (n, p)-type CE reactions, they play important roles in GT transition studies. The (n, p) reaction at intermediate energies has been studied at Uppsala [214] and at TRIUMF, where measurements have been carried out extensively for various target nuclei [5,215–218]. A considerable effort has been devoted to advancing the use of the $(d, {}^2\mathrm{He})$ reaction at RIKEN ($E_d = 135$ MeV/nucleon) [219,220]. At KVI a resolution of 110–150 keV has been realised at incoming energies of $E_d = 85$–92 MeV/nucleon [172,221–224]. It was found that the comparison of the results obtained with $({}^3\mathrm{He}, t)$ results was fruitful [25,225]. Reactions using heavier incoming beams such as the $({}^{12}\mathrm{C}, {}^{12}\mathrm{N})$ [226] and $({}^{13}\mathrm{C}, {}^{13}\mathrm{N})$ [227] reactions have also been performed at RIKEN. At NSCL, MSU, secondary beams of tritons have been produced and used to study $(t, {}^3\mathrm{He})$ reactions on stable targets [9,112,115,228]. Another interesting (n, p)-type reaction is the $({}^7\mathrm{Li}, {}^7\mathrm{Be}\gamma)$ reaction [91,229,230]. Since the $J^\pi = 1/2^-$, 0.429 MeV first excited state and the $3/2^-$ g.s of ${}^7\mathrm{Be}$ are particle bound, the spin-flip and non-spin-flip excitations can be distinguished by measuring the particle-γ-ray coincidences (see Section 5.1).

The (n, p)-type reactions on stable target nuclei with $T_0 = 1/2$, 1 and larger values excite only $T_0 + 1$ states (see Fig. 3 in Section 2.3 and Fig. 7 in Section 2.5). By combining with the results from (p, n)-type measurements on the same $T = T_0$ target nucleus and assuming isospin symmetry, the $T_0 + 1$ GT states and their GT strengths were studied [24,25,112,216]. From the combined studies of (p, n)-type and (n, p)-type CE reactions, the nuclear matrix elements that are needed for the determination of the rate of two-neutrino double-β decay, except the ambiguity of phase relationship, can be obtained [7, 222,224,231].

How will all of this develop in the future? Up to the present we have been largely concerned with CE reactions on stable targets and β decays far from the line-of-nuclear-stability, but still not at the limits. It is clear that the future of this area of nuclear science is firmly focused on the development of beams of radioactive nuclear species and their use to study nuclear structure. Accordingly we can anticipate that CE reaction and β decay studies involving unstable, exotic nuclei will become part of the major extension of our traditional repertoire of experimental methods.

The reader will find many articles devoted to the development and construction of facilities intended to produce accelerated beams of radioactive nuclear species. These facilities fall into two main categories, namely ISOL and In-Flight (or Fragmentation) facilities. The great advantage of the former is that the accelerated beams are of high quality as discussed in Section 4.1. However, the beams produced at ISOL facilities depend on the chemistry of the species involved. In general, beam intensity is another difficulty. Probably reasonable intensities will be available only at the future EURISOL facility [232]. In the case of fragmentation (or high energy fission)-based facilities beam production is independent of the chemistry. However the beam quality is poor compared with ISOL facilities. The beams at RIKEN, GSI, GANIL and MSU are all produced after passage through a fragment separator [233–236]. In general the beams are not fully separated physically but are delivered as a cocktail of species of neighbouring A and Z (see Section 4.1). They also suffer from poor energy resolution. This will make comparison with the analogous states produced in other ways very difficult since one cannot be sure one is seeing the same states. One way round this is to detect the γ rays emitted in CE reactions in coincidence with the heavy ejectile [230], if the states are particle bound. One can then identify the states based on the higher resolution in the γ-ray spectrum. The other possibility is to use cooled beams in storage rings, this however imposes a limitation on the nuclei which can be studied depending on their half-life (short-lived nuclei will not survive the cooling period). In addition, in inverse kinematics, measurements at 0° are difficult, because the energy of light particles emitted close to 90° is almost zero.

If we are to exploit CE and β decay fully at these new facilities, we must develop new and improved detection methods as well as the new beams. In this context the direction of improvement in the β decay studies has been set by experiments already undertaken at MSU (see e.g. [237,238]), at GANIL [58] and also at GSI (see e.g. [164]). Here the relevant radioactive species is identified using the time-of-flight and energy loss of the ion and the $B\rho$ of the separator magnets. The identified ion is stopped in a highly pixellated set of double-sided Si Strip detectors (DSSDs). The subsequent β rays and β delayed radiation are then recorded in coincidence with the heavy ion implant (for details, see Section 7.3). As beam intensities increase by the orders of magnitude promised at the new facilities it will also require improvements in electronics and data acquisition. In addition one will also need to develop improved techniques for detecting the β-delayed neutrons emitted far from stability and allowing the use of the TAS technique. A concerted development programme is underway in conjunction with the FAIR facility at GSI [239] and at the DESIR-SPIRAL 2 facility in France [240].

As a conclusion, if one can develop these techniques to the point where one can start with the g.s of the nucleus and study exactly the same transition in CE and β decay, we will be able to look in detail at the differences in the two processes. This holy grail remains in the distant future at this point.

Acknowledgements

The high energy resolution $({}^3\mathrm{He}, t)$ experiments were performed at RCNP, Osaka University. The authors are grateful to the RCNP accelerator group, especially to Professors K. Hatanaka and T. Saito. They are also grateful to all the participants in the high resolution $({}^3\mathrm{He}, t)$ experiments. They came from Japan, Asia, Europe, USA and South Africa. The project seeking a higher energy resolution at intermediate energies started in 1995 at RCNP, when Professor G. Berg (IUCF, now at Notre Dame) stayed in Osaka supported by JSPS. YF greatly acknowledges his contribution. The authors are also grateful to their collaborators at ISOLDE, GSI (FRS and Rising groups), GANIL (Lise3 and CEN Bordeaux groups), and KU-Leuven (Lisol group), who made many of the difficult β-decay experiments a reality.

YF acknowledges the work of Drs. H. Fujita (Osaka), Y. Shimbara (Niigata), T. Adachi (KVI) and Prof. A. Tamii (RCNP, Osaka), who put in the effort needed for the achievement of high energy resolution. YF is also grateful for discussions made with various people, especially with Professors and Drs. B. Blank (Bordeaux), B.A. Brown (NSCL, MSU), M. Fujiwara (Osaka), I. Hamamoto (Lund), M.N. Harakeh (KVI), J. Jänecke (Michigan), K. Muto (TIT), H. Nakada (Chiba), T. Otsuka (Tokyo), L. Popescu (Gent and SCK-CEN), H. Sakai (Tokyo), P. von Brentano (Köln), P. von Neumann-Cosel (TUDA) and R.G.T. Zegers (NSCL, MSU). He acknowledges the encouragement of Professors H. Toki and H. Horiuchi (RCNP, Osaka), and S. Sasaki (Osaka).

BR is grateful to F. Molina for the careful analysis of the β-decay experiments at Louvain la Nueve and GSI, and his dedicated effort to obtain a precise half-life value of ^{54}Ni.

This work was supported in part by MEXT, Japan under Grant Nos. 15540274, 18540270 and 22540310 and also by the Japan–Spain collaboration programme of JSPS and CSIC. This work was also supported in part by the Spanish MEC under Grant No. EPA2005-03993, the Spanish MICINN Grant No. FPA200806419-C02-01, the Brix-IAP Research Programme (P06/23), FWO-Vlaanderen, Belgium, and the UK Science and Technology Facilities Council (STFC) Grant No. ST/F012012/1. The β-decay experiments were partly supported through EURONS No. 506065.

References

[1] F. Osterfeld, Rev. Modern Phys. 64 (1992) 491 and references therein.
[2] A. Bohr, B.R. Mottelson, Nuclear Structure, vol. 1, Benjamin, New York, 1969.
[3] K. Langanke, G. Martínez-Pinedo, Rev. Modern Phys. 75 (2003) 819 and references therein.
[4] J. Rapaport, E. Sugarbaker, Annu. Rev. Nucl. Part. Sci. 44 (1994) 109 and references therein.
[5] Papers in Can. J. Phys. 65 (6) (1987) 535–698.
[6] M. Fujiwara, Nuclear Phys. A 687 (2001) 18c and references therein.
[7] D. Frekers, Prog. Part. Nucl. Phys. 57 (2006) 217 and references therein.
[8] M. Ichimura, H. Sakai, T. Wakasa, Prog. Part. Nucl. Phys. 56 (2006) 446 and references therein.
[9] B.M. Sherrill, et al., Nucl. Instrum. Methods Phys. Res. A 432 (1999) 299.
[10] T.N. Taddeucci, et al., Nuclear Phys. A 469 (1987) 125 and references therein.
[11] D.H. Wilkinson (Ed.), Isospin in Nuclear Physics, North-Holland, Amsterdam, 1969.
[12] A. Bohr, B.R. Mottelson, Nuclear Structure, vol. 2, Benjamin, New York, 1975.
[13] C. Djalali, et al., Nuclear Phys. A 388 (1982) 1.
[14] C. Djalali, et al., Nuclear Phys. A 410 (1983) 399; Nuclear Phys. A 417 (1984) 564.
[15] G.M. Crawley, et al., Phys. Rev. C 39 (1989) 311.
[16] A. Willis, et al., Nuclear Phys. A 499 (1989) 367.
[17] A. Tamii, et al., Nucl. Instrum. Methods Phys. Res. A 605 (2009) 326.
[18] E.K. Warburton, J. Weneser, in: D.H. Wilkinson (Ed.), Isospin in Nuclear Physics, North-Holland, Amsterdam, 1969 (Chapter 5).
[19] S.S. Hanna, in: D.H. Wilkinson (Ed.), Isospin in Nuclear Physics, North-Holland, Amsterdam, 1969 (Chapter 12).
[20] A. Richter, Prog. Part. Nucl. Phys. 34 (1995) 261.
[21] Y. Fujita, Nuclear Phys. A 805 (2008) 408c.
[22] Y. Fujita, et al., Phys. Rev. C 55 (1997) 1137.
[23] C.C. Foster, G.P.A. Berg, IUCF Sci. Tech. Rep. 1988–1989, p. 193 (unpublished).
[24] H. Fujita, et al., Phys. Rev. C 75 (2007) 034310.
[25] L. Popescu, et al., Phys. Rev. C 79 (2009) 064312.
[26] N. Anantaraman, et al., Phys. Rev. C 78 (2008) 065803.
[27] J.C. Hardy, I.S. Towner, Phys. Rev. Lett. 88 (2002) 252501.
[28] T. Eronen, et al., Phys. Rev. Lett. 97 (2006) 232501.
[29] T. Eronen, et al., Phys. Rev. Lett. 100 (2008) 132502.
[30] J.C. Hardy, I.S. Towner, Phys. Rev. C 79 (2009) 055502 and references therein.
[31] Y. Fujita, et al., Phys. Rev. C 75 (2007) 057305.
[32] Y. Fujita, B.A. Brown, H. Ejiri, K. Katori, S. Mizutori, H. Ueno, Phys. Rev. C 62 (2000) 044314 and references therein.
[33] H. Morinaga, T. Yamazaki, Beam Gamma-Ray Spectroscopy, North-Holland, Amsterdam, 1976 and references therein.
[34] H. Ejiri, M.J.A. de Voigt, Gamma-Ray and Electron Spectroscopy in Nuclear Physics, Clarendon, Oxford, 1989 and references therein.
[35] A.R. Edmonds, Angular Momentum in Quantum Mechanics, Princeton University Press, Princeton, 1960.
[36] L. Zamick, D.C. Zheng, Phys. Rev. C 37 (1988) 1675.
[37] W.G. Love, M.A. Franey, Phys. Rev. C 24 (1981) 1073.
[38] A. Arima, K. Shimizu, W. Bentz, H. Hyuga, in: J.W. Negele, E. Vogt (Eds.), Advances in Nuclear Physics, vol. 18, Plenum, New York, 1987, p. 1 and references therein.
[39] I.S. Towner, Phys. Rep. 155 (1987) 263.
[40] A. Richter, A. Weiss, O. Häusser, B.A. Brown, Phys. Rev. Lett. 65 (1990) 2519.
[41] C. Lüttge, et al., Phys. Rev. C 53 (1996) 127.
[42] P. von Neumann-Cosel, A. Richter, Y. Fujita, B.D. Anderson, Phys. Rev. C 55 (1997) 532.
[43] Y. Fujita, et al., Phys. Rev. C 59 (1999) 90.
[44] W. Pauli, Rapports du Septieme Conseil de Physique Solvay, Brussels, 1933.
[45] E. Fermi, Z. Phys. 88 (1934) 161.
[46] J.C. Hardy, I.S. Towner, Nucl. Phys. News 16 (2006) 11.
[47] I.S. Towner, J.C. Hardy, Phys. Rev. C 66 (2002) 035501.
[48] A.H. Wapstra, G. Audi, Nuclear Phys. A 432 (1985) 1.
[49] A.H. Wapstra, G. Audi, Nuclear Phys. A 565 (1993) 1.
[50] G. Audi, et al., Nuclear Phys. A 729 (2003) 1.
[51] K. Blaum, Sz. NagyWerth, J. Phys. B 42 (2006) 154015.
[52] K. Blaum, Phys. Rep. 425 (2006) 1.
[53] F. Bosch, Lecture Notes in Phys. 651 (2004) 137.
[54] I. Ahmad, et al., Phys. Rev. C 74 (2006) 065803 and references therein.
[55] S.-C. Wu, Nucl. Data Sheets 91 (2000) 1.
[56] C.G. Ball, et al., Phys. Rev. Lett. 86 (2001) 1454.
[57] I. Dillman, et al., Phys. Rev. Lett. 91 (2003) 162503.
[58] C. Dossat, et al., Nuclear Phys. A 792 (2007) 18.
[59] H. Geissel, et al., Nucl. Instrum. Methods Phys. Res. B 70 (1992) 286.

[60] H. Morrisey, et al., Nucl. Instrum. Methods Phys. Res. B 204 (2003) 90.
[61] A.C. Muller, et al., Nucl. Instrum. Methods Phys. Res. B 56–57 (1991) 559.
[62] T. Kubo, et al., Nucl. Instrum. Methods Phys. Res. B 204 (2003) 97.
[63] S. Pietri, et al., Nucl. Instrum. Methods Phys. Res. B 261 (2007) 1079.
[64] T. Kurtukian-Nieto, Nucl. Instrum. Methods Phys. Res. A 589 (2008) 472.
[65] J. Pereira, et al., Phys. Rev. C 79 (2009) 035806.
[66] J.C. Hardy, et al., Phys. Lett. B 71 (1977) 307.
[67] J. Milton, Paradise Lost, Book I, 1667.
[68] B. Rubio, et al., J. Phys. G: Nucl. Part. Phys. 31 (2005) S1477.
[69] M. Karny, et al., Nucl. Instrum. Methods Phys. Res. B 126 (1997) 411.
[70] J.L. Tain, D. Cano-Ott, Nucl. Instrum. Methods Phys. Res. A 571 (2007) 719.
[71] J.L. Tain, D. Cano-Ott, Nucl. Instrum. Methods Phys. Res. A 571 (2007) 728.
[72] W. Nazarewicz, et al., Nuclear Phys. A 435 (1985) 397.
[73] P. Bonche, et al., Nuclear Phys. A 443 (1985) 39.
[74] J.H. Hamilton, et al., Phys. Rev. Lett. 32 (1974) 239.
[75] C. Chandler, et al., Phys. Rev. C 56 (1997) R2924.
[76] R. Neugart, G. Neyens, Lecture Notes in Phys. 700 (2006) 135.
[77] E. Davni, et al., Phys. Rev. Lett. 50 (1983) 1652.
[78] F. Hardeman, et al., Phys. Rev. C 43 (1991) 130.
[79] I. Hamamoto, et al., Z. Phys. A 353 (1995) 145.
[80] P. Sarriguren, et al., Nuclear Phys. A 691 (2001) 631.
[81] E. Nacher, et al., Phys. Rev. Lett. 92 (2004) 232501.
[82] C.J. Lister, et al., Phys. Rev. C 42 (1990) R1191.
[83] L. Grodzins, Phys. Lett. 2 (1966) 88.
[84] Ch. Miehe, et al., in: H. Sakai (Ed.), New Facet of Spin Giant Resonances in Nuclei, World Scientific, Singapore, 1997, p. 140.
[85] D. Cano-Ott, et al., Nucl. Instrum. Methods Phys. Res. A 430 (1999) 488.
[86] Ph. Dessagne, et al., Eur. Phys. J. A 20 (2004) 405.
[87] E. Poirier, et al., Phys. Rev. C 69 (2004) 034307.
[88] C. Chandler, et al., Phys. Rev. C 56 (1997) R2924.
[89] W. Korten, et al., Nuclear Phys. A 746 (2004) 90c.
[90] M.N. Harakeh, A. Van Der Woude, Giant Resonances, in: Oxford Studies in Nucl. Phys., vol. 24, Oxford University Press, Oxford, 2001.
[91] T. Annakkage, et al., Nuclear Phys. A 648 (1999) 3.
[92] Web page: http://www.nndc.bnl.gov/ensdf/.
[93] Web page: http://www.rcnp.osaka-u.ac.jp.
[94] T. Wakasa, et al., Nucl. Instrum. Methods Phys. Res. A 482 (2002) 79.
[95] M. Fujiwara, et al., Nucl. Instrum. Methods Phys. Res. A 422 (1999) 484.
[96] Y. Fujita, et al., Nucl. Instrum. Methods Phys. Res. B 126 (1997) 274.
[97] Y. Fujita, et al., Nuclear Phys. A 687 (2001) 311c.
[98] H. Fujita, et al., Nucl. Instrum. Methods Phys. Res. A 484 (2002) 17.
[99] H.A. Enge, Nucl. Instrum. Methods 162 (1979) 161 and references therein;
H.A. Enge, Nucl. Instrum. Methods 187 (1981) 1 and references therein.
[100] S.A. Martin, et al., Nucl. Instrum. Methods 214 (1983) 281.
[101] H. Ikegami, et al., Nucl. Instrum. Methods Phys. Res. 175 (1980) 335;
Y. Fujita, et al., Nucl. Instrum. Methods Phys. Res. 225 (1984) 298.
[102] G.P.A. Berg, et al. IUCF Sci. and Tech. Report 1986–1987, p. 152 (unpublished).
[103] C.C. Foster, G.P.A. Berg, IUCF Sci. and Tech. Report 1988–1989, p. 193.
[104] A.M. van den Berg, Nucl. Instrum. Methods B 99 (1995) 637.
[105] B.L. Cohen, Rev. Sci. Instrum. 30 (1959) 415.
[106] B. Sjögren, Nucl. Instrum. Methods 7 (1960) 76.
[107] D.L. Hendrie, in: J. Cerny (Ed.), Nuclear Spectroscopy and Reactions Part A, Academic Press, New York, 1974, p. 365.
[108] A.M. van den Berg, KVI Report KVI-165i, 1991.
[109] J. Rapaport, et al., Nuclear Phys. A 410 (1983) 371.
[110] C.D. Goodman, et al., Phys. Rev. Lett. 44 (1980) 1755.
[111] W.G. Love, K. Nakayama, M.A. Franey, Phys. Rev. Lett. 59 (1987) 1401.
[112] R. Zegers, et al., Phys. Rev. C 74 (2006) 024309.
[113] Y. Fujita, et al., Phys. Rev. C 67 (2003) 064312.
[114] Y. Fujita, et al., Phys. Rev. C 66 (2002) 044313.
[115] A.L. Cole, et al., Phys. Rev. C 74 (2006) 034333.
[116] J.W. Watson, et al., Phys. Rev. Lett. 55 (1985) 1369.
[117] J.W. Watson, Q.Q. Du, Nuclear Phys. A 687 (2001) 32c.
[118] R. Zegers, et al., Phys. Rev. C 77 (2008) 024307.
[119] R. Zegers, et al., Phys. Rev. Lett. 99 (2007) 202501.
[120] D.R. Tilley, C.M. Cheves, J.L. Godwin, G.M. Hale, H.M. Hofmann, J.H. Kelley, C.G. Sheu, H.R. Weller, Nuclear Phys. A 708 (2002) 3.
[121] N. Ryezayeva, et al., Phys. Lett. B 639 (2006) 623.
[122] J.H. Kelley, C.G. Sheu, J.L. Godwin, et al., Nuclear Phys. A 745 (2004) 155.
[123] H. Akimune, et al., Phys. Rev. C 64 (2001) 041305(R).
[124] Y. Kanada-En'yo, H. Horiuchi, A. Ono, Phys. Rev. C 52 (1995) 638 and Private communication.
[125] C. Forssén, P. Navrátil, W.E. Ormand, E. Caurier, Phys. Rev. C 71 (2005) 044312;
P. Navrátil, Private communication.
[126] T. Suzuki, R. Fujimoto, T. Otsuka, Phys. Rev. C 67 (2003) 044302;
T. Suzuki, Private communication.
[127] C. Scholl, et al., AIP Conf. Proc. 1090 (2009) 544.
[128] Y. Fujita, et al., Phys. Rev. C 70 (2004) 011306(R).
[129] T.N. Taddeucci, et al., Phys. Rev. C 42 (1990) 935.
[130] P. Navrátil, W.E. Ormand, Phys. Rev. C 68 (2003) 034305.
[131] P. Navrátil, et al., Phys. Rev. Lett. 99 (2007) 042501.
[132] F. Ajzenberg-Selove, J.H. Kelley, Nuclear Phys. A 506 (1990) 1.
[133] Y. Kanada-En'yo, Phys. Rev. C 75 (2007) 024302.
[134] A. Tohsaki, H. Horiuchi, P. Schuck, G. Röpke, Phys. Rev. Lett. 87 (2001) 192501.
[135] Y. Funaki, A. Tohsaki, H. Horiuchi, P. Schuck, G. Röpke, Phys. Rev. C 67 (2003) 051306(R).
[136] M. Chernykh, H. Feldmeier, T. Neff, P. von Neumann-Cosel, A. Richter, Phys. Rev. Lett. 98 (2007) 032501.

[137] T. Kawabata, et al., Phys. Rev. C 70 (2004) 034318.
[138] Y. Shimbara, et al., Eur. Phys. J. A 19 (2004) 25.
[139] M. Guttormsen, et al., Nuclear Phys. A 338 (1980) 141.
[140] A.E. Litherland, et al., Can. J. Phys. 36 (1958) 378.
[141] A. Heger, et al., Phys. Rev. Lett. 86 (2001) 1678.
[142] A.B. Balantekin, G.M. Fuller, J. Phys. G: Nucl. Part. Phys. 29 (2003) 2513.
[143] K. Langanke, et al., Phys. Rev. Lett. 93 (2004) 202501.
[144] Y. Shimbara, et al., Nucl. Instrum. Methods Phys. Res. A 522 (2004) 205.
[145] A. Honkanen, et al., Nuclear Phys. A 621 (1997) 689.
[146] W. Liu, et al., Phys. Rev. C 58 (1998) 2677.
[147] Y. Fujita, et al., Phys. Rev. C 70 (2004) 054311.
[148] J.A. Cameron, B. Singh, Nucl. Data Sheets 94 (2001) 429 and references therein.
[149] J.A. Nolen, J.P. Schiffer, Annu. Rev. Nucl. Part. Sci. 19 (1969) 471.
[150] N. Auerbach, Phys. Rep. 98 (1983) 273.
[151] T. Adachi, et al., Nuclear Phys. A 788 (2007) 70c.
[152] T. Adachi, et al., Phys. Rev. C 73 (2006) 024311.
[153] Y. Fujita, et al., Phys. Rev. Lett. 95 (2005) 212501.
[154] T.K. Onishi, et al., Phys. Rev. C 72 (2005) 024308.
[155] V.T. Koslowsky, et al., Nuclear Phys. A 624 (1997) 293.
[156] I. Reusen, et al., Phys. Rev. C 59 (1999) 2416.
[157] A. Jokinen, et al., Eur. Phys. J. A 3 (1998) 271.
[158] T.W. Burrows, Nucl. Data Sheets 75 (1995) 1.
[159] A. Schmidt, et al., Phys. Rev. C 62 (2000) 044319.
[160] N. Pietralla, et al., Phys. Rev. C 65 (2002) 024317.
[161] F. Molina, Ph.D. Thesis, Valencia (2010) (unpublished).
[162] D.H. Wilkinson, B.E.F. Macefield, Nuclear Phys. A 232 (1974) 58.
[163] Y. Fujita, B. Rubio, W. Gelletly, AIP Conf. Proc. 1072 (2008) 3.
[164] F. Molina, B. Rubio, Y. Fujita, W. Gelletly, AIP Conf. Proc. 1265 (2010) 49.
[165] P.H. Regan, J. Gerl, H.J. Wollersheim, "Stopped beam" RISING experimental campaign at GSI, spokespersons.
[166] F. Molina, http://arxiv.org/abs/1006.0960.
[167] B.D. Anderson, et al., Phys. Rev. C 41 (1990) 1474.
[168] Y. Fujita, et al., Eur. Phys. J. A 13 (2002) 411.
[169] C.D. Nesaraja, S.D. Geraedts, B. Singh, Nucl. Data Sheets 111 (2010) 897.
[170] F. Bauwens, et al., Phys. Rev. C 62 (2000) 024302.
[171] M. Hagemann, et al., Phys. Lett. B 579 (2004) 251.
[172] M. Hagemann, et al., Phys. Rev. C 71 (2005) 014606.
[173] W. Mettner, et al., Nuclear Phys. A 473 (1987) 160.
[174] S. El-Kateb, et al., Phys. Rev. C 49 (1994) 3128.
[175] E. Caurier, K. Langanke, G. Martínez-Pinedo, F. Nowacki, Nuclear Phys. A 653 (1999) 439.
[176] A. Poves, J. Sánchez-Solano, E. Caurier, F. Nowacki, Nuclear Phys. A 694 (2001) 157.
[177] M. Honma, T. Otsuka, B.A. Brown, T. Mizusaki, Phys. Rev. C 69 (2004) 034335.
[178] M. Honma, T. Otsuka, T. Mizusaki, M. Hjort-Jensen, B.A. Brown, J. Phys. Conf. Ser. 20 (2005) 7.
[179] M.R. Bhat, Nucl. Data Sheets 85 (1998) 415.
[180] P.M. Endt, Nuclear Phys. A 521 (1990) 1.
[181] T. Niizeki, et al. Bulletin, Annual Meeting of the Physical Society of Japan, No. 50 (1995) (31p-P-4), p. 112.
[182] P.M. Endt, J. Blachot, R.B. Firestone, Nuclear Phys. A 633 (1998) 1.
[183] Y. Fujita, et al., Phys. Rev. Lett. 92 (2004) 062502.
[184] S.G. Nilsson, Mat. Fys. Medd. Dan. Vid. Selsk. 29 (16) (1955).
[185] B.R. Mottelson, S.G. Nilsson, Mat. Fys. Skr. Dan. Vid. Selsk. 1 (8) (1959).
[186] J.P. Schiffer, W.W. True, Rev. Modern Phys. 48 (1996) 191.
[187] R.R. Doering, et al., Phys. Rev. Lett. 35 (1975) 1691.
[188] C. Gaarde, et al., Nuclear Phys. A 334 (1980) 248.
[189] D.J. Horen, et al., Phys. Lett. B 99 (1981) 383.
[190] C. Gaarde, et al., Nuclear Phys. A 369 (1981) 258.
[191] C. Gaarde, Nuclear Phys. A 396 (1983) 127c.
[192] J. Jänecke, M.N. Harakeh, S.Y. van der Werf, Nuclear Phys. A 463 (1987) 571.
[193] J. Jänecke, J.A. Bordewijk, S.Y. van der Werf, M.N. Harakeh, Nuclear Phys. A 552 (1993) 323.
[194] K. Pham, et al., Phys. Rev. C 51 (1995) 526.
[195] Y. Kalmykov, et al., Phys. Rev. Lett. 96 (2006) 012502.
[196] B. Rubio, in: H. Sagawa, H. Iwasaki (Eds.), Frontiers of Collective Motions, World Scientific, Singapore, 2002, p. 102.
[197] A. Algora, et al., Phys. Rev. C 68 (2003) 034301.
[198] P. Kleinheinz, et al., Z. Phys. A 290 (1979) 279.
[199] P. Kleinheinz, et al., Phys. Rev. Lett. 55 (1985) 2664.
[200] J. Eberth, et al., Nucl. Instrum. Methods Phys. Res. A 369 (1996) 135.
[201] Z. Hu, et al., Phys. Rev. C 60 (1999) 024315.
[202] Z. Hu, et al., Phys. Rev. C 62 (2000) 064315.
[203] M. Gierlik, et al., Nuclear Phys. A 724 (2003) 313.
[204] D. Wang, et al., Nuclear Phys. A 480 (1988) 285.
[205] Huo Junde, Huo Su, M.A. Chunhui, Nucl. Data Sheets 108 (2007) 773.
[206] H. Fujita, et al. OULNS Annual Report, Osaka University 2006, p. 91 (unpublished).
[207] R. Anne, A.C. Mueller, Nucl. Instrum. Methods Phys. Res. B 70 (1992) 276.
[208] M.J. López Jiménez, et al., Phys. Rev. C 66 (2002) 025803.
[209] B.D. Anderson, et al., Phys. Rev. C 43 (1991) 50.
[210] H. Akimune, et al., Phys. Rev. C 52 (1995) 604.
[211] J. Jänecke, et al., Nuclear Phys. A 687 (2001) 270c.
[212] H. Fujimura, et al., Phys. Rev. C 69 (2004) 064327.
[213] H. Ueno, et al., Phys. Lett. B 465 (1999) 67.
[214] T. Rönnqvist, et al., Nuclear Phys. A 563 (1993) 225.
[215] K.P. Jackson, et al., Phys. Lett. B 201 (1988) 25.
[216] M.C. Vetterli, et al., Phys. Rev. C 40 (1989) 559.
[217] S. El-Kateb, et al., Phys. Rev. C 49 (1994) 3128.

[218] S.A. Long, et al., Phys. Rev. C 57 (1998) 3191.
[219] H. Okamura, et al., Phys. Lett. B 345 (1995) 1.
[220] T. Niizeki, et al., Nuclear Phys. A 577 (1994) 37c.
[221] S. Rakers, et al., Phys. Rev. C 65 (2002) 044323.
[222] S. Rakers, et al., Phys. Rev. C 70 (2004) 054302.
[223] L. Popescu, et al., Phys. Rev. C 75 (2007) 054312.
[224] E.-W. Grewe, et al., Phys. Rev. C 76 (2007) 054307.
[225] A. Negret, et al., Phys. Rev. Lett. 97 (2006) 062502.
[226] T. Ichihara, et al., Nuclear Phys. A 569 (1994) 287c.
[227] T. Ichihara, et al., Phys. Rev. Lett. 89 (2002) 142501.
[228] I. Daito, et al., Phys. Lett. B 418 (1998) 27.
[229] S. Nakayama, Nuclear Phys. A 687 (2001) 84c.
[230] R. Zegers, et al., Phys. Rev. Lett. 104 (2010) 212504.
[231] K. Yako, et al., Phys. Rev. Lett. 103 (2009) 012503.
[232] http://www.eurisol.org.
[233] T. Kubo, et al., Nucl. Instrum. Methods Phys. Res. B 204 (2003) 97 and refereces therin.
[234] H. Geissel, et al., Nucl. Instrum. Methods Phys. Res. B 70 (1992) 286.
[235] A.C. Mueller, R. Anne, Nucl. Instrum. Methods Phys. Res. B 56–57 (1991) 559.
[236] D.J. Morrisey, et al., Nucl. Instrum. Methods Phys. Res. B 204 (2003) 90 and refereces therin.
[237] P. Hosmer, et al., Phys. Rev. Lett. 94 (2005) 112501.
[238] S.N. Liddick, et al., Phys. Rev. C 73 (2006) 044322.
[239] B. Rubio, Internat. J. Modern Phys. E 15 (8) (2006) 1979.
[240] http://www.cenbg.in2p3.fr/desir/.